University of Alberta

Ice Dynamics and Recent Geometric Changes of the Devon Island Ice

Cap, Nunavut, Canada

by

David Burgess ©

A thesis submitted to the Faculty of Graduate Studies and Research in partial

fulfillment of the requirements for the degree of Doctor of Philosophy

Department of Earth and Atmospheric Sciences

Edmonton, Alberta

Spring, 2006

Library and
Archives Canada

Bibliothèque et
Archives Canada

Published Heritage
Branch

Direction du
Patrimoine de l'édition

395 Wellington Street
Ottawa ON K1A 0N4
Canada

395, rue Wellington
Ottawa ON K1A 0N4
Canada

NOTICE:
The author has granted a non-exclusive license allowing Library and Archives Canada to reproduce, publish, archive, preserve, conserve, communicate to the public by telecommunication or on the Internet, loan, distribute and sell theses worldwide, for commercial or non-commercial purposes, in microform, paper, electronic and/or any other formats.

AVIS:
L'auteur a accordé une licence non exclusive permettant à la Bibliothèque et Archives Canada de reproduire, publier, archiver, sauvegarder, conserver, transmettre au public par télécommunication ou par l'Internet, prêter, distribuer et vendre des thèses partout dans le monde, à des fins commerciales ou autres, sur support microforme, papier, électronique et/ou autres formats.

The author retains copyright ownership and moral rights in this thesis. Neither the thesis nor substantial extracts from it may be printed or otherwise reproduced without the author's permission.

L'auteur conserve la propriété du droit d'auteur et des droits moraux qui protège cette thèse. Ni la thèse ni des extraits substantiels de celle-ci ne doivent être imprimés ou autrement reproduits sans son autorisation.

In compliance with the Canadian Privacy Act some supporting forms may have been removed from this thesis.

Conformément à la loi canadienne sur la protection de la vie privée, quelques formulaires secondaires ont été enlevés de cette thèse.

While these forms may be included in the document page count, their removal does not represent any loss of content from the thesis.

Bien que ces formulaires aient inclus dans la pagination, il n'y aura aucun contenu manquant.

Canada

ABSTRACT

In this study, recent changes in geometry and dynamics of the Devon Island ice cap are quantified from remote sensing techniques and field observations. Comparisons of the ice margin position in 1960's aerial photography and 1999 Landsat7 ETM+ imagery indicate a net decrease in area by -338 ± 40 km^2 or 2.4%, over this time period. The dominant changes include retreat of tidewater glacier margins on the eastern side of the ice cap, shrinkage of the southwest arm, and increased bedrock exposure in the ice cap interior. Variability in the changes observed reflect inter-basin differences in the sensitivity of glacier mass balance to climate warming.

Surface velocity fields mapped across ~95% of the ice cap using satellite radar interferometry indicate that the western half of the ice cap is dominated by relatively uniform 'sheet' flow, but 3 fast-flowing outlet glaciers that extend 14 – 23 km beyond the ice cap margin also drain this region. Several outlet glaciers that extend up to 60 km inland from the eastern margin drain the eastern side of the ice cap. Four dominant ice flow regimes were derived from the relationship between the driving stress and the ratio of surface velocity to ice thickness and indicate that ~22% (8%) of the east (west) half of the ice cap is sliding at the glacier bed. The volume of ice calved between 1960 and 1999 was estimated to be 20.5 +/- 4.7 km^3 of ice which accounted for ~30% of the total ablation for this interval.

Long-term thickness change rates were derived at several spatial scales across most of the Devon Island ice cap. Results reveal accumulation zone thinning throughout the southern and eastern basins with a maximum rate of ~ -0.23 m a^{-1} in the southeast sector. Dynamic thinning by of the Southeast 1 and possibly Southeast 2 outlet glaciers above the ELA likely contributes to the basin-wide thinning of the southeast accumulation zone. Dynamic thinning of ~ -2 m occurs near the terminus of the Belcher Glacier as well as thinning by ~ -2 m along the lower reaches of the South Croker Bay Glacier. Dynamic thickening by up to ~ 2 m along the lower reaches of the North Croker Bay Glacier and by ~1 m in the ablation zone of the southeast region along the Southeast 1 and 2 Glaciers prevails. In total, the main portion of the Devon Island ice cap has decreased by -74 ± 9 km^3 of ice (67 ± 7 km^3 water equivalent) between 1960 and 1999, contributing ~0.19 mm to global sea-level rise over this time period.

ACKNOWLEDGMENTS

TABLE OF CONTENTS

LIST OF TABLES

LIST OF FIGURES

CHAPTER 3

CHAPTER 1

INTRODUCTION

The primary objective of this thesis is to provide insight into the ice dynamics, recent changes in geometry, and overall mass balance of the Devon Island ice cap, Nunavut. The Devon Island ice cap is one of the largest ice caps in the Canadian Arctic which, in total, contains the greatest proportion of land ice in the Northern hemisphere outside the Greenland ice sheet. It is currently estimated that ice caps and glaciers have contributed ~0.51 mm a^{-1} to sea level rise from 1960 to 1994, increasing to ~0.93 mm a^{-1} for the period 1994-2003 (Dyurgerov and Meier, 2005). In light of the fact that climate warming is expected to be larger in high northern latitudes than in other regions (IPCC 2001), it is likely that contribution from glaciers and ice caps in these regions will increase significantly. It is therefore critical to quantify long-term changes in the geometry of these ice masses in order to provide accurate estimates of their contribution to global sea-level rise, and to determine the dominant factors (ie. surface mass balance, dynamics, or rates of iceberg calving) that are responsible for these changes in order to predict their response to future climate warming.

The Devon Island ice cap occupies ~14,000 km^2 of the eastern third of Devon Island (Figure 1.1) with a volume of 3962 +/- 140 km^3 based on radio-echo sounding measurements performed in 2000 (Dowdeswell and others, 2004). *In situ* mass balance data collected along the northwest transect by Dr. R. Koerner (Geological Survey of Canada) since the early 1960's indicate a slightly negative balance of ~ -0.086 mWe a^{-1}. Accumulation across the ice cap is derived primarily from distal moisture sources

1

with the exception of the southeast sector, which receives significant mass input from the North Open Water polynya at the head of Baffin Bay (Koerner, 1970). The southeast sector also experiences the highest surface ablation rates across the ice cap (up to ~ -2 m a^{-1}) resulting in a steeper mass balance gradient throughout this region (0.0027 m a^{-1} m^{-1}) than the northwest (0.0015 m a^{-1} m^{-1}). The net annual surface mass balance between these regions however is similar, and is driven primarily by the intensity and duration of summer melt (Koerner, 2002).

Observed, modelled, and proxy data indicate that mean annual air temperatures at high northern latitudes have experienced a net increase by ~1°C since the end of the Little Ice Age (IPCC, 2001, Johannessen and others, 2004, Serreze and others, 2000). Warming took place primarily through two distinct warming events with the first event recorded between 1926 and 1940. During this event, average temperatures across the Arctic increased by ~1°C over a 10 year period of time resulting in high concentrations of ice in the stratigraphic record of firn cores retrieved from the Devon, Agassiz, and Axel Heiberg ice caps (Koerner, 1977), and a 16 m snow pit on the Grant Ice cap, Northern Ellesmere Island (Hattersley-Smith, 1963). With the exception of moderate warming between 1947 and 1963 (Bradley and England, 1978), general cooling prevailed in the Canadian Arctic until the early 1980's, at which time a second major stage of anthropogenically induced warming commenced. Global temperatures associated with this event increased by ~1.5 °C (Johannessen and others, 2004) resulting in a significantly negative trend in surface mass balance along the northwest transect of the Devon Island ice cap since 1988 (Cogley, personal communication, 2005).

2

Our current knowledge of the large-scale ice flow dynamics on the geometry and mass balance of land ice in the Canadian Arctic is limited (Koerner, 2002). Previous studies however, have shown that the influence of changes in ice dynamics on the geometry of and mass loss from northern hemisphere land ice outside Canada is significant. It is estimated that iceberg calving accounts for up to 50% of the total mass loss from the Greenland ice sheet (Weidick, 1985). Repeat airborne laser altimetry measurements along most of the major outlet glaciers that drain the Greenland ice sheet reveal that dynamic thinning associated with many of these calving fronts is responsible for enhanced thinning throughout much of the ablation zone of these outlet glaciers with the highest and most extensive thinning in the southeast and southwest regions (Abdalati, 2001). In the southeast region, channelized fast flow extends up to 70 km inland from the ice margin along the Helheim Glacier where dynamic thinning of ~ -1 m a^{-1} occurs well into the accumulation zone of the ice sheet (Abdalati, 2001). In the northeast region, channelized flow associated with the Northeast Ice Stream, as identified in C-band ERS-1 SAR imagery by Fahnestock and others (1993), extends up to 550 km inland from the ice sheet margin. Zwally and others (2002) detected seasonally enhanced flow of the Greenland ice sheet at Swiss Camp approximately 35 km inland of the ice sheet margin in west-central Greenland where the ice is ~1220 m thick. This finding revealed important linkages between the transmission of melt water from the ice surface to the glacier bed and rates of flow by basal sliding, which may have important implications for the role played by changes in large-scale flow dynamics in ice sheet response to global warming (Parizek and Alley, 2004). Dowdeswell and others (1999) used repeat InSAR techniques to detect time

3

varying flow over Austfonna, the largest ice cap in the Eurasian Arctic (~8100 km^2). Dynamic thinning along a major tidewater glacier that drains this ice cap was observed to extend inland to the interior drainage divide and was associated with significant mass loss from this region by iceberg calving (Unwin, Unpublished PhD Thesis). Similarly, iceberg calving was estimated to account for ~30% of the total volume ablated from the Academy of Sciences ice cap, the largest ice cap in the Russian high Arctic (~5600 km^2) (Dowdeswell and others, 2002).

In a series of three papers, this thesis provides new insight into the recent geometric changes, the dynamic behavior, and the influence of ice dynamics on the mass balance of the Devon Island ice cap, Nunavut, Canada. In the first paper (Chapter 2), areal changes of the Devon Island Ice cap since 1960 are quantified by comparing the ice margin identifiable in aerial photography with the margin in 1999 Landsat7 ETM+ satellite imagery. Analyses of theoretical glacier response times and drainage basin hypsometry, as derived from the Canadian Digital Elevation Dataset (CDED), are used to classify all ice cap drainage basins according to their relative sensitivity to future climate warming and to explain the spatial variability in the observed changes in ice extent. In the second paper (Chapter 3), the surface velocity field of most of the Devon Island ice cap is mapped using satellite radar interferometry (InSAR). In conjunction with ice thickness data obtained from Dowdeswell and others (2004), downslope surface velocities are used to identify and map the dominant ice flow regimes of the ice cap and to quantify the current rate of iceberg calving from 96% of that part of the ice margin that terminates in the ocean. In the third paper (Chapter 4), rates of ice cap thickness change are investigated. Rates of thickness

4

change are calculated separately for the accumulation and ablation areas of individual drainage basins. For the accumulation areas, comparisons between the observed flux out of the accumulation zone and the theoretical balance flux are used to estimate the mean rate of thickness change. For the ablation zones, the observed flux into the ablation zone was compared with the rates of mass loss by iceberg calving determined in the second paper and rates of surface melt computed by Mair and others (2004) to estimate the rate of thickness change. Along most of the major outlet glaciers, rates of thickness change were computed as a function of the continuity of ice flow by comparing values of ice flux at successive gates along these features. Finally, field measurements were used to determine rates of thickness change at 3 locations in the southwest region of the ice cap. The results presented in this thesis provide new insight into the magnitude and distribution of recent changes in the geometry of one of the largest ice masses in the northern hemisphere, and provide the basis for a new assessment of their implications for global sea level.

To date, 2 of the 3 papers in this thesis have been published (or accepted for publication) in peer-reviewed scientific journals. The first paper, *Recent changes in the areal extent of the Devon Island ice cap, Nunavut, Canada,* has been published in the journal Arctic, Antarctic, and Alpine Research. The second paper, *Dynamics and iceberg calving rates of the Devon Island ice cap, Nunavut,* has been accepted for publication in the Journal of Glaciology, and the third paper, *Recent changes in the thickness of the Devon Island ice cap, Nunavut, Arctic Canada,* has been submitted for publication to the Journal of Geophysical Research. Co-authorship on these papers represents contributions in the form of data input from other researchers and editing

5

from Dr. Sharp. All data compilation, processing, and analysis was performed by myself.

In addition to the publications produced from this thesis, work performed during the course of this research has resulted in a further 2 co-authored publications. In the first co-authored paper entitled '*37-year mass balance across the Devon Ice Cap*' (published in the Journal of Geophysical Research; Mair and others, 2004), I contributed field measurements of long-term accumulation rates across the Devon Ice Cap. New information on the surface velocity fields derived from InSAR techniques, controls on the inland extent of fast glacier flow along the North and South Croker Bay Glaciers, and the delineation of major drainage basins was contributed to the second co-authored paper entitled '*Flow and form of the Devon Island Ice Cap, Canadian Arctic*' (published in the Journal of Geophysical Research; Dowdeswell and others, 2004).

1.2 REFERENCES

Abdalati, W., W. Krabill, E. Frederick, S. Manizade, C. Martin, J. Sonntag, R. Swift, R. Thomas, W. Wright, and J. Yungel. 2001. Outlet glacier and margin elevation changes: Near-coastal thinning of the Greenland Ice Sheet. *J. Geoph. Res.*, **106**(D24), 33,729-33,741.

Bradley. R.S. and J. England. 1978. Recent climatic fluctuations of the Canadian high Arctic and their significance for glaciology. *Arctic and Alpine Research.* **10**(4), 715-731.

Cogley, J.G. 2005. Personal communication. Department of Geography, Trent University, ON, Canada.

Dowdeswell, J.A., B. Unwin, A.M.Nuttall, D.J. Wingham. 1999. Velocity structure, flow instability and mass flux on a large Arctic ice cap from satellite radar interferometry. *Earth. and Planet. Sci. Lett., 106, 131-140.*

Dowdeswell, J.A., Bassford, R.P., Gorman, M.R., Williams, M., Glazovsky, A.F., Macheret, Y.Y., Shepherd, A.P., Vasilenko, Y.V., Savatyuguin, L.M., Hubberten, H.-W. and Miller, H., 2002. Form and flow of the Academy of Sciences Ice Cap, Severnaya Zemlya, Russian High Arctic. *J. Geophys. Res., 107,* *doi:10.1029/2000/JB000129.*

Dowdeswell, J. A., T. J. Benham, M.R. Gorman, D. Burgess, and M. Sharp. 2004. Form and flow of the Devon Island ice cap, Canadian Arctic. *J. Geophys. Res.* **109**, F02002, doi:10.1029/2003JF000095.

Dyurgerov, M.B. and M.F. Meier. 2005. Glaciers and the Changing Earth system: A 2004 snapshot. *University of Colorado Institute of Arctic and Alpine Research Occasional Paper 58.*

Fahnestock, M., R. Bindschadler, R. Kwok, K. Jezek. 1993. Greenland ice sheet surface properties and ice dynamics from ERS-1 SAR imagery. *Science.* **262**,1530-1534.

Hattersley-Smith, G. 1963. Climatic inferences from firn studies in northern Ellesmere Island. *Geografiska Annaler.* **XLV**, 139-151.

7

Intergovernmental Panel on Climate Change. 2001. Climate Change 2001: Impacts, Adaptation, and Vulnerability, edited by J.J. McCarthy et al., Cambridge Univ. Press, New York.

Johannessen, O.M. and 11 others. 2004. Arctic climate change: observed and modelled temperature and sea-ice variability. *Tellus*. **56A**. 328-341.

Koerner, R. 2002. Glaciers of the High Arctic Islands, in *Satellite Image Atlas of Glaciers of the World. Glaciers of North America – Glaciers of Canada*. Edited by R.S. Williams, Jr. and J.G. Ferrigno, U.S. Geological Survey Professional Paper 1386-J,j111-j146.

Koerner, R.M., 1977. Devon Island ice cap: core stratigraphy and paleoclimate. *Science*. **196**, No.4285,15-18.

Koerner, R.M., 1970: The mass balance of Devon Island ice cap Northwest Territories, Canada, 1961-1966. *J. Glaciol.*, 9(57): 325-336.

Mair, D.W.F., D.O. Burgess, and M.J. Sharp. 2004. Thirty-seven year mass balance of the Devon Ice Cap, Nunavut, Canada determined by shallow ice coring and melt modelling. *J. Geophys. Res.* **110**, F01011, doi:10.1029/2003JF000099.

Parizek, B.R. and R. Alley. Implications of increased Greenland surface melt under global-warming scenarios: ice-sheet simulations. *Quat. Sci. Rev.* **23**, 1013-1027.

Serreze, M.C. and 9 others. 2000. Observational evidence of recent change in the northern high-latitude environment. *Climatic Change*. **46**. 159-207

Unwin, B., Arctic ice cap velocity variations revealed by ERS SAR interferometry. Unpubl. Ph.D. Thesis, University of London, 1998.

Weidick, A.1985. Review of glacier changes in west Greenland. *Z. Gletscherkd.*
Glacialgeol., **21**, 301-309.

Zwally, H.J., W. Abdalati, T. Herring, K.Larson, J. Saba, K. Steffen. 2002. Surface
melt-induced acceleration of Greenland ice-sheet flow. *Science,* **297**, 218-222.
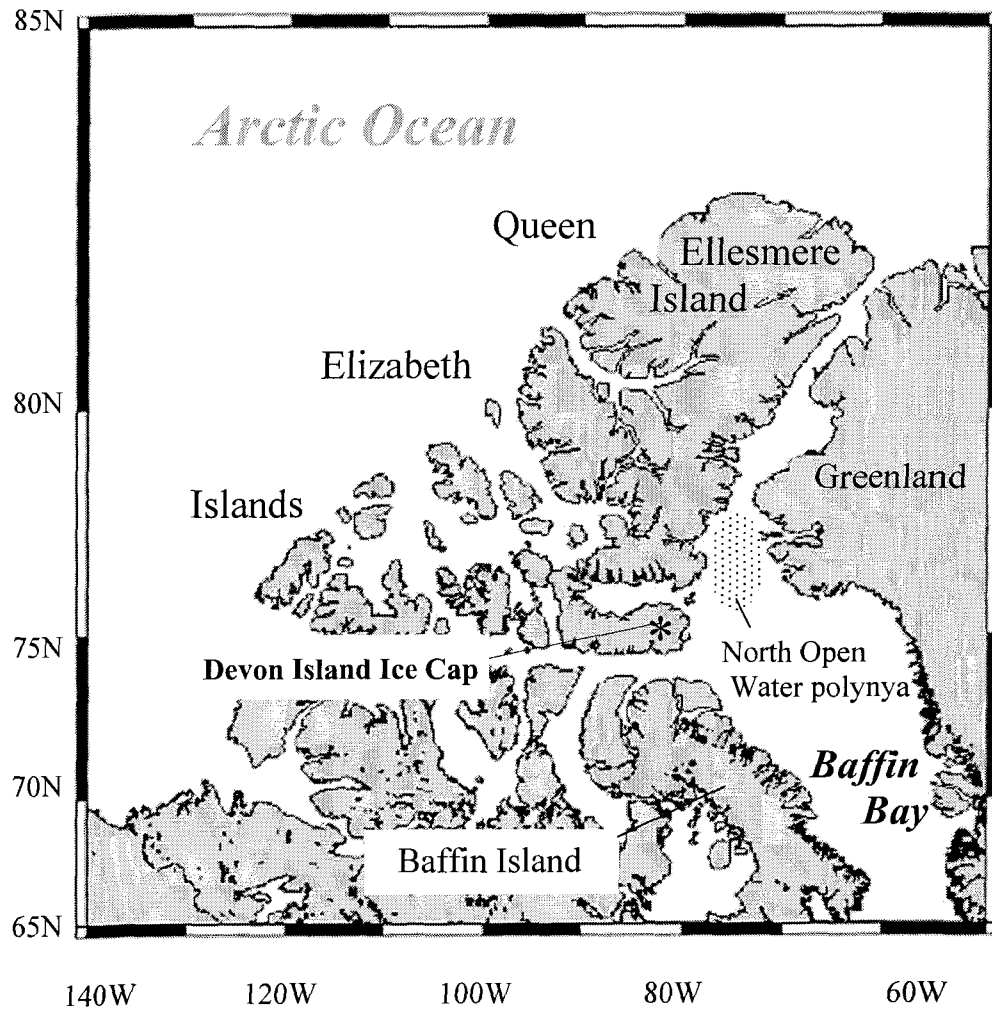
Figure 1.1. Location of the Devon Island ice cap in the Canadian Arctic archipelago.

10

CHAPTER 2

RECENT CHANGES IN AREAL EXTENT OF THE DEVON

ISLAND ICE CAP, NUNAVUT, CANADA

2.1 INTRODUCTION

Global climate models consistently predict that anthropogenic climate warming will be manifested most strongly in northern high latitudes (IPCC, 2001; Johns, and others, 1997; Mitchell, 1995). There is already considerable evidence that the predicted changes are occurring (Overpeck and others, 1997; Serreze and others, 2000). The predicted temperature changes would impact strongly on the mass balance and extent of the glaciers, ice caps and ice sheets in the region, and the resulting shrinkage of these ice masses could contribute significantly to global sea level change over the next century (Meier and Dyurgerov, 2002; Van de Wal and Wild, 2001; Meier, 1984).

Outside Greenland, the largest amounts of land ice (~150,000 km^2) in the Northern Hemisphere are found in the Canadian Arctic islands (Koerner, 1966). However, little is known about recent changes in the extent of these ice masses. Areal change measurements have been made for a section of the Barnes Ice Cap (BIC) on Baffin Island (Jacobs, and others, 1996) and for the small, stagnant Murray Ice Cap (MIC) on northern Ellesmere Island (Braun, and others, 2001). Over the period 1961 to 1993, the area of the measured sector of the BIC decreased by ~1%, while that of the MIC decreased by ~28% between 1959 and 2000. Here we report results of an

11

investigation into recent changes in the extent of the Devon ice cap, Nunavut. Investigation of glacier change at the scale of the whole ice cap is of particular interest because there are strong spatial gradients in climate, mass balance characteristics, glacier geometry, and terminus conditions across the ice cap. Thus, different sectors of the ice cap may be subjected to different climate forcings, they may have different inherent mass balance sensitivity to specific forcings, and they may respond to these forcings at different rates.

Glacier response times are influenced by a combination of ice mass geometry, mass balance gradient, and terminus ablation rates (Johannessen, 1989; Bahr and others, 1998). All of these factors vary significantly across the Devon ice cap. Differences in mass balance gradient between the east and west sides of the ice cap have been attributed to the effect of the Baffin Bay moisture source on regional accumulation patterns. These patterns are believed to have influenced the long-term evolution of the ice cap geometry such that glaciers draining to its eastern margin occupy larger basins and descend to lower elevations than glaciers draining to the west (Koerner, 1977a). Large differences in terminus ablation rates between the east and west margins may have a significant effect on response times characteristic of these regions.

This study quantifies recent changes in the areal extent of the Devon Island ice cap by comparing the position of ice margins extracted from 1959/1960 aerial photographs and 1999/2000 satellite imagery. Information on the topography of the ice cap surface, obtained from the Canadian Digital Elevation Dataset (CDED), was used to delineate drainage basins within the ice cap, and changes were analysed at the

12

scale of individual drainage basins. Relationships among the magnitudes of observed changes, the characteristic response times, and the hypsometry of drainage basins were investigated to provide insight into the mechanisms controlling ice margin variations. Also, two independent methods were used to estimate volume change for selected basins and for the ice cap as a whole.

2.2   STUDY AREA

The Devon Island ice cap occupies approximately 14,400 km^2 (between 74° 30' N and 75° 50'N and 80° 00'W and 86° 00'W) on Devon Island, which is located in the south east of the Queen Elizabeth Islands, Nunavut, Canada (Figure 2.1). Recent radio echo sounding data indicate that the current ice cap volume is 3962 +/- 140 km^3 with a maximum ice thickness of approximately 750 m at the head of the eastward flowing basins (Dowdeswell, and others, 2004). The highest elevation is 1901 m at the ice cap summit. The eastern margin of the ice cap faces the North Open Water (NOW) polynya at the head of Baffin Bay. Large outlet glaciers that descend to sea level in this region experience high rates of accumulation (up to 0.5 m a^{-1}) and surface ablation (up to -2 m a^{-1}) as well as mass loss by iceberg calving, resulting in relatively steep mass balance-elevation gradients (0.0027 m a^{-1} m^{-1}; Koerner, 1970). Smaller tidewater glaciers reach the ocean along the northern and southern margins of the ice cap. By contrast, the western margin of the ice cap terminates entirely on land at elevations of 300-500 m. This part of the ice cap is located in a precipitation shadow, where rates of accumulation and ablation (up to 0.2 m a^{-1} and ~ -1 m a^{-1} respectively), along with mass balance gradients (0.0015 m a^{-1} m^{-1}) are much reduced. An arm extending

13

approximately 80 km to the south-west of the main ice cap consists largely of near stagnant, ablating ice. Nearly all of this sector of the ice cap lies below the equilibrium line altitude (ELA) as defined by mass balance data compiled by Koerner (1970).

Proxy data and field measurements provide insight into the climate history of the ice cap since the end of the Little Ice Age (LIA). Records of summer melt layers from ice cores in the Canadian Arctic indicate an abrupt warming trend beginning ca. 1850 AD, with a second significant temperature increase after ca. 1925 (Koerner, 1977b). Stake measurements made across the northwest part of the ice cap (Sverdrup Glacier) since 1960 indicate a negative mass balance since observations began, with a trend towards increasingly negative balances since the late 1980's (Koerner and Lundgaard, 1995).

2.3 METHODS

Changes in the surface area of the Devon Island ice cap were determined from remotely sensed imagery acquired in 1959/1960 and 1999/2000. Ice margins were digitized for each data set and drainage basin boundaries common to both data sets were delineated. Overlay analysis and raster cartographic techniques were then employed to detect and quantify areal differences between the extracted data sets.

2.3.1 Data Sources

The satellite image data used in this study were obtained from 3 Landsat 7 ETM+ panchromatic (15 m resolution) scenes acquired on July 13, 1999 (path 38 rows 6 and 7) and August 2, 2000 (path 36 row 7). All satellite images were purchased as L1G (radiometrically and geometrically corrected) processed data. The aerial

14

photography consisted of 250 1:60,000 photographs acquired in late July and early August of 1959/1960 by the Government of Canada. The digital elevation model (DEM) used in this study was a subset of the Canadian Digital Elevation Dataset (CDED) produced from the National Topographic System (NTS) 1:250,000 map sheets which, in turn, were derived from the 1959/1960 aerial photography mentioned above. The DEM's were re-projected from the WGS-84 geographic coordinate system (3 x 6 arc seconds) to a 100 m resolution NAD83 UTM grid. Vertical accuracy of the DEM is +/- 20 m over bedrock and ice margins and increases to +/- 50 m throughout the interior regions of the ice cap (A. Gagne, personal communication, 2002).

2.3.2 Image Preparation

All image data were referenced to the UTM projection on the NAD83 datum. Satellite images were georeferenced to the 1:250,000 NTS map sheets using at least 40 ground control points (GCPs) that were clearly identified in both images (RMS error < 60 m). The satellite imagery was orthorectified in PCI Orthoengine™ V8.0 using the *Satellite Orbital Modeler* and the CDED DEM to correct for terrain distortions. The orthorectified images were manually mosaiced to produce a 15 m resolution ortho-image of the entire Devon Island ice cap. The aerial photographs were obtained as contact prints and digitized at 300dpi (5 meters ground resolution) using a Vidar 36" upright scanner. Each digital photograph was georeferenced to the Landsat 7 ortho-mosaic by selecting between 7 and 12 GCPs (depending on the amount of exposed bedrock) over bedrock features clearly identifiable in both images (RMS error < 15 m). The digital photos were then orthorectified in the PCI Orthoengine™ V8.0 *Aerial*

15

Photography Modeler using the CDED DEM to correct for terrain distortions. Four mosaics of the aerial photography were generated in Orthovista™ (image mosaicing software) and clipped to the geographic extents of the corresponding 1:250,000 map sheets.

2.3.3 Linework Capture

Ice margins and boundaries of interior bedrock regions were captured through on-screen digitizing techniques in ArcView 3.2™ geographic information system from both orthorectified digital data sets. Linework representing ice margins was digitized in 'point mode' as a series of line segments and later converted to single polygon coverage in ArcInfo 8.0™. Interior bedrock regions were digitized directly as polygons in ArcView 3.2™. The 1960 ice margin was digitized from the contiguous ice mass. Any parts of the ice cap that were separated from the main ice cap by melting between 1960 and 1999 were included in the 1999 surface area calculations.

2.3.4 Drainage Basin Delineation

Drainage basins were delineated to allow areal changes to be associated with distinct catchment regions (Figure 2.2). A river network for the ice cap surface was initially simulated from the DEM and overlayed on the satellite image mosaic. Using the *'Basin'* utility in ArcView 3.2™, outlet locations (points where the simulated drainage paths flow off the ice cap edge) were identified interactively and the associated catchment areas were delineated based on flow accumulation and direction grids. Due to inaccurate representation of the ice surface by the DEM in some areas,

16

particularly towards the margins, ice flow (as observed from the Landsat image) is not always consistent with the downslope direction derived from the DEM. In these cases, manual editing of the boundaries was necessary to prevent drainage basin boundaries from cross-cutting ice flow lines. This was done through visual interpretation of the Landsat ortho-mosaic. Drainage basin boundaries were then clipped by both the 1960 and 1999 ice margin polygons.

2.3.5 Area Calculation

Calculation of area change in each drainage basin was performed using raster overlay techniques in ArcView GIS. The drainage basin boundary layer was clipped by the 1960 and 1999 ice margin polygons to produce the same internal drainage divide structure for both years. The polygon coverages and interior bedrock regions were then converted to a 15 m resolution raster grid. Cells were coded with unique arbitrary values assigned to each polygon with the same polygons having the same coded value for both years. For each data set (1959/1960 and 1999/2000) the interior bedrock regions were subtracted from the ice surface polygon coverage, resulting in 'ice surface only' coverages. Areal changes were then calculated by comparing tabulated pixel counts for each gridded ice surface coverage on a per polygon basis.

2.3.6 Error Analysis

Errors associated with the ice cap area measured from the air photos were a function of both the accuracy of the co-registration between the air photos and the Landsat 7 ETM+ ortho-mosaic and the accuracy with which the ice cap margin was identified and digitized. Errors of the Landsat 7 ETM+ derived areas were only a

17

function of the accuracy with which the ice cap margin was identified and digitized. Ice cap margins were digitized using on-screen digitizing in ArcView GIS that allowed the operator to zoom in to the pixel level for point data collection. Digitizing inaccuracies over unobscured sections of the ice cap margin were therefore based on (a) image resolution and (b) contrast between the ice cap surface and the adjacent terrain.

Co-registration errors between the air photo ortho-mosaics and the Landsat 7 ETM+ ortho-mosaic were estimated to be +/- 22 m based on residual values between 40 (10 points from each air photo mosaic) independent check points identified in each data set. However, for the area measurement to be affected by the maximum amount, the co-registration error would have to displace each mosaic in equal and opposite directions from each other. Since it is more likely that these errors are random, a value of +/- 11 m (50% of the co-registration error) was chosen as a more realistic estimate of the error attributed to co-registration (see Table 2.1).

Measurement uncertainty of the unobscured sections of the ice margin was judged to be no greater than the pixel size of the image being digitized (+/- 15 meters for the satellite mosaic and +/- 5 meters for the aerial photography mosaic). This error was calculated as the product of the total ice cap boundary length minus the length obscured, and the pixel width. For obscured sections of the ice cap perimeter, error was estimated as the product of the obscured segment length and a maximum estimated line offset value applied to each type of obscurity (Table 2.1). Because all missing or obscured sections of the aerial photography ortho-mosaic were digitized from the 1:250,000 NTS map sheets, estimated offset distances were based on the co-

18

registration accuracy between the aerial photography ortho-mosaic and the 1:250,000 NTS map sheets (+/- 75 meters).

Offset distances were estimated for the satellite ortho-image based on the confidence with which the ice margin could be identified within each type of obscurity. Because the margin was generally not completely obscured by cloud and shadow, error along these sections was estimated at +/- 90 meters. Sections of the ice margin under cloud were faintly (intermittently) identified through semi-transparent (broken) cloud cover. Similarly, sections of the ice cap margin obscured by shadow were enhanced by applying a contrast stretching function to the imagery that allowed the margin to be identified with some degree of confidence in these areas. Ice margins obscured by late lying snow pack, however, were less distinct and identification accuracy was estimated at +/- 120 meters. Along these sections, the margin was digitized at the angle of inflection between the ice cap boundary and the snow-covered ground that was highlighted by differential illumination as a result of the local incidence angle of the sun. In total, the ice cap margin was obscured (either partially or fully) by 3% and 0.8% in the satellite imagery and the aerial photography respectively.

Additional error could potentially have been generated in the orthorectification process due to registration errors between the imagery and the DEM. The DEM used in this study is essentially a digital version of the NTS topographic map sheets to which the Landsat 7 imagery was georeferenced with an RMS error of +/- 75 meters. The aerial photography was subsequently georeferenced to the Landsat 7 imagery (RMS error of +/- 15 meters) increasing the registration error between the aerial

19

photography and the DEM to +/- 90 meters. Therefore, the uncorrected aerial photography and Landsat 7 imagery may have been orthorectified based on topographic information offset by up to 90 meters from the associated features on the imagery. Orthorectification errors resulting from inaccurate co-registration between the DEM and imagery however were not considered in this study because both data sets would be affected equally by this problem therefore the relative difference in area measurements would be minimal.

2.3.7 Area Estimates and Total Error

The total error (TE) of the area measured from each data source was computed from the formula;

$$TE = \sqrt{g1^2 + g2^2 + ...gn^2} \tag{1}$$

where g1 ... gn represent the individual sources of error as specified in Table 2.1. The total area (TA) and the associated error as measured from the 1999 Landsat imagery therefore is;

$$TA_{Landsat} = 14,004 +/- 40 \text{ km}^2$$

and for the 1960 Aerial photography is;

$$TA_{aerial\ photography} = 14,342 +/- 31 \text{ km}^2$$

20

The error associated with the change of areal extent (difference between the 1999 area and the 1960 area measurement) was taken as the greater of the 2 error estimates.

Therefore,

Total area change $= 338 +/- 40 \text{ km}^2$

Area change measurements derived for individual drainage basins were estimated to be accuate to +/- 11% for basins with unobscured margins. For all other drainage basins, error was estimated as a function of the length (and type) of the obscured margin within the basin.

The error analysis presented in this study likely overestimates the actual error because it assumes a maximum digitizing offset along the entire perimeter of the ice cap boundary. Previous work based on repeat digitizing experiments has demonstrated that errors associated with digitizing points along the perimeter of a polygon are limited to a statistically derived epsilon band which is significantly smaller than the maximum offset width (Dunn, and others,1990). It is beyond the scope of this study however, to minimize the stated error by deriving a statistical distribution of digitized points about the ice cap margin.

21

2.4 RESULTS

The Devon ice cap has experienced a net decrease in area of 338 +/- 40 km^2 over the past 40 years. Surface area changes were most significant in 4 distinct regions of the ice cap.

(1)   Retreat of the 4 major tidewater glaciers on the east coast (Figure 2.3) accounted for 38 +/- 4 km^2 of the decrease in area of the ice cap. The most northerly glaciers (i) and (ii) experienced retreat of up to 1300 m from the 1960 terminus location and the central glacier (iii) retreated approximately 750 m. The most southerly glacier (iv) experienced maximum retreat of up to 3000 m.

(2)   Increase in the area of exposed bedrock in the interior regions of the ice cap accounted for 28 +/- 5 km^2 of the decrease in ice surface area (Figure 2.3). The basins most affected are located in the mountainous north-east and south-east regions of the ice cap. The increase in exposed bedrock area in these regions indicates a lowering of the ice cap surface.

(3)   Marginal retreat of the south-west arm (Figure 2.4) accounted for a 200 +/- 17 km^2 decrease in surface area of the ice cap.

(4)   Ice margin advance by an average of 130 meters along a 80 km section of the northwest margin (Figure 2.5) accounted for a 10.5 +/- 2 km^2 increase in surface area of the ice cap.

22

The changes described above account for approximately 76% of the total change experienced by the Devon ice cap. The remaining changes in terms of area decrease have occurred primarily as a result of glacier retreat within small basins located throughout the south and north-east sectors of the ice cap. The remaining increases in area have resulted from advance of the Sverdrup glacier (basin 12) by up to 250 meters and the 2 major outlet glaciers that drain south into Croker Bay (basins 42 and 40) which have experienced advance of between 100 – 400 meters along their termini.

2.5   ANALYSIS

Variability in the areal changes observed could be due to regional differences in climate forcing, to variations in the sensitivity of glacier mass balance to given changes in climate, or to differences in the response time of different sectors of the ice cap to mass balance changes. It is also probable, however, that the variations in ice margin fluctuations have resulted from a complex interaction of these factors combined with the fact that tidewater terminating glaciers are likely to respond different from land-terminating glaciers given similar climatic conditions.

2.5.1   Prevailing Climate Pattern

Differential changes at the ice margin may reflect growth related to the influence of a prevailing climate pattern on the ice cap geometry. The predominant moisture supply for the ice cap is derived from the cyclonic weather systems that move across the ice cap from Baffin Bay. These systems deposit over two times as

23

much precipitation over the east sector of the ice cap than the west (Koerner, 1966). Ice cap growth in the extreme southeast is also encouraged by the maritime effect associated with the North Open Water polynya, which suppresses summer melt in this region (Koerner, personal communication, 2002). Koerner (1977a) has suggested that this pattern has likely persisted since at least 6000 - 5000 years B.P. to produce the asymmetric geometry of the ice cap that exists today. The eastern basins are typically larger and descend to lower elevations than basins in the west. This results in the east side of the ice cap being subjected to greater amounts of surface ablation and mass loss due to ice berg calving than basins on the west side. The significant mass losses that have occurred along the east side of the ice cap may therefore suggest that those regions of the ice cap that experienced preferential growth in the past as a result of this prevailing climate pattern are most susceptible to recent increases in average air temperature.

2.5.2   Basin Hypsometry

Analysis of the hypsometry of the major basins was performed to investigate the influence of basin topography on ice cap response to recent climate changes. Two parameters were used to characterize the basin topography: a Balance Ratio (BR; Furbish and Andrews, 1984) and a sensitivity index derived in this study which provides a measure of the relative change in glacier mass balance resulting from a prescribed change in ELA.

The balance ratio (BR) was calculated from the equation:

$$BR = (Zm - ELA) / (ELA - Zt) \qquad\qquad (2)$$

where Zm = maximum elevation of the glacier, Zt = terminus elevation of the glacier, and ELA = equilibrium line altitude. For a rectangular glacier, the change in the altitude of the glacier terminus that results from a prescribed change in the ELA is an inverse linear function of the Balance Ratio. For glaciers with other shapes, the relationship is still inverse, but non-linear (Furbish and Andrews, 1984, p202-203). Thus if the ice cap as a whole were subjected to a spatially uniform change in ELA, the change in terminus position resulting from that ELA change would primarily be a function of the BR and planimetric shape of the basin.

BR's were calculated for the major drainage basins of the Devon Island ice cap using ELA estimates derived from the 1960-1966 mass balance observations by Koerner (1970). The ice cap was divided into quadrants, with boundaries following the watershed divides and appropriate ELA values were applied to each region. ELAs for the northwest and southeast zones were identified directly from Koerner's measurements (950 meters a.s.l. and 800 meters a.s.l. respectively) and ELA's within the northeast and southwest zones were taken as the average of the 2 adjacent zones (875 meters a.s.l.). Basin hypsometry was derived from the CDED data and analysis was limited to basins larger than 170 km^2, which comprise more than 85% of the total ice cap area.

Although the ELA used to calculate the balance ratio index should be that for an ice cap in steady state, the mass balance associated with the ELAs chosen above is slightly negative. Based on analysis of the mass balance / ELA relationship, Koerner

25

however, suggests that a steady state ELA for the northwest sector of the ice cap is 920 +/- 80 meters. As the ELA assumed for the north-west region of 950 meters falls in this range, we are therefore confident that our method of estimating the ELA for the rest of the ice cap is adequate for proper balance ratio calculations.

The calculated BRs display a strong logarithmic relationship (r^2 = 0.78) with percent area change of the major drainage basins (Figure 2.6). Most basins with BR values below 1.0 have experienced a significant reduction in surface area. Maximum elevations of these basins are collectively among the lowest on the ice cap (Table 2.2) resulting in a relatively small altitudinal range above the ELA. In particular, Basins 39 and 48 reach maximum elevations of only 998 and 1169 meters a.s.l. respectively, resulting in extremely low BR values for these basins. Basins with BR's greater than 1.0 have experienced much less of an area decrease, and in some cases, these basins have increased in size. Those that have experienced growth (42, 40, 25, and 17) are concentrated mainly along the western margin. Although these basins only reach 1500 – 1600 meters a.s.l., their average terminus elevation is 400 meters a.s.l., which results in a small elevational range below the ELA. Also, because the termini of these basins are relatively high, they experience cooler temperatures that inhibit glacier retreat. Basins that have experienced limited shrinkage (< -1 %) and have BR's greater than 1.0 (2, 44, 41, 43 and 45) extend up to elevations equal to or close to those of the ice cap summit. These basins generally have larger accumulation area ratios (AARs) than glaciers that have shrunk significantly, and their mass balance was presumably less strongly affected by the post LIA rise in ELA.

26

Excluding the southwest arm, basin shape appears to have had some influence on the amount of area loss at the ice cap margin. Basin shapes were grouped into 3 main categories according to the Furbish and Andrews (1984) classification scheme: Type "A" – rectangular shaped basins, type "C" – basins that taper up-glacier, and type "D" – basins with wide mid sections that narrow in both up and down glacier directions. For glaciers with BR's less than 1.0, type "D" shaped basins have decreased in size by an average of 3.4% whereas those in type "A" basins have only shrunk by an average of 1.7%. Areal change of glaciers in basins with balance ratios greater than 1.0, show no correlation with shape, however.

Basin hypsometry was analyzed further to determine the sensitivity of major drainage basins to climate warming. Basin sensitivity (BS) values were estimated as the fractional change in AAR resulting from a 100 meter rise in the ELA:

$$BS = \Delta AAR_{+100m} / AAR \tag{3}$$

where,

$$AAR = Accumulation\ area\ /\ Total\ Basin\ Area \tag{4}$$

AAR (accumulation area ratio) represents the proportion of the basin area within the accumulation zone and ΔAAR_{+100m} is the change in accumulation area ratio resulting from a 100 meter rise in ELA as documented in the CDED DEM for 1959/1960 (year of the aerial photography used to derive the CDED DEM).

27

Overall, the calculated BS values display a strong linear relationship ($r^2 = 0.79$) with percent area change of the major drainage basins (Figure 2.7). This relationship is controlled mainly by BS values of the basins situated at lower elevations (ie. basins 38,52,48, and 39). These basins have relatively high BS values (> 0.2) and have experienced significant areal change over the past 40 years. A trend is less obvious for basins with BS values < 0.2.

The spatial distribution of BS values highlights the relative susceptibility of various regions of the ice cap to climate warming (Figure 2.8; Table 2.2). Basins with BS values greater than 0.23 ('VH'; basins 38, 39, 48, 52) have small AARs and have experienced the greatest average retreat of all major basins since 1960. These basins are restricted to lower elevations (ie. have low maximum and terminus elevations; see Table 2.2) where shrinkage appears to be a direct function of the relative loss of accumulation area due to raising the ELA. Drainage basins classified as 'highly sensitive' ('H'; 31,29, 43, 45, 17, and 25) include those that occupy the western margin and have experienced recent advance. These basins are predominantly type 'C' in shape implying that the accumulation area ratio increases rapidly as the ELA is lowered. Recent advance throughout this region indicates that these basins may not yet have reacted fully to recent climate warming. Medium sensitivity basins ('M'; 46,15, 44, and 41) are concentrated on the eastern side of the ice cap. They are predominantly type 'A' in planimetric shape (accumulation area ratio decrease is directly proportional to a rise in ELA) and reach near-summit elevations with AAR's averaging 0.71. Finally, low sensitivity drainage basins ('L'; 12, 42, 2, and 40) have properties very

28

similar to the 'M' basins except that they drain towards the north and south coasts and have an average AAR of 0.81.

The hypsometric curves plotted in Figure 2.9 indicate the distribution of surface area within a basin in relation to elevation above or below the ELA. Basins in which the ELA intersects the steepest section of the curve (basins 38 and 52) are most sensitive to climate change because moving the ELA from the current location results in changes in accumulation area that are large relative to the total basin area. In some cases however, the ELA intersects the hypsometric curve close to the upper limit of the cumulative basin area (basins 39 and 48). The accumulation areas within these basins have almost entirely disappeared resulting in consistently high ELAs regardless of fluctuations of the ELA. The ELAs of highly sensitive basins ('H') intersect steep sections of the hypsometric curves. The sensitivity of these basins is reduced however by the fact that the areal fraction of these basins below the ELA is generally less than 0.4. Medium sensitivity basins ('M') have between 0.2 and 0.3 of their cumulative area below the ELA whereas low sensitivity basins consistently have less than 0.2 of their area below the ELA. Both of these basin types intersect relatively low sloping sections near the inflection point along the hypsometric curves, indicating that the accumulation area of these basins will decrease at a much faster rate as the ELA is raised than it will increase as the ELA is lowered.

29

2.5.3 Response Time

Approximate response times (RT) were calculated for each of the major drainage basins using the volume time scale following Johannessen, and others, (1989);

$$RT = H / b_t \qquad\qquad (5)$$

where H is the maximum thickness of ice within the basin and b_t is the mass balance at the glacier terminus. Ice thickness data were obtained from Dowdeswell's 2000 RES data set (Dowdeswell, and others, 2004) and terminus ablation rates were interpolated from Koerner's, 1961 – 1998 mass balance observations as compiled by Dyurgerov (2002).

A moderate inverse relationship ($r^2 = 0.65$) exists between RT and percent area change of the major basins across the ice cap (Figure 2.10). The maximum areal changes have occurred in those basins with the shortest calculated response times, and the magnitude of change decreases logarithmically (and in some cases the basins grow rather than shrink) as the calculated response times increase.

Three distinct groupings emerged from these RT calculations (Table 2.3). RTs in the first group of basins range from ca. 125 years to ca. 380 years. This group includes ~70% of all major basins. Although all basins in this group terminate at or near sea level where ablation rates are highest, basins with the shortest RTs in this group (29, 38, 39, 46, 48, and 52) are restricted to the peripheral regions (ie. their source regions do not extend to the ice cap summit region) where the ice is thinnest.

30

Except for basin 39 (southwest arm), all basins in this category are located along the east or south margins of the ice cap. Other basins within this group (2, 40, 42, 12, 41, 15, and 44) extend further inland towards the ice cap summit, lengthening the RT due to increased ice thickness. Basins exhibiting intermediate (ca. 700 years) and long (ca. 950 years) RTs terminate at higher elevations (500 – 600 meters a.s.l.) where terminus ablation rates are relatively small. These basins are concentrated along the western margin and they also extend inland towards the interior summit region where ice thickness is greatest.

The RTs calculated here are consistent with characteristic RTs suggested by Bahr, and others (1998). Glaciers in larger basins with steeper mass balance gradients (east side) have significantly shorter RTs than glaciers in smaller basins with shallower mass balance gradients (west margin). This difference suggests that the east and west sectors of the ice cap may be responding to distinctly separate periods of climate forcing.

2.5.4 Multiple Regression Analysis of Areal Change

To determine the influence of BS, BR, and RT on the areal changes (AC) measured, multiple regression analysis was performed, resulting in the equation:

$$AC = (-9.87 (+/- 0.86) * BS) + (0.002 (+/- 0.0005) * RT) \qquad (6)$$

31

($r^2 = 0.854$). BR was highly correlated with RT ($r^2 = 0.86$) and was therefore excluded from this analysis. *P*-values of 0.00001, and 0.002, were obtained for the coefficients of BS and RT respectively.

2.5.5 Volume Change Estimates

Ice cap volume change was calculated using 2 independent methods. The first method was based on calculating the difference between the 1960 ice cap volume, derived from the volume-area scaling (VA) technique (Bahr and others, 1997), and the 2000 ice cap volume derived from Dowdeswell's RES data. Using this method, the 1960 volume was calculated for the southwest arm and the main ice cap separately, and summed for a total ice cap volume estimate. The second method calculates the change in volume of a glacier as the product of the maximum thickness and the length change at the terminus (MT) (Hooke, 1998, p219). In order to account for the influence of glacier width, the total area change measured in each basin was multiplied by the maximum thickness to estimate the resulting change in volume. Using this method, volume change was calculated for each major drainage basin separately and summed to estimate the total ice cap volume change.

The 1960 ice cap volume (VOL_{1960}) was calculated from the VA method using the formula:

$$VOL_{1960} = SC * A_{1960}{}^{1.25} \tag{7}$$

32

where, A_{1960} is the area of the ice cap in 1960 and 1.25 is the appropriate exponent for small ice caps (Bahr and others, 1997). The scaling constant (SC) is derived from the formula:

$$SC = VOL_{2000} / (A_{1999}^{1.25})$$ (8)

where A_{1999} is the area in 1999 and VOL_{2000} is the volume in 2000 taken from Dowdeswell's RES data. VOL_{2000} measurements of 3854 km^3 and 107 km^3 produced scaling constants of 0.0299 and 0.0095 for the main ice cap and the southwest arm respectively. Applying the scaling constants to the 1960 measurements resulted in a total volume estimate of 4030 km^3 (124 and 3906 km^3 for the southwest arm and main ice cap respectively). Differences between the 1960 and 2000 volume estimates derived from the VA method and from Dowdeswell's RES measurements respectively indicate a loss of 68 km^3 for the entire ice cap and 16 km^3 for the southwest arm over the past 40 years. Volume changes estimated using the MT method were a loss of 62 km^3 for the whole ice cap and 18 km^3 for the southwest arm. These estimates imply a thinning of ~3 meters averaged over the main part of the ice cap and ~8 meters over the southwest arm.

The error for the VA method was estimated at +/- 12 km^3, based on the 1960's area measurement error of +/- 30 km^2. For the MT method the error of +/- 9 km^3 was estimated as the product of the average area measurement error between 1960 and 1999 (+/- 35 km^2) and the average ice cap thickness (284 meters). The total volume

33

loss of the Devon ice cap between 1960 and 1999 was therefore estimated as 65 +/- 12 km^3.

Our computed volume loss of 65 km^3 equates to a 0.15 mm contribution to global sea level between 1960 and 1999. When extrapolated to all ice cover in the Canadian arctic, this would represent a total contribution of ~1.5 mm. This is approximately one-sixth the current estimated contribution from all Alaskan glaciers (Arendt, and others, 2002) which cover ~40% less surface area than ice in the Canadian Arctic.

2.6   CONCLUSIONS

Remotely sensed imagery acquired in 1959/1960 and 1999/2000 reveals a net decrease in surface area of the Devon Island ice cap of 338 +/- 40 km^2 with an associated volume loss of 65 +/- 12 km^3. The dominant trends in geometric change are retreat (thinning) of the eastern margin, growth of the western basins, and rapid shrinkage of the southwest arm. Major tidewater glaciers along the east coast have retreated up to 3 km over the past 40 years. These glaciers drain from basins that have experienced increased bedrock exposure indicating that the ice surface within these basins has lowered. Advance of the north-west margin suggests either that conditions favourable to ice sheet growth are prevalent in this region, or that this sector of the ice cap is still responding to the cooler conditions of the Little Ice Age. The southwest arm of the Devon Island ice cap lies almost entirely below the regional ELA (Koerner, 1970). Thus, rapid retreat of the ice margin in this region reflects the loss of the accumulation area for this sector as a result of ELA rise driven by post LIA warming.

34

Statistical analysis has shown that 85.4% of the variance in basin area change is explained by variations in the basin sensitivity and response times of different drainage basins. The logarithmic relationship between BR and AC suggests that the ice cap will shrink at a much faster rate in response to a given rise in the ELA than it will grow in response to an equivalent lowering of the ELA. Similarly, cumulative area curves for most basins indicate that the rate of accumulation area loss as the ELA is raised is greater than the rate of accumulation area gain when the ELA is lowered. Finally, response times of 700 to 1000 years throughout the western region indicate that the advance of these basins is likely a delayed response to cooler LIA climatic conditions. In contrast, shorter response times (100 – 400 years) for the remaining basins suggest that the observed retreat over these regions is likely a response to post LIA warming.

2.7 REFERENCES

Arendt, A., Eckelmeyer, K., Harrison, W.D., Lingle, C.S., and Valentine, V.B., 2002: Rapid wastage of Alaska glaciers and their contribution to rising sea level. *Science,* 297(5580): 382-386.

Bahr, D.B., Pfeffer, W. Tad, Sassolas, C., Meir., M.F., 1998: Response time of glaciers as a function of size and mass balance: 1. Theory. *J. Geoph. Res.,* 103(B5): 9777-9782.

Bahr, D.B., Meier, M.F., and Peckham, S.D., 1997: The physical basis of glacier volume-area scaling. *J. Geoph. Res.,* 102(20): 355-362.

35

Braun, C., Hardy, D., and Bradley, R., 2001: Recent recession of a small plateau ice cap, Ellesmere Island, Canada. *J. Glac.*, 47(156): 154.

Dowdeswell, J. A., T. J. Benham, M.R. Gorman, D. Burgess, and M. Sharp. 2004. Form and flow of the Devon Island ice cap, Canadian Arctic. *J. Geophys. Res.* **109**, F02002, doi:10.1029/2003JF000095.

Dunn, R., Harrison, A.R., and White, J.C., 1990: Positional accuracy and measurement error in digital databases of land use: an empirical study. *Int. J. Geogr. Inf. Syst.*, 4(4): 385-398.

Dyurgerov M. 2002. Glacier mass balance and regime: Data of measurements and analysis. [M. Dyurgerov and R. Armstrong (eds.)]. CD ROM.

Furbish, D.J. and Andrews, J.T., 1984: The use of hypsometry to indicate long-term stability and response of valley glaciers to changes in mass transfer. *J. Glac.*, 30: 199-210.

Gagne, A. Personal communication. Geomatics Canada, 615 Booth St., Ottawa, Canada.

Hooke, LeB. R., 1998: *Principles of glacier mechanics*. Upper Saddle River, JJ, Prentice Hall. 248.

IPCC, 2001: Climate change 2001: impacts, adaptation, and vulnerability. [J.J. McCarthy, O.F. Canziani, N.A. Leary, D.J.Dokken, K.S.White (eds.)].

Jacobs, J.D., Simms, E.L., Simms, A., 1996: Recession of the southern part of Barnes Ice Cap, Baffin Island, Canada, between 1961 and 1993, determined from digital mapping of Landsat TM. *J. Glaciol.*, 3(143): 98-102.

36

Johannessen, T., Raymond, C.F., and Waddington, E.D., 1989: A simple method for determining the response time of glaciers. *Glacier fluctuations and climate change,* J.Oerlemans (ed.). 343-352.

Johns, T. C., Carnell, R.E., Crossley, J.F., Gregory, J.M., Mitchell, J.F.B., Senior, C.A., Tett, S.F.B., and Wood, R.A., 1977. The second Hadley Centre coupled ocean–atmosphere GCM: Model description, spinup and validation. *Clim. Dynam.,* 13. 103–134.

Koerner, R.M., and Lundgaard, L., 1995: Glaciers and global warming. *Geogr. Phys. Quatern.,* 49(3): 429-434.

Koerner, R.M., 1977a: Ice thickness measurements and their imlications with respect to past and present ice volumes in the Canadian High Arctic ice caps. *Can. J. Earth Sci.,* 14: 2697-2705.

Koerner, R.M., 1977b: Devon Island ice cap: core stratigraphy and paleoclimate. *Science,* 196: 15-18.

Koerner, R.M., 1970: The mass balance of Devon Island ice cap Northwest Territories, Canada, 1961-1966. *J. Glaciol.,* 9(57): 325-336.

Koerner, R.M., 1966: Accumulation on the Devon Island ice cap, Northwest Territories, Canada. *J. Glac.,* 6(45): 383-392.

Meier, M.F. and Dyurgerov, M.B., 2002: How Alaska affects the world. *Science,* 297 (5580): 350-351.

Meier, M.F., 1984: Contribution of small glaciers to global sea level. *Science,* 226 (4681): 1418-1420.

Mitchell, J. F. B., Johns, T. C., Gregory, J. M., and Tett, S. F. B., 1995: Climate response to increasing levels of greenhouse gases and sulphate aerosols. *Nature*, 376: 501–504.

Overpeck, J., Hughen, K., Hardy, D., Bradley, R., Case, R., Douglas, M., Finney, B., Gajewski, K., Jacoby, G., Jennings, A., Lamoureux, S., Lasca, A., MacDonald, G., Moore, J., Retelle, M., Smith, S., Wolfe, A., and Zielinski, G., 1997: Arctic environmental change of the last four centuries. *Science,* 278: 1251-1256.

Serreze, M.C., Walsh, J.E., Chapin III, F.E., Osterkamp, T., Dyurgerov, M., Romanovsky, V., Oechel, Morison, J., Zhang, T., and Barry, R.G., 2000: Observational evidence of recent change in the northern high latitude environment. *Climatic Change,* 46: 159-207.

Van de Wal, R.S.W., and Wild, M., 2001: Modelling the response of glaciers to climate change by applying volume-area scaling in combination with a high resolution GCM. *Clim. Dynam.,* 18: 359-366.

Image Type	Error Source	Line Segment Length (km)	Line Placement Error (m)	Area Estimate Error (+/-km^{-2})
Landsat 7	Digitizing	2678	15	40
Landsat 7	Cloud	19	90	2
Landsat 7	Shadow	14	90	1
Landsat 7	Snow	50	120	6
Landsat 7 Total				**40**
Aerial Photography	Digitizing	2546	5	13
Aerial Photography	Co-registration	2567	11	28
Aerial Photography	Obscured and missing imagery	21	75	2
Aerial Photography Total				**31**

Table 2.1 Summary of error associated with extracting linework from the satellite and aerial photography image data.

39

Basin ID	ELA Zone	Balance Ratio	Basin Sensitivity	% Area Change	Basin Shape	Accumulation Area Ratio	Minimum Elevation (m)	Max. Elevation (meters above sea level)
12	NW	0.91	L(0.09)	-0.4	A	0.83	0	1854
42	SW	1.2	L(0.09)	0.3	D	0.77	0	1835
2	NE	1.37	L(0.07)	-0.2	A	0.82	0	1901
40	SW	1.38	L(0.09)	0.3	A	0.81	5	1897
46	SE	1.2	M(0.14)	-1.9	C	0.65	0	1674
15	NE	1.37	M(0.13)	-1.4	A	0.69	0	1901
44	SE	1.74	M(0.10)	-0.4	A	0.77	0	1853
41	SE	1.89	M(0.14)	-0.3	D	0.57	0	1901
25	NW	3.06	M(0.14)	0.3	A	0.87	540	1667
31	NW	0.8	H(0.23)	1.1	C	0.59	312	1521
29	NE	0.91	H(0.18)	-2.4	D	0.61	0	1708
43	SW	2.53	H(0.16)	0	C	0.73	398	1633
45	SW	2.84	H(0.20)	-1.2	C	0.77	538	1443
17	NW	3.38	H(0.22)	0.8	C	0.73	561	1666
39	SW	0.03	VH(0.90)	-10.3	N/A	0	119	998
52	SE	0.2	VH(0.46)	-2.5	A	0.45	34	1141
48	SE	0.21	VH(0.59)	-4.3	D	0.01	0	1169
38	SE	0.73	VH(0.31)	-2.2	A	0.43	0	1484

Table 2.2 Hypsometrically derived index values and associated glacier attributes for all major drainage basins. Shaded rows indicate basins with balance ratios below 1.0.

40

Basin ID	Quadrant	% Area Change	Terminus Mass Balance $(Kg\ m^{-2}\ a^{-1})$	Maximum Thickness (m)	Response Time (yrs)
25	Nw	0.3	-680	666	979
45	Sw	-1.2	-595	571	959
17	Nw	0.8	-620	589	950
31	Nw	1.1	-850	576	677
43	Sw	0	-940	621	660
2	Ne	-0.2	-1875	712	379
40	Sw	0.3	-1875	705	376
42	Sw	0.3	-1875	695	370
12	Nw	-0.4	-1500	555	370
41	Se	-0.3	-2250	775	344
15	Ne	-1.4	-1875	597	318
44	Se	-0.4	-2250	706	313
48	Se	-4.3	-2250	539	239
46	Se	-1.9	-2250	463	205
52	Se	-2.5	-2200	403	183
29	Ne	-2.4	-1875	318	169
38	Se	-2.2	-2250	330	146
39	Sw	-10.3	-1600	200	125

Table 2.3 Response time estimates and associated glacier attributes for each major drainage basin across the ice cap. Shaded rows highlight the intermediate class of response time estimates.

41
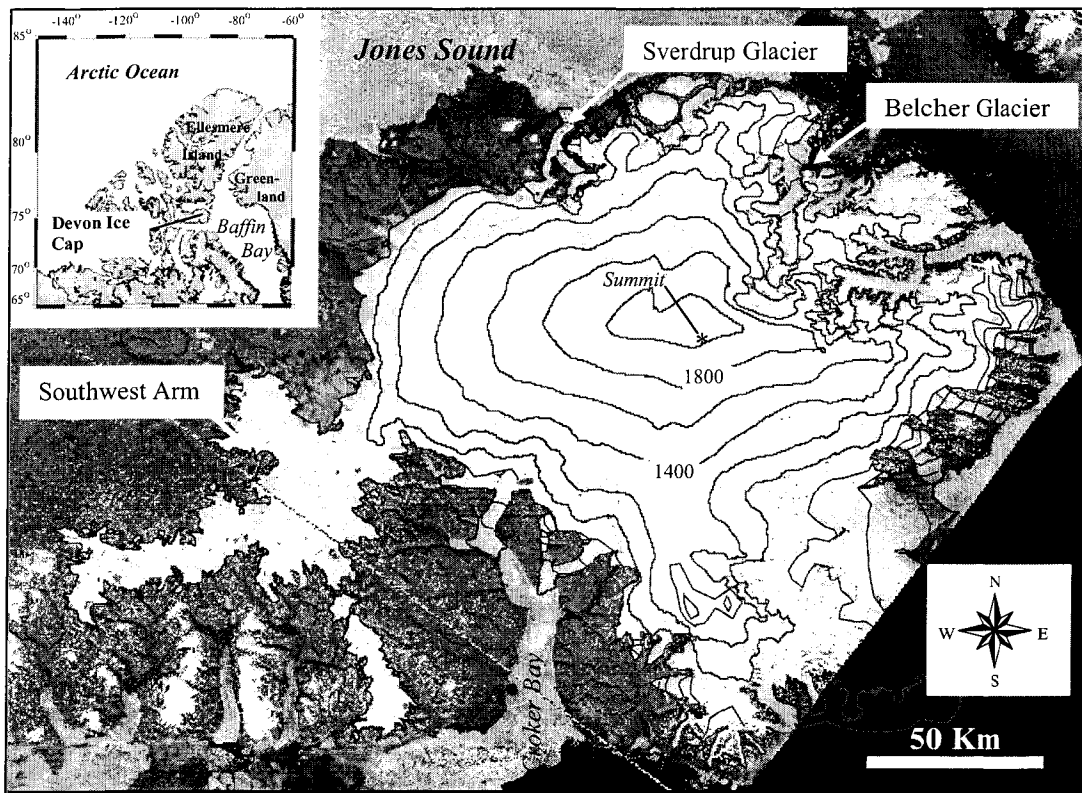
Figure 2.1 Location of the Devon Island ice cap in the Canadian Arctic Archipelago. Image of the ice cap is an orthorectified mosaic of Landsat 7 satellite panchromatic data acquired on July 13, 1999 and August 2, 2000. Contour interval is 200 meters.

42
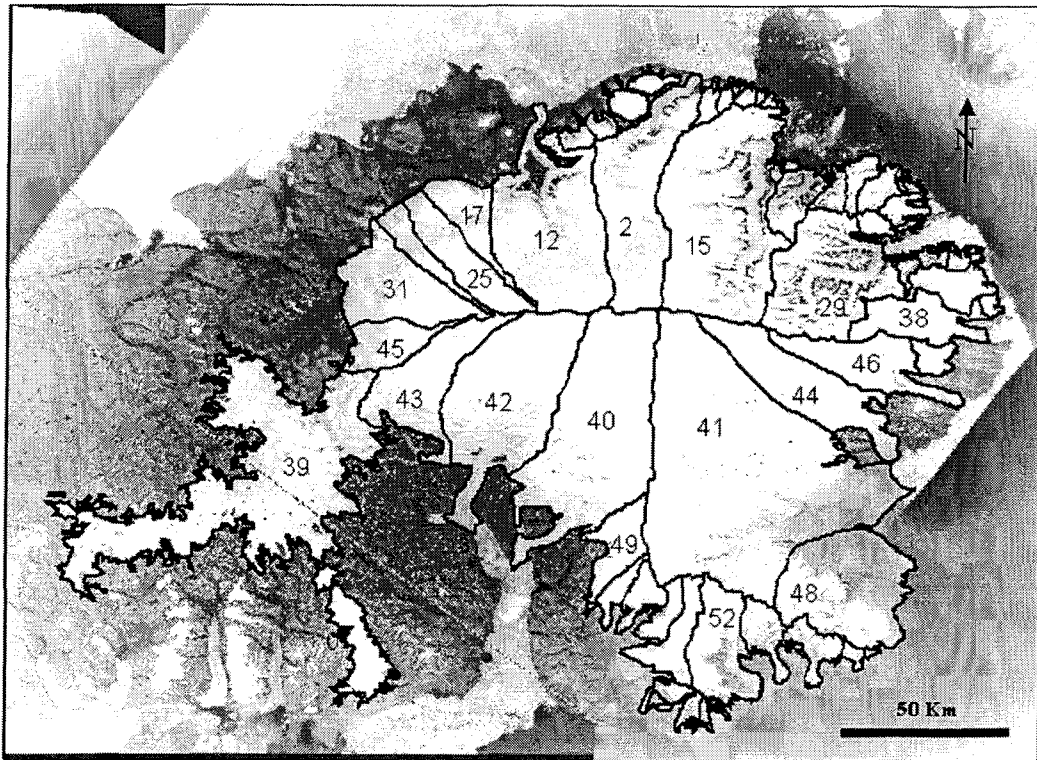
Drainage Basin Divide   *52*   Basin ID

Figure 2.2 Drainage basins of the Devon Island ice cap. Only the basins labelled with unique identification numbers were used for analysis in this study.

43
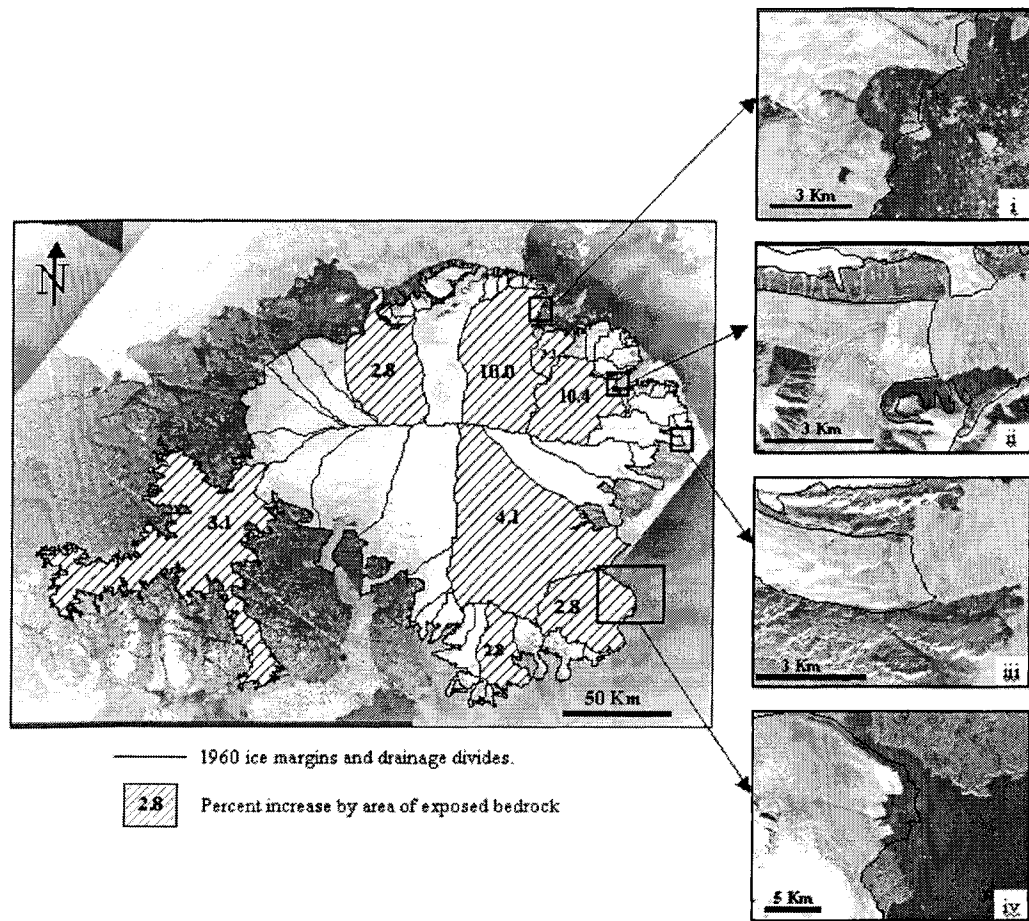
Figure 2.3. 1960 ice margins superimposed on 1999/2000 Landsat image mosaics highlight retreat of the major tidewater glaciers over the past 40 years. Shaded basins have experienced a minimum increase of 2 km^2 of exposed bedrock area between 1960 and 1999 within the ice cap interior.

44
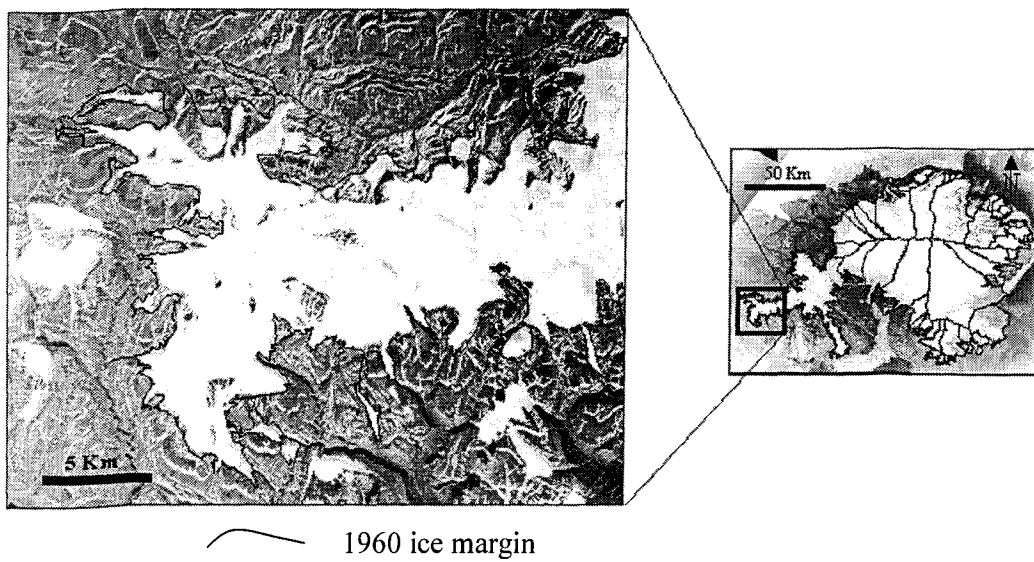
1960 ice margin

Figure 2.4 Ice margin retreat and apparent thinning of the southwest arm.

45

——— 1960 ice margin
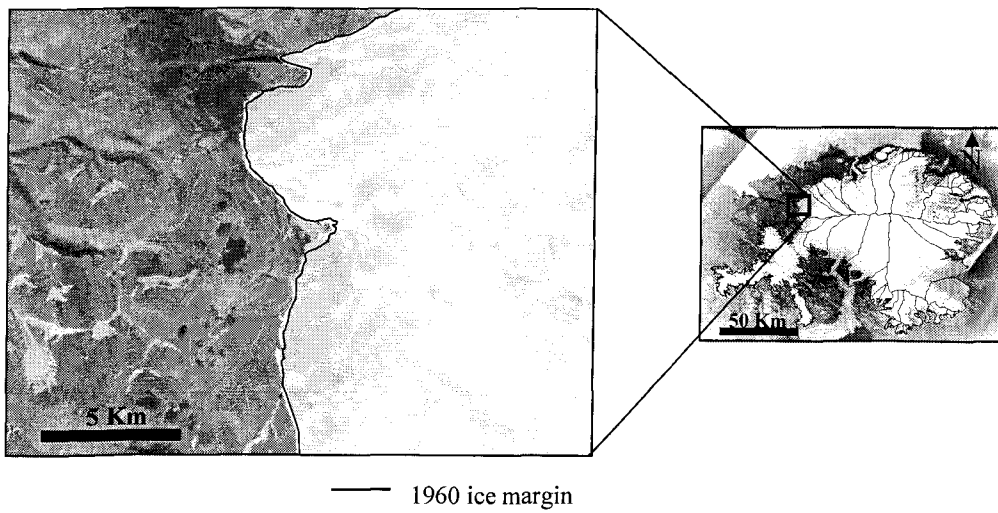
Figure 2.5 Section of the advancing northwest margin.

46
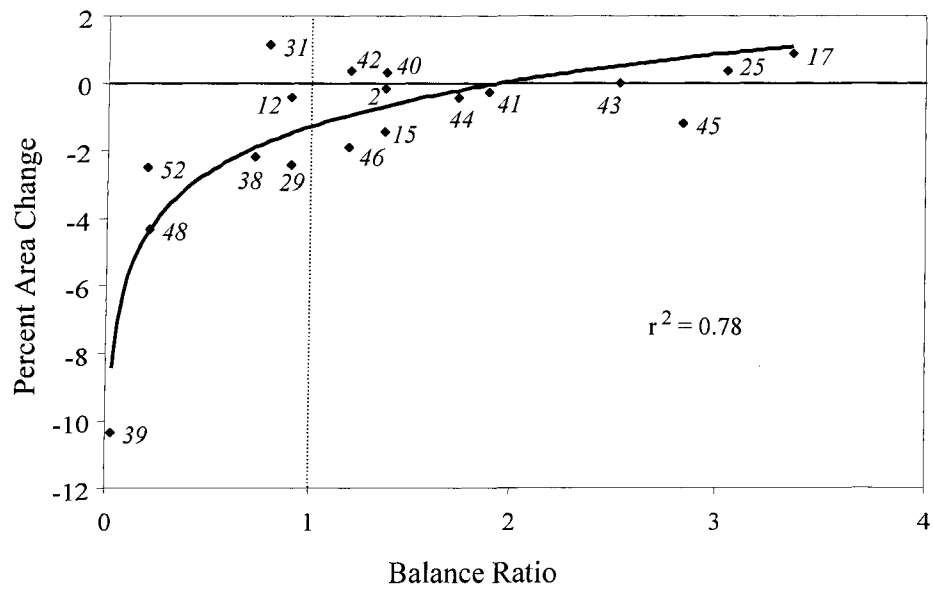
Figure 2.6 Plot of the logarithmic relationship between calculated balance ratios and percent area change of glaciers in the major drainage basins between 1959/1960 and 1999/2000.

47
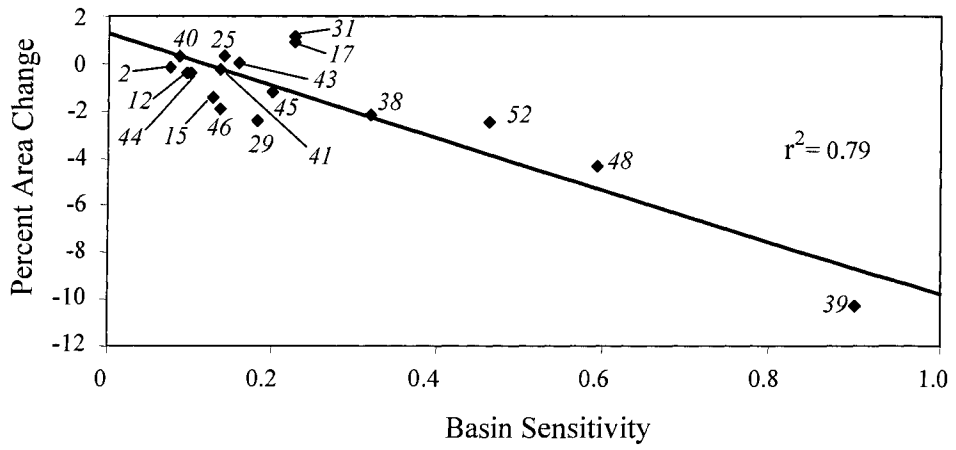
Figure 2.7 Plot of the linear relationship between basin sensitivity and percent area change of glaciers in the major drainage basins measured between 1959/1960 and 1999/2000.

48
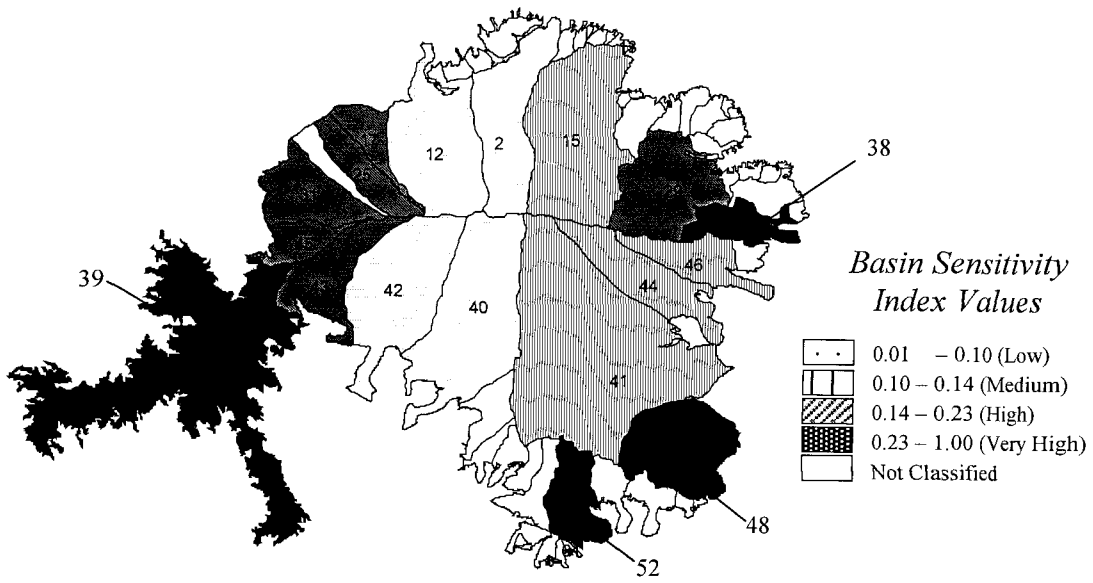
Figure 2.8 Relative sensitivity of glaciers in the major drainage basins to increasing the ELA by 100 meters.

49
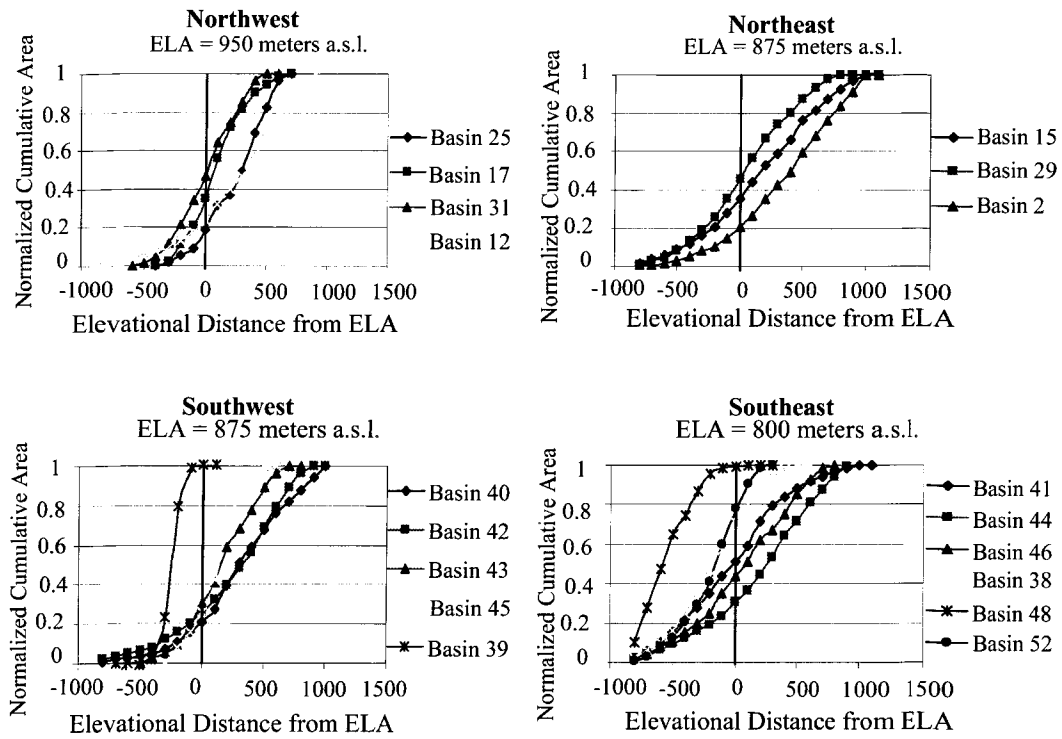
Figure 2.9 Hypsometric curves of the normalized cumulative area for each major drainage basin plotted in relation to the ELA (vertical line at 0) for each quadrant of the ice cap.

50
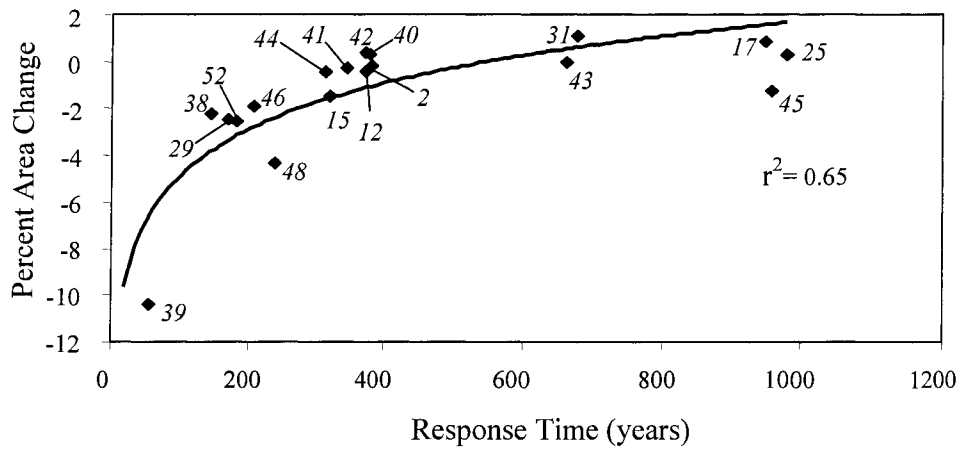
Figure 2.10 Plot of the logarithmic relationship between response time and percent area change of glaciers in the major drainage basins measured between 1959/1960 and 1999/2000.

51

CHAPTER 3

FLOW DYNAMICS AND ICEBERG CALVING RATES OF THE

DEVON ISLAND ICE CAP, NUNAVUT, CANADA

3.1   INTRODUCTION

Most of the outlet glaciers that drain the interior regions of the Devon Island ice cap, Nunavut, Canada, terminate in tidewater, making them potentially sensitive to changes in both climate and sea-level. Iceberg calving from the termini of these glaciers has not previously been quantified, but may constitute a significant mode of mass loss from the ice cap. The rate of calving may be sensitive to changes in the flow dynamics of the glaciers and to changes in terminus position related to instabilities of the grounding line. Knowledge of the velocity structure of the ice cap is essential for identifying the major pathways by which ice is removed from the ice cap, and for estimating the rate of mass loss by iceberg calving and its relative contribution to overall changes in the mass of the ice cap. A recent study by Burgess and Sharp (2004) estimated that the Devon Island ice cap has decreased in volume by ~67 km^3 between 1960 and 1999. Mair and others (in review) suggest that surface melting may account for between 60 – 90% of this loss indicating that iceberg calving may account for up to 40% (27 km^3) of the total mass loss over this time interval.

In this study, surface velocities were derived for almost the entire Devon ice Island cap using satellite radar interferometry (InSAR). The pattern of surface

52

velocities in the look direction of the satellite was analysed to identify the dominant ice flow regimes and the spatial relationships between slow and fast flowing sectors of the ice cap. Downslope surface velocities were projected from look direction velocities in order to quantify the flow rates of all major glaciers on the ice cap. Ice thickness data acquired using airborne radio echo sounding (Dowdeswell and others, 2004) were used in conjunction with surface velocity values to calculate calving fluxes at the terminus of 94% of all tidewater glaciers draining the ice cap. The velocity and ice thickness data were also used to investigate the nature of the transition zones between slow and fast ice flow, and the mechanisms of ice flow along the major glaciers that drain the interior regions of the ice cap.

3.2   STUDY AREA

The Devon Island ice cap occupies approximately 14,000 km^2 of the eastern part of Devon Island, Nunavut, in the Canadian high Arctic (Figure 3.1). Landsat 7 ETM$^+$ imagery acquired in 1999 suggests that ice flow patterns are strongly influenced by the form of the underlying bedrock surface, and that they differ significantly between the east and west sides of the ice cap. West of the central north-south divide, the ice cap rests on a relatively flat plateau and flows westwards as a single broad lobe (~82 km long) that terminates on land between 400 and 600 m a.s.l. This region is also drained by 2 outlet glaciers that flow south into Croker Bay and by the Sverdrup Glacier that flows north into Jones Sound (Figure 3.2). These glaciers all extend more than 14 km beyond the main ice cap margin. East of the central divide, the topography is primarily mountainous. Large outlet glaciers that extend up to 41 km inland from

53

the coast drain the north-east sector. The east-central region is dissected by a series of outlet glaciers that extend up to 60 km inland from the ice cap margin. Most of these outlet glaciers terminate in tidewater, and they comprise 89% of the 73 km of the ice cap margin that reaches the sea (Dowdeswell and others, 2004). Flow stripes (Figure 3.3) are characteristic surface features along these glaciers indicating that ice motion is likely due to sliding at the glacier bed (Gudmundsson and others, 2003; Gudmundsson and others, 1998). Margin - parallel layering and surface parallel melt streams are surface features common to the remaining areas of the ice cap below ~1000 m a.s.l.

3.3 INTERFEROMETRIC MEASUREMENTS

Surface velocity fields across the Devon Island ice cap were derived from InSAR which measures topography and displacement of the Earth's surface as a result of the interference pattern created between a coherent pair of radar images acquired from successive satellite passes along the same orbital path (Massonnet and Feigl, 1998). In order to isolate the component of surface motion in the interferogram, the effects of topography must be removed by either subtracting an independent DEM from the InSAR pair (Joughin, and others, 1996) or through double-differencing with a second coherent InSAR pair (Gabriel and Goldstein, 1989). In this study, double differencing was performed with 2 radar pairs acquired over the south-east region of the ice cap during the ERS1/2 tandem mode mission in 1996 (see Table 3.1 for orbital pairs and Figure 3.2 for the footprint of the radar images). Topography was removed from the interferograms over the western half and the north-east region (where only

54

single radar pairs were available) using the Canadian Digital Elevation Dataset (CDED) as the external DEM. The 'motion only' interferograms were unwrapped and converted to absolute values by referencing bedrock features identifiable in the radar imagery to zero velocity (Zebker and others, 1994). The 3 'motion only' interferograms were then manually mosaicked to produce line of sight velocity fields (V_{LOS}) over 98% of the ice cap surface (Figure 3.2). Line of sight velocities were projected to true downslope velocities (V_{DS}) based on the satellite-ice surface geometry (Cumming and Zhang, 1999; Vachon and others, 1996) according to the formula;

$$V_{DS} = V_{LOS} / ((\cos\alpha \sin\nu \sin\theta) + (\sin\alpha \cos\theta)) \qquad (1)$$

where α = slope of the ice cap surface, ν = angle between the look direction of the satellite and the direction of ice flow, and θ = incidence angle of the radar beam (33 ° for the ERS satellites). Throughout the interior regions of the ice cap, ice was assumed to flow in the direction of maximum slope of ice cap surface. Surface slopes were computed from the Canadian Digital Elevation Dataset (CDED) that was smoothed at a horizontal scale equivalent to ~6 times the local ice thickness. The direction of ice flow over outlet glaciers was mapped from the orientation of flow stripes visible in the Landsat 7 ETM+ imagery. Projecting line of sight velocities to downslope velocities produces unreliable results over regions where ice flow is nearly perpendicular to the look direction of the satellite (Unwin, 1998). Therefore, since InSAR from only a

55

single look direction was available, true surface velocities could be computed for only ~75% of the ice cap surface.

3.3.1 Error estimates for InSAR measurements

The main source of velocity error (V_{error}) associated with the measurements of downslope surface displacement derives from projecting the line of sight velocities from a single look angle. Throughout the interior regions where ice velocity is generally < 20 m a^{-1}, V_{error} was quantified by comparing the projected InSAR data with point velocity values from repeat differential global positioning system (GPS) measured in the field. The positions of thirteen velocity stakes deployed above the equilibrium line altitude (Figure 3.2) were measured during May 2000 using Leica Geosystems Series 500 GPS dual frequency antennae. GPS tracking data was collected for 3-4 hours at each site. The data were post-processed using the GIPSY-OASIS II software package (Webb and Zumberge, 1995), which includes models and estimation algorithms, developed by NASA's Jet Propulsion Laboratory (JPL), that account for orbit, Earth orientation, clock biases and a range of other geodetic and astronomic parameters. The 1σ uncertainty in horizontal positioning was <0.02 m (J.F. Zumberge, personal communication, 2004). Repeat measurements were made at each stake in April 2001. Slight measurement errors may have been incurred in the repositioning of antennae on the stakes and from wind induced movement during measurement periods. We estimate the error in the annual surface displacement measurements to be < 0.05 m. Measured annual surface displacements ranged from

56

2.33 m, near the saddle of the southern half of the north-south ice divide, to 12.24 m

just above the equilibrium line in the south-eastern sector (A8 and A9 respectively in

Figure 3.2). The average discrepancy between the velocity stake data and the

associated InSAR pixel data agreed to within an average of +/- 2.54 m a^{-1} indicating a

conservative V_{error} of +/- 3 m a^{-1} throughout the interior regions of the ice cap.

V_{error} over ice moving greater than 20 m a^{-1} (where DGPS velocity

measurements not performed) were determined to be a function of the accuracy with

which the direction of ice flow was measured. The direction of ice flow over these

regions was determined from the visual inspection of flow stripes in the Landsat 7

imagery and was estimated to be accurate to within +/- 2° in azimuth. This error

translated into an accuracy of 2 – 10% of the projected surface velocity values,

depending on the angle between the direction of ice flow and look angle of the

satellite.

Significant variability in seasonal velocity measured over several high arctic

glaciers (Cress and Wyness, 1961; Iken, 1972; Copland and others, 2003a; Bingham

and others, 2003) suggests that additional error may be introduced when extrapolating

InSAR derived velocity measurements to annual values. Summer velocities up to

100% higher than winter velocities were recorded at certain low elevation velocity

stakes by Copland (2001) on the John Evans Glacier, Nunavut. Such variability would

not be detected in the short-term (1 – 3 day) InSAR velocity measurements. Although

the effects of seasonal variability cannot be quantified due to a lack of summer

velocity measurements over the ice cap, it is likely that the areas affected are restricted

to the main outlet glaciers. Since the radar imagery used in this study was acquired in

57

the winter and spring months (before the onset of melt), velocities derived from these data likely represent minimum annual values.

3.4 SPECKLE TRACKING MEASUREMENTS

Intense crevassing and relatively high velocities at the termini of the Eastern, Belcher, and Unnamed Glaciers caused de-correlation between the ERS 3-day repeat pass image pairs over these regions. The technique of speckle tracking (Gray and others, 2001; Joughin, 2002) was therefore used to measure surface velocities over the terminus of the Belcher Glacier. Speckle tracking measures movement of the surface of the earth between 2 coherent radar images acquired from successive orbital cycles (Gray and others, 2001). Coherence is based on the backscatter properties of each image, which allow the pairs to be co-registered to within a fraction of a pixel. In this study, pixels were re-sampled to 250 m resolution. Displacement rates and directions are measured by matching the speckle pattern of a roving chip (several pixels in size) to a reference image. Unfortunately, poor coherence between the Radarsat 1 pairs precluded the application of this technique to other areas of the ice cap. Ice velocities of $180 - 300$ m a^{-1} were measured throughout the terminal reaches of the Belcher Glacier. Velocities of up to 21 m a^{-1} were, however, measured over adjacent bedrock outcrops (where velocity should be 0 m a^{-1}), indicating that the error of the velocity estimates is up to 10% of the measured value.

58

3.5 ICEBERG CALVING RATES

The volume of ice calved was quantified for 94% of that part of the perimeter of the ice cap that terminates at sea-level. Total discharge was calculated as;

$$Q_{Total} = Q_{flux} + Q_{v\_loss} \tag{2}$$

where Q_{flux} is the volume of ice flux discharged at the tidewater termini between 1960 and 1999 and Q_{v_loss} is the volume loss due to the observed change of terminus position over that interval (Burgess and Sharp, 2004).

Although the predominant ice flow regimes at the location of the flux gates for which Q_{flux} was determined are known (derived in a later section), the exact ratio of sliding to ice deformation at each gate is not known. A range of estimates of Q_{flux} was therefore made, based on different assumptions regarding the contribution of internal deformation to overall glacier motion. The maximum estimate was based on the assumption that glacier flow was entirely by basal sliding or bed deformation ($V_{sliding} = V_{DS}$). The minimum estimate assumed that internal deformation also contributed to glacier flow, and that the depth averaged velocity was equal to 80% of the measured downslope surface velocity ($V_{depth\_avg} = V_{DS} \times 0.8$; Paterson, 1994). The occurrence of flow stripes on all major glaciers however suggest that basal motion is likely more important to glacier flow than internal deformation indicating that the upper velocity estimate is probably closer to the actual value.

Flux gates were located as close as possible to the termini of all tidewater glaciers. However, flux gates of the Eastern and Unnamed Glaciers had to be

59

positioned 3 kilometres up-glacier from their termini due to a lack of surface velocity data for regions further downstream. Also, ice flux from 6% of that part of the ice cap perimeter that terminates at sea-level could not be derived due to an absence of surface velocity data. The glaciers concerned originate from relatively small basins isolated from the main ice cap, however, and probably do not contribute significantly to the volume of ice discharged from the ice cap.

Another important source of error associated with the iceberg calving flux measurements (besides V_{error}) is inaccuracies in the ice thickness data (h_{error}). Point measurements of ice thickness were obtained in 2000 (Dowdeswell and others, 2004) along transects flown 5 – 10 km apart in north-south and east-west directions across the main part of the ice cap, and up the centrelines of most of the main outlet glaciers. The data were then interpolated across the entire ice cap using an inverse distance weighted surfacing algorithm constrained by exposed bedrock visible in the 1999 Landsat ETM+ imagery in order to properly constrain channelized flow (Dowdeswell and others, 2004). The spatial resolution of the resultant grid cells was 1 km with an estimated error in ice thickness of ± 10 m. Errors associated with glacier width (W) at the location of the flux gate were considered insignificant.

Other sources of error associated with extrapolating calving flux estimates over the period of 1960 – 1999 are introduced by the variability in velocity of these glaciers on seasonal and/or long term time scales. As mentioned above, velocities near the glacier termini may fluctuate on a seasonal time scale indicating that the spring InSAR data used to derive velocity estimates in this study likely underestimate the actual annual velocities, and hence rates of calving flux. Since significant summer melting

60

generally only extends from early July to early August (Alt, 1978), the resulting fluctuations in flow rate should not affect the annual velocity measurements by more than ~10%. It is difficult to estimate the long term variability in glacier flow due to the lack of velocity data across most of the ice cap over the past 40 years. However, a point velocity of 36 m a^{-1} measured on the Sverdrup Glacier by Cress and Wyness (1960) agrees to within 5 m a^{-1} of the 1996 InSAR measured velecity suggesting a reasonably consistent rate of flow at this location since 1960. On the other hand, evidence of fast glacier flow (see Figure 3.3) near the termini of the Southeast 1 and Southeast2 glaciers indicates that the velocity throughout this region (which is currently <15 m a^{-1}) has decreased significantly since the formation of these surface features. If this apparent reduction in velocity has occurred since 1960 then the extrapolated calving flux derived from the InSAR data would be an underestimate of the 40 year average across this calving front.

Upper and lower estimates of flux (Q_{max} and Q_{min} respectively) at each gate were calculated from the formulae;

$$Q_{max} = VT_{max} \, W \tag{3}$$

$$Q_{min} = VT_{min} \, W \tag{4}$$

where

$$VT_{max} = (V_{sliding} + V_{error}) \, (h + h_{error}) \tag{5}$$

and

61

$$VT_{min} = (V_{depth\_avg} - V_{error})(h - h_{error}) \qquad (6)$$

VT_{max} and VT_{min} represent average values across the flux gates, which were then multiplied by the flux gate width. This technique of averaging pixel values along the flux gate, as opposed to a summation of the pixel values, was chosen to avoid including extra pixels in the calculation which can occur when representing irregular or diagonal lines in a gridded format.

The value of Q_{v_loss} was calculated as the product of the 1960 – 1999 area change and the average of all gridded ice thickness values across the tidewater terminus of each outlet glacier. Area changes were determined as the difference between the 1960 and 1999 outlines of the ice cap margin (Burgess and Sharp, 2004). The estimated accuracy of volume change measurements at the glacier termini was derived by assuming a +/- 15 meter digitizing error around the perimeter of the area of change and a +/- 10 meter error in the measured ice thickness. Due to the absence of bathymetry data beyond the tidewater termini, volume changes were derived assuming that the thickness of ice throughout the area of change is consistent with ice thickness along the current ice margin.

3.6 RESULTS

3.6.1 Flow pattern of the Devon Island ice cap

The line of sight velocity map reveals a significant difference in the pattern of ice flow between the eastern and western sectors of the Devon ice cap (Figure 3.2). In the western half of the ice cap, ice movement occurs predominantly by slow 'sheet'

62

flow ($<$ ~15 metres a^{-1}), although several areas of more rapid flow occur along the southwest margin. The largest of these areas occurs upglacier of the North Croker Bay Glacier, where more rapid flow penetrates up to 30 km inland from the ice cap margin. Flow associated with the South Croker Bay Glacier penetrates up to 20 km inland of the ice cap margin. The Croker Bay glaciers terminate in Lancaster Sound, and their velocities reach maxima of ~210 and ~240 m a^{-1} for the north and south glaciers respectively. A third region of more rapid flow is associated with the Sverdrup Glacier which flows north into Jones Sound. Unfortunately, a lack of velocity data precludes analysis of the inland extent of enhanced glacier flow in this region. However, Koerner (personal communication, 2004) indicated that the inland extent of fast glacier flow associated with the Sverdrup Glacier is defined by the concave up form of the ice cap surface which extends ~5 km inland of where the glacier enters the main valley. The Sverdrup Glacier draws ice from both its main tributary (Main Branch - Figure 3.2), and an eastern arm (East Branch – Figure 3.2), the up-glacier extension of which is restricted by the head of the Eastern Glacier. Enhanced ice flow at the head of a third flow feature to the west of the main tributary (West Branch – Figure 3.2) is limited as it terminates approximately 14 km downglacier of its head and does not contribute to the flow of the Sverdrup Glacier.

Ice drainage from the north-east sector of the ice cap occurs primarily via large outlet glaciers that flow through mountain valleys to reach sea-level. Most of the glaciers in this region originate at valley heads that restrict the inland extension of fast ice flow. Exceptions to this are the Eastern Glacier (basin 3) and 3 tributary glaciers to the Belcher (Belcher Tributary1, Belcher Tributary2, and Belcher Tributary3 – Figure

63

3.2) all of which draw from the slower flowing ice of the interior region. The Belcher Glacier itself originates along the north slope of the main east-west ice divide. In the upper reaches of this glacier, velocity increases to ~75 m a^{-1} upstream of the confluence with Belcher Tributary1 ~15 km upglacier from the terminus. Velocities increase to ~120 m a^{-1} at this confluence reaching maximum values of ~290 m a^{-1} at the glacier terminus. Belcher Tributary2 and 3 merge with the main glacier at the terminus, forming the widest 'fast flowing' calving front on the ice cap.

Velocities of the Eastern Glacier increase over approximately 30 km from the slow-moving interior regions to reach a maximum of ~120 m a^{-1}, 10 km up-glacier from the terminus. Although velocities at the terminus of the Eastern Glacier could not be measured, intense crevassing suggests that the speed of this glacier increases as it approaches marine waters. The remaining ice in the northeast sector is drained through a series of tidewater glaciers that range in maximum speed from 30 to 100 m a^{-1}. These glaciers drain relatively small basins (< ~15 km^2) that are separate from the main ice cap accumulation area.

'Fast' flow along the Southeast 1 and Southeast 2 glaciers extends farther into the accumulation zone than any other flow feature across the ice cap (Figure 3.2). The ice divide at the head of Southeast 1 has a convex upglacier form suggesting that this outlet glacier may be extending headwards into the less active basin to the west (basin 54). Both glaciers converge 40 km downglacier from the head resulting in a near stagnant region (<10 m a^{-1}) approximately 250 km^2 that terminates along an 8 km ice front in Hyde Inlet (Figure 3.2). Despite low velocities throughout this region, flow stripes visible on the surface of the Southeast 1 Glacier suggest that this feature was

64

once flowing faster than at present (Figure 3.3). Sharp shear zones along both margins and folded moraines near the terminus are indicators that this glacier may have surged in the past (Copland and others, 2003b; Dowdeswell and Williams, 1997).

Ice from the southern slopes of the Cunningham Mountains drains through a series of steep valley glaciers towards Lancaster Sound, most of which terminate on land. Included in this group is a possible surge-type glacier identified by Copland and others (2003b). Measured velocities on this glacier reach a maximum of ~150 m a^{-1}, but the surface morphology of the glacier suggests that, if it is indeed a surge-type glacier, it is currently in the quiescent phase of a surge cycle.

3.6.2 Glacier flow regimes

Four major flow regimes were identified based on the relationship between the ratio of surface velocity to ice thickness (v/h) and the driving stress (τ_d) analysed along the North Croker Bay, Southeast 1, Belcher Glaciers and across the western lobe. When the ice flow is solely due to ice deformation, the parameter (v/h) represents the mean shear strain rate in a vertical profile through the ice. When basal motion is important, this parameter no longer represents the shear strain rate in the ice, but the inverse of the ratio of (v/h) to (τ_d) has units of Pa s and is therefore a measure of the "effective viscosity" of the glacier system.

τ_d was derived from:

$$\tau_d = \rho_i \, g \, h \sin\alpha \qquad (7)$$

65

where ρ_i is the density of ice (910 kg m^{-3}) and g is the acceleration due to gravity (9.81 m s^{-2}). The effects of local variations in surface slope due to longitudinal stress gradients in the ice were removed by averaging surface slope values over distances equivalent to ~10 times the ice thickness. Figure 3.4 illustrates the theoretical relationships between v/h and τ_d that characterize the major flow regimes identified in this study.

Flow Regime 1 is distinguished by values of v/h < 0.075 a^{-1} and a high positive correlation with τ_d (r^2 > 0.85), though the sensitivity of v/h to changes in τ_d is low (Figures 3.4a – d). This behaviour suggests that the ice is frozen to the bed and glacier movement is by internal deformation alone (Cooper and others,1982; Budd and Smith, 1981). Within this flow regime, however, the ratio of v/h to τ_d may increase downstream (Figures 3.5a - c). This is probably a reflection of softening of the ice as it warms up with increasing distance of transport. Flow Regime 1 is characteristic of the upper reaches leading into major outlet glaciers (Figures 3.6a – c) and of the whole western lobe (Figure 3.6d). In these regions, glaciers have convex upward surface profiles (Figures 3.7a – d), and flow is not constrained laterally by bedrock topography. Flow Regime 1 is also observed in the terminal reaches of the Southeast 1 Glacier flow line where the velocity, and hence v/h, is low (see Figures 3.3 and 3.7c). In this region, v/h decreases as τ_d rises, suggesting increased flow resistance and "effective viscosity" towards the glacier terminus. This may be indicative of a frozen bed at the glacier margin.

The relationship between v/h and τ_d changes significantly at v/h ~ 0.075 a^{-1} (Flow Regime 2; Figure 3.5a – c). In this flow regime, the ratio of v/h to τ_d is

66

generally higher, the relationship between the two variables is more sensitive, and the sign of the relationship may be opposite to that observed in Flow Regime 1 (Figures 3.5b, c). This is not, however, always the case (Figure 3.5a). The ensemble of changes observed suggests a down flow reduction in "effective viscosity" and flow resistance and a contribution of basal motion to the surface velocity. The beginning of Flow Regime 2 coincides with convergent flow at the head of the major outlet glaciers (Figures 3.6a, c) and the appearance of flow stripes on the ice surface (Figures 3.6a – c). Gudmundsson and others (1998) argued that flow stripes form only where the velocity at the bed is large relative to the shearing through the ice thickness, supporting the argument that basal motion must be significant in regions with this flow regime. Flow Regime 2 commences ~5 km upglacier from steps in the bedrock topography along the North Croker Bay and Southeast 1 Glaciers (Figures 3.7a, c). These locations also coincide with the transformation to a concave up surface profile (Figures 3.7a – c) from the convex up profile, which is characteristic of Flow Regime 1. Rapid acceleration of V_{DS} and ice thinning at the cusp of the bedrock steps (Figures 3.7a,c) indicate that the onset of basal sliding is controlled primarily by the subglacial topography at these locations (McIntyre, 1985).

Ice Flow Regime 3 appears to be defined by threshold values of v/h $>$ ~ 0.28 a^{-}^{1} and τ_d $>$ ~0.75 bars (Figures 3.5a, b). In this region, v/h is inversely related to τ_d and the slope of the relationship between the two variables is steeper than in Flow Regime 2. The ratio of v/h to τ_d is higher again than in Flow Regime 2, implying a further reduction in viscosity and probably an increase in the relative contribution of basal motion to the surface velocity. Regions of Flow Regime 3 occur throughout the mid to

lower reaches of the major glaciers where flow stripes are well developed on the ice surface. Along the North Croker Bay Glacier flow line, Flow Regime 3 begins where the glacier enters the bedrock valley at km 48 (Figure 3.6a) and V_{DS} increases rapidly $(60 - 170$ m a^{-1} over a 1 km distance). A rapid increase of V_{DS} (and hence v/h) marks the beginning of Flow Regime 3 at km 42 along the Belcher Glacier flow line (Figure 3.6b). In contrast to the North Croker Bay Glacier, however, the flow of ice within this region is driven mainly by large values of τ_d that occur over steeply sloping (and rough) bed topography that descends to ~300 m b.s.l. within 2 km of the glacier terminus. In both situations, intense crevassing at the onset of Flow Regime 3 suggests that an increase in the rate of ice deformation occurs at the transition from Flow Regime 2 to Flow Regime 3. In addition, meltwater channels terminating at these crevasse fields (visible in the 1960's aerial photography) indicate that surface run-off may penetrate to the glacier bed via the crevasses and potentially enhance flow rates throughout this zone during the summer months A fourth regime, Flow Regime 4, is defined by threshold values of v/h > 0.28 a^{-1} and τ_d < 0.75 bars (Figure 3.5a). In this region, the wide range of values of v/h for consistently low values of τ_d is indicative of low friction at the glacier bed. This may suggest that deformation of subglacial sediments contributes to basal motion, which remains a major component of the surface velocity of the glacier. Flow Regime 4 is characteristic of the terminal reaches of the North Croker Bay Glacier, where the glacier is grounded below sea level (Figure 3.7a). It is not, however, found along the Belcher and Southeast 1 Glaciers that are also grounded below sea level.

68

Identification of distinct flow regimes across the ice cap indicates that the mode of ice movement evolves as one of a few possible sequences along a flow line between the interior region and the ice cap margin. The initial transition occurs at the head of the outlet glaciers where cold-based ice moving by internal deformation only (Bentley, 1987) transforms to warm-based flow and basal sliding commences. This mode of flow continues until the glacier either (a) reverts back to being cold-based (where flow is by internal deformation only) or (b) is enhanced by high driving stresses or narrowing bedrock valleys. Glaciers that transform into (b) likely experience high rates of internal deformation (Truffer and Echelmeyer, 2003) and enhanced basal sliding as a result of the penetration of surface meltwater through crevasses during the summer melt season (Zwally and others, 2002; Boon and Sharp, 2003, Copland and Sharp, 2003a). A third transition occurs near the termini of a few glaciers where τ_d is greatly reduced while high velocities are maintained. The mechanics of this mode of glacier flow are likely similar to ice stream flow where glacier movement occurs over a highly deformable and/or lubricated bed and the main resistance to flow occurs at the glacier margins (Truffer and Echelmeyer, 2003; Bentley, 1987).

Threshold values of v/h and τ_d separating the 4 distinct flow regimes in the scatter plots were applied to raster datasets of these parameters in order to map the distribution of ice flow regimes across the entire ice cap. For the raster grids, surface slope was averaged as a function of area rather than in an along profile direction. This spatial averaging has the effect of slightly over (under) estimating the slope relative to

69

the profile analyses over high (low) slope areas. These variations however did not have any affect on the flow regime classification.

Further uncertainties in τ_d may also derive from the fact that the glacier shape factors were not included in the computed values of τ_d. A few representative shape factor values were computed along the major outlet glaciers (assuming a parabolic glacier cross-section; Paterson, 1984) and they indicated that applying this correction could reduce the computed values of τ_d by up to ~25%. Also, it is possible that the longitudinal averaging used in this study (10h) was inadequate to fully remove the effects of longitudinal stress gradients from τ_d. In particular, near the glacier termini where averaging was less than 10h, computed values of τ_d may be slightly higher than the true values. In any case, slight discrepancies between the actual and computed values of τ_d would have only minor implications for flow regime classification relating exclusively to the separation of Flow Regime 3 from Flow Regime 4.

Approximately 50% of the mapped area of the ice cap was classified as Flow Regime 1, which includes the interior region above 1000 m a.s.l. as well as ~600 km^2 of the southeast sector which lies below 300 m a.s.l (Figure 3.8). Flow Regime 2 is confined mainly to the outlet glaciers, but it also occurs in some small areas along the western margin. Excluding the areas that were not mapped, this regime comprises approximately 22% of the total area east of the central divide (basins 3, 10, 11, 15, 20, 24, 25, 29, 30, 33, 35, 36, 37, 40, 39, 60, 66, 70, 73) but only 8% of the area west of the central divide (basins 9, 13, 38, 43, 54, 61, 65, and 67), indicating that basal motion is much more prevalent in the east. Flow Regime 3 occurs up to 22 km upglacier from the termini of the North and South Croker Bay Glaciers and up to 25

70

km upglacier from the terminus of the Belcher Glacier (along Belcher Tributary2), reflecting the combination of relatively high driving stresses and high velocities in these regions. Flow Regime 4 is confined to the termini of the North Croker Bay, East3, East Central1, and the South Cunningham Glaciers as well as a small section along the Southeast2 Glacier. The glaciers classified as Flow Regime 4 are all grounded above sea-level except for the terminus region of the North Croker Bay Glacier, suggesting that reduced basal friction of these glaciers may be attributed to the presence of deformable sediments at the bed rather than to buoyancy effects at tidewater margins.

3.6.3 Rates of Iceberg Calving

The rate of ice calved directly into the ocean due to flux at the tidewater margins was estimated to be 0.42 +/- 0.14 km^3 a^{-1}. This equates to a calving flux rate of 16.8 +/- 5.7 km^3 between 1960 and 1999 assuming invariant glacier flow velocities over this time interval. Volume loss due to retreat of the tidewater termini increase the total mass loss by 3.6 +/- 0.026 km^3 resulting in a total volume loss due to iceberg calving of 20.5 +/- 4.7 km^3 over the past 40 years. The northeast sector (basins 10, 11, 15, 20, 24, 25, 29, 30, 31, 33, and 36) produced 67% of the total volume of ice calved. The Belcher Glacier alone was responsible for 70% of this amount, which equates to almost half (47%) of the ice cap total (Figure 3.8). Most of the mass lost from the Belcher Glacier (~93%) is accounted for by ice flux as opposed to terminus change. This reflects the relatively thick ice (~250 m) and high velocity (up to 290 m a^{-1}) at this ice front. Although 2 major glaciers terminating at the southeast margin of the ice

71

cap (basins 39 and 60) have extensive calving fronts (~18 km long), this region accounts for only 16% of the total calving flux. This is due mainly to the low surface velocities of these glaciers. The southern most calving front (basin 60) is unique in that the majority of mass calved from this terminus is due to retreat of the ice front (~60%) rather than ice flux. The North and South Croker Bay glaciers have advanced since 1960. This reduces the calculated volume loss due to flux by 12%. Similarly, glacier advance reduced the calculated calving flux of the Sverdrup Glacier by 13%. Mass loss due to calving from the western glaciers accounts for ~10% of the total volume of ice calved from the Devon Island ice cap. In total, the 8 major tidewater glaciers draining the ice cap (indicated in Figure 3.9) are responsible for ~90% of the total discharge of ice calved. The rest is derived from small alpine glaciers (generally < 1 km wide) that flow from basins in the northeast and eastern sectors.

3.7 CONCLUSIONS

The continuous surface velocity field of the Devon Island ice cap mapped using InSAR techniques reveals a significant contrast in ice flow dynamics between the east and west sides of the ice cap. The eastern half of the ice cap is drained by several fast flowing outlet glaciers that extend up to 60 km inland from the ice cap margin, and in some cases reach within a few kilometres of the central ice divides. The western half of the ice cap is drained primarily by sheet flow, but also by a few outlet glaciers that are restricted to within less than 30 km of the ice cap margins.

The predominant ice flow regimes were classified based on the relationship between the ratio of surface velocity to ice thickness and the driving stress derived

72

along 4 flow lines from distinctly different regions across the ice cap. The classified regimes were mapped across ~75% of the ice cap surface for which both surface velocity and ice thickness data are available. The interior and southeast ice regions were classified as Flow Regime 1 type flow and are characterized by frozen bed conditions where ice movement is solely by internal deformation. The main sections of most outlet glaciers were classified as Flow Regime 2, in which basal motion occurs. The transition to Flow Regime 2 along a flow line marks the onset of basal sliding and is usually associated with ice flow over a step in the bedrock topography. The appearance of flow stripes on the ice surface in regions of Flow Regime 2 supports the argument that significant basal motion contributes to the surface velocity in these areas. Flow Regime 3 is characterized by enhanced basal motion and internal deformation due to a significant increase in driving stress. Flow Regime 4 is characterized by a wide range in values of (v/h) (including maximum values) within sections of the glacier with consistently low values of driving stress. This flow regime occurs within a few kilometres of the termini and is indicative of minimal basal friction that may result from the presence of deformable sediments at the glacier bed.

Approximately 20.5 km^3 of ice was calved from the Devon Island ice cap between 1960 and 1999. Approximately 89% of the total volume of ice calved was discharged from the eastern margin, with the largest single source being the Belcher Glacier which was responsible for ~50% of the total amount. Comparing the total volume of ice lost due to calving and total mass loss of ~67 km^3 from the Devon Island ice cap between 1960 and 1999 (Burgess and Sharp, 2004) indicates that iceberg calving may account for up to 30% of the total volume loss over the past 40

73

years. Iceberg calving therefore represents a significant form of ablation from the Devon Island ice cap and should be accounted for when determining the state of health of this ice mass as a whole. Dowdeswell and others (2002) also found that about 40% of mass loss from the 5,575 km^2 Academy of Sciences Ice Cap in Russian Severnaya Zemlya was lost by iceberg calving. Together with the evidence from Devon Island ice cap, this suggests that iceberg production is an important component of the total mass loss from large Arctic ice caps.

3.8 REFERENCES

Alt, B.T. 1978. Synoptic climate controls of mass-balance variations on Devon Island Ice Cap. *Arct. Alp. Res.*, **10**(1). 61-80.

Benham, T., J.A. Dowdeswell. 2002. Devon Dems, *CD ROM*, V.1.1a.

Bentley, C.R. 1987. Antarctic ice streams: A review. *J. Geophys. Res.,* **92**(B9), 8843-8858.

Bingham, R., P.W. Nienow and M.J. Sharp. 2003. Intra-annual and intra-seasonal flow dynamics of a high Arctic polythermal valley glacier. *Ann. Glaciol.*, **37**,181-188.

Boon, S. and M.J. Sharp. 2003. The role of hydorlogically-driven ice fracture in drainage system evolution on an Arctic glacier. *Geophys. Res. Lett.*, **30.**

Budd, W.F. and I.N. Smith, 1981. The growth and retreat of ice sheets in response to orbital radiation changes. *Int. Ass. Hydro. Sci. Pub.,* **131** (Symposium at Canberra 1979 – S*ea level, ice and climatic change: 369-409*

Burgess, D. O. and M. J. Sharp, 2004. Recent changes in areal extent of the Devon ice

74

cap, Nunavut, Canada. *Arc., Ant., and Alp. Res.*, **36**(2), 27pp.

Cooper, A.P.R., N.F. McIntyre, and G.de Q. Robin. 1982. Driving stresses in the Antarctic Ice Sheet. *Ann. Glaciol.*, **3,** 59-64.

Copland, L., M. Sharp. 2001. Mapping thermal and hydrological conditions beneath a polythermal glacier with radio-echo sounding. *J. Glaciol.*, **47**(157), 232-242.

Copland, L., M. Sharp, P. Nienow, and R. Bingham. 2003(a). The distribution of basal motion beneath a high Arctic polythermal glacier. *J. Glaciol.*, **49**(106).

Copland, L., M. Sharp, and Dowdeswell, J.A. 2003(b). The distribution and flow characteristics of surge-type glaciers in the Canadian High Arctic. *Ann. Glaciol.*, **36**.

Cress, P., and Wyness, R. 1961, The Devon Island expedition, observations of glacial Movements. *Arctic*, **14**(4), 257-259.

Cumming, I. G. and J. Zhang. Measuring the 3-D Flow of the Lowell Glacier with InSAR. FRINGE'99 - Advancing ERS SAR interferometry from applications towards operations. 10-12 November 1999, Centre Spatial de Liege, Belgium, ESA Publications Division, 2000

Dowdeswell, J.A., and M. Williams. 1997. Surge-type glaciers n the Russian High Arctic identified from digital satellite imagery. *J. Glaciol., 43(145), 489-494.*

Dowdeswell, J.A., Bassford, R.P., Gorman, M.R., Williams, M., Glazovsky, A.F., Macheret, Y.Y., Shepherd, A.P., Vasilenko, Y.V., Savatyuguin, L.M., Hubberten, H.-W. and Miller, H., 2002. Form and flow of the Academy of Sciences Ice Cap, Severnaya Zemlya, Russian High Arctic. *J. Geophys. Res., 107, doi:10.1029/2000/JB000129.*

75

Dowdeswell, J. A., T. J. Benham, M.R. Gorman, D. Burgess, and M. Sharp. 2004. Form and flow of the Devon Island ice cap, Canadian Arctic. *J. Geophys. Res.* **109**, F02002, doi:10.1029/2003JF000095.

Gabriel, A. K. and R. M. Goldstein.1989. Mapping small elevation changes over large areas: differential radar interferometry. *J. Geophys. Res.*, **94**(B7), 9183-9191.

Gray, L., N. Short, K.E. Mattar, K.C. Jezek. 2001. Velocities and Flux of the Filchner Ice Shelf and its tributaries determined from speckle tracking interferometry. *Can. J. Rem. Sen.*, **27**(3), 193-206.

Gudmundsson, G.H., Adalgeirsdottir, G., Bjornsson, H. 2003. Observational verification of predicted increase in bedrock-to-surface amplitude transfer during a glacier surge. *Ann. Glaciol.,* **36**.

Gudmundsson, G.H., C.F. Raymond and R.A. Bindschadler. 1998. The origin and longevity of flow stripes on Antarctic ice streams. *Ann. Glaciol.* **27**, 145-152

Iken, A.1972. Measurements of water pressure in moulins as part of a movement study of the White Glacier, Axel Heiberg Island, Northwest Territories, Canada. *J. Glaciol.*, **11**(61), 53-58.

Joughin, I. 2002. Ice-sheet velocity mapping: a combined interferometric and speckle-tracking approach. *Ann. Glaciol.,* **34**,195-201.

Joughin, I., R. Kwok, and M. Fahnestock.1996. Estimation of ice-sheet motion using satellite radar interferometry: method and error analysis with application to Humboldt Glacier, Greenland. *J. Glaciol.*, **42**(142), 564-575.

Koerner, R.M., 1970. The mass balance of Devon Island ice cap Northwest Territories, Canada, 1961 - 1966. *J. Glaciol.*, **9**(57): 325-336.

76

Koerner, R.M. 2004. Personal communication, Geological Survey of Canada, Terrain Sciences Division, 601 Booth St., Ottawa, Canada.

Mair, D.W.F., D.O. Burgess, and M.J. Sharp. 2004. Thirty-seven year mass balance of the Devon Ice Cap, Nunavut, Canada determined by shallow ice coring and melt modelling. *J. Geophys. Res.* **110**, F01011, doi:10.1029/2003JF000099.

Massonnet, D. and K. L. Feigl.1998. Radar interferometry and its application to changes in the earth's surface. *Reviews of Geophysics*, **36**(4), 441-500.

McIntyre, N. F.1985. The dynamics of ice-sheet outlets. *J. Glaciol.*, **31**(108), 99-107.

Paterson, W. S. B. 1994. *The Physics of Glaciers.3rd.* Oxford, etc., Elsevier.

Truffer, M. and K.A. Echelmeyer. 2003. Of isbrae and ice streams. *Ann. Glaciol.*, **36**, 66-72.

Unwin, B. 1998. Arctic ice cap velocity variations revealed by ERS SAR interferometry, *Unpubl. Ph.D. Thesis*, University of London.

Vachon, P. W., D. Geudtner, K. Mattar, Gray, A.L., M. Brugman, and I. Cumming.1996. Differential SAR interferometry measurements of Athabasca and Saskatchewan glacier flow rate. *Int. J. Rem. Sen.*, **22**(3), 287-296.

Webb, F.H. and Zumberge, J.F. 1995. An introduction to GIPSY/OASIS-II, *NASA/Jet Propul. Lab./Calif. Inst. Technol.*, Pasadena, Cal, USA. 442pp.

Zebker, H. A., P.A. Rosen, R.M. Goldstein, A.Gabriel, and C.L. Werner.1994. On the derivation of coseismic displacement fields using differential radar interferometry: The Landers earthquake. *J. Geophys. Res.*, **99**(19), 19,617-19,634.

Zumberge, J.F. 2004. Personal communication. *NASA/Jet Propul. Lab./Calif. Inst. Technol.*, Pasadena, Cal, USA.

Zwally, H.J., W.Abdalati, T.Herring, K. Larson, J.Saba, K.Steffen. 2002. Surface melt-induced acceleration of Greenland ice-sheet flow. *Science,* **297**, 218-222.

Ice cap region	Radarsat Orbit	ERS Orbit	ERS Image Dates	Perp. Baseline(m)
South East	-	24397/4724, 24898/5225	Mar15-16, Apr19-20, 1996	-187, -6
West	-	24894 / 5311	Apr25-26, 1996	-1
		2924 / 2967	Feb6/9,1992	-60
Belcher terminus	25810 / 26153	-	Oct14-Nov7,2000	-
Belcher terminus	26345/ 26688	-	Nov20-Dec14,2000	-

Table 3.1. Orbit numbers and dates of radar imagery used for velocity mapping over the Devon Island ice cap.
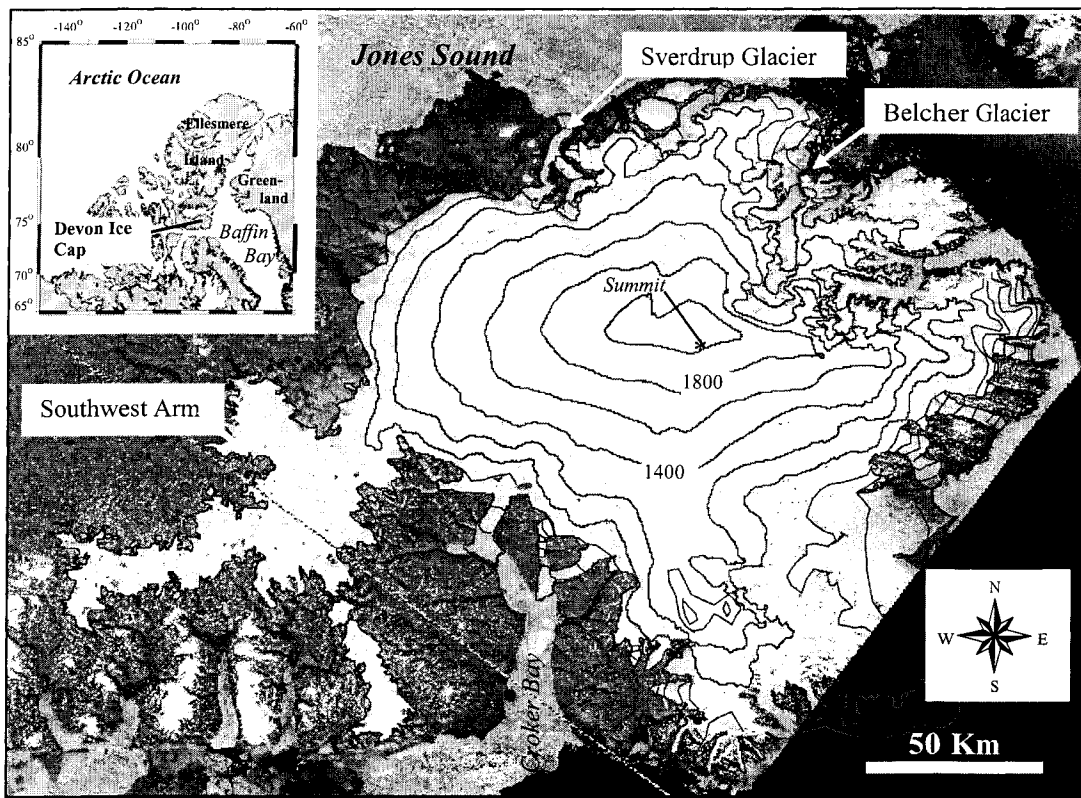
Figure 3.1. 1999 Landsat 7 ETM+ ortho-mosaic of the Devon Island ice cap, Nunavut, Canada. Inset shows the location of the Devon Island ice cap in the Canadian Arctic Archipelago.
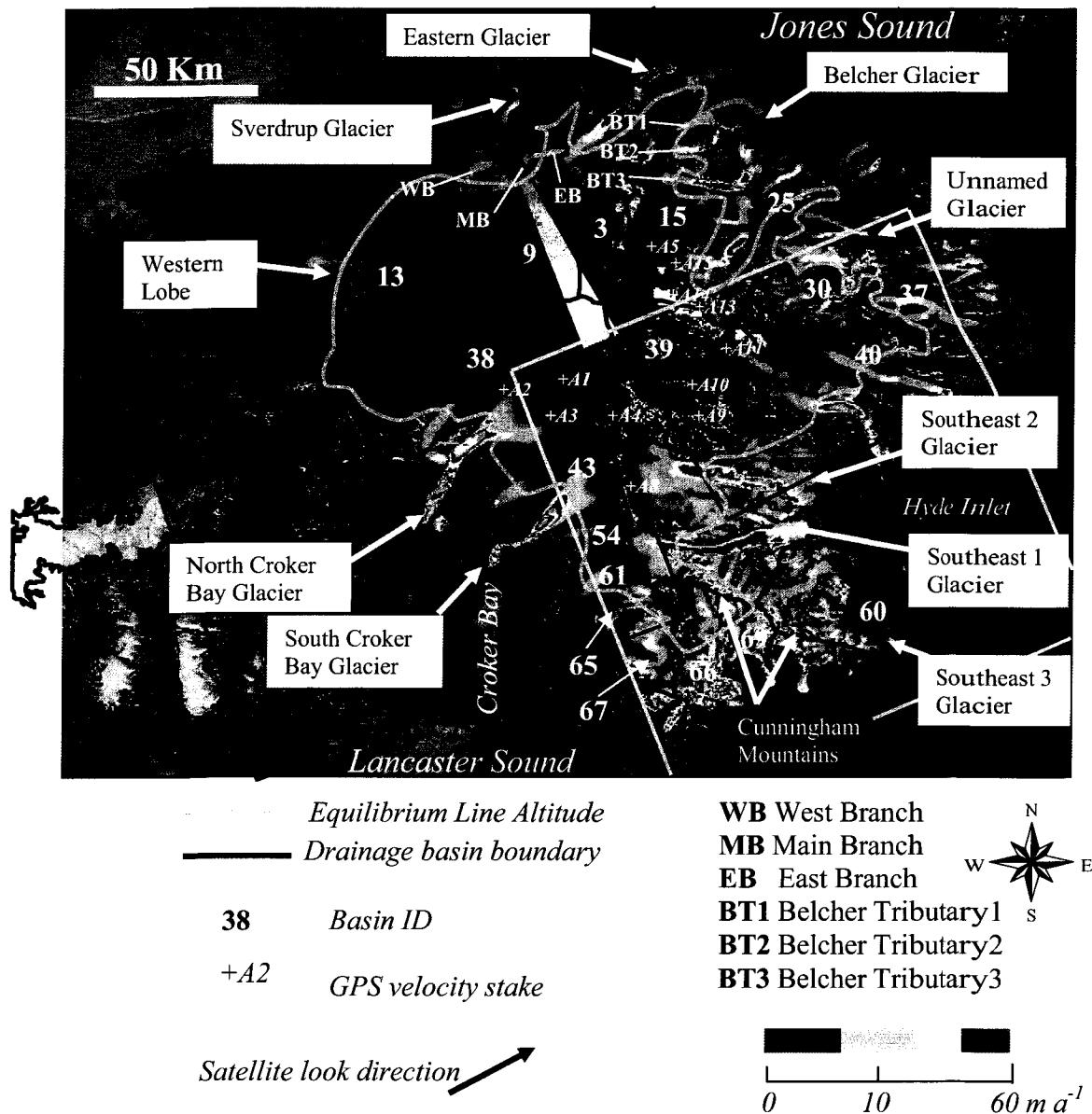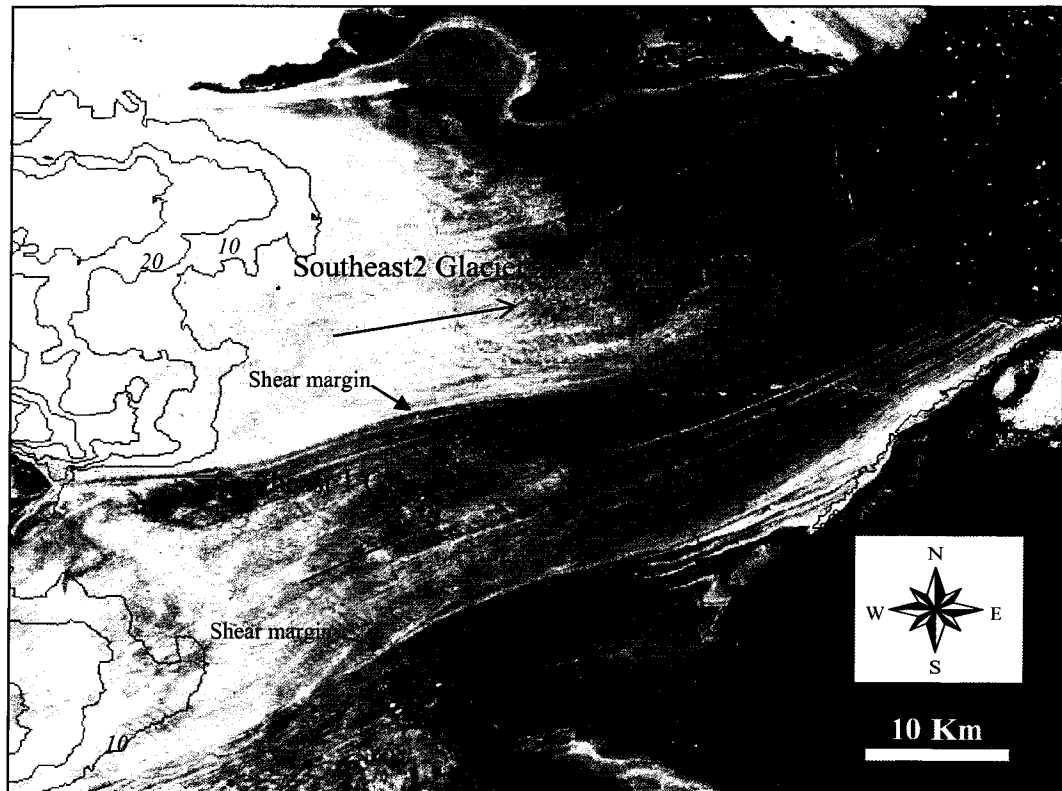
80

Figure 3.2. Look direction surface velocities overlayed onto a 1999 Landsat 7 ETM+ satellite ortho-mosaic of the Devon Island ice cap. Accelerated glacier flow is identified by the closely spaced colored fringes which are evident along the entire length of most of the major outlet glaciers. Red, green, and blue boxes outline the footprints for the west, southeast, and northeast ERS radar image pairs respectively. Orbital numbers are listed in Table 3.1. The equilibrium line altitude (ELA) used here is situated at ~800 m a.s.l. throughout the southeast, ~950 m a.s.l. throughout the northwest, and 875 throughout the southwest and northeast regions of the ice cap (Koerner, 1970).

Figure 3.3. A subset of a 2000 Landsat 7 ETM+ image mosaic highlighting surface features indicative of fast glacier flow throughout the terminus region of the Southeast 1 and Southeast 2 glaciers.
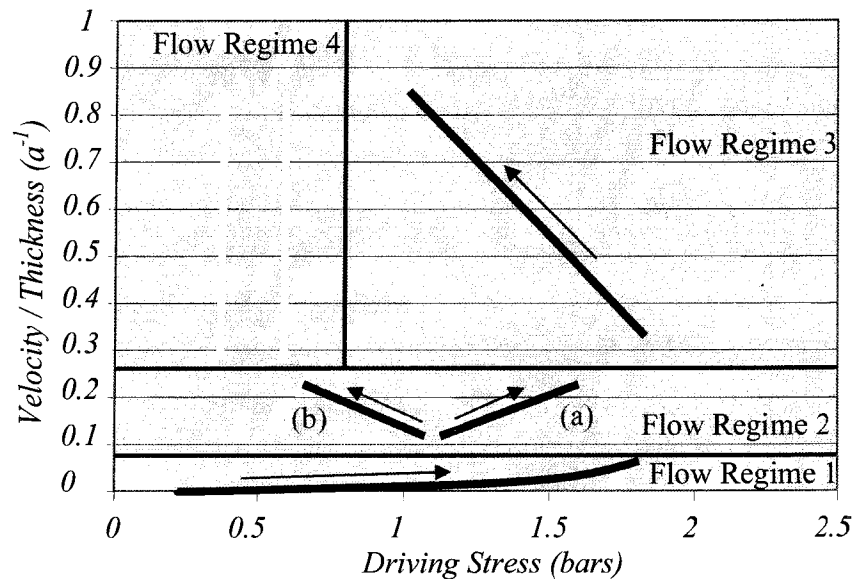
82

Figure 3.4. Theoretical relationships between (v/h) and driving stress (τ_d) for each of the major flow regimes across the Devon Island ice cap. Solid arrows indicate the direction of glacier flow. In Flow Regime 1 v/h increases slightly, indicating non-linear viscous flow (in response to relatively large increases in τ_d). This relationship reflects the shear strain rate within the ice suggesting that flow is by internal deformation alone. An increase in the slope of the relationship in Flow Regime 2 (a) indicates sliding (probably over bedrock) at the glacier bed or warmer (less viscous) ice. The inverse of this relationship (b) indicates reduced basal friction in the direction of flow, implying increased sliding downstream. Flow Regime 3 is characterized by a further increase in the sensitivity of v/h to changes in τ_d. The inverse relationship between v/h and τ_d in this flow regime likely indicates reduced till strength or increased basal lubrication towards the glacier terminus. The vertical relationship characteristic of Flow Regime 4 indicates sliding over sediments deforming according to Coulomb-plastic flow at the glacier bed. The x-intercept of this relationship indicates the yield strength of the subglacial sediment, which may decrease (as indicated by dotted arrow) toward the glacier terminus.

83

Figure 3.5a. The predominant modes of glacier flow across the Devon Island ice cap identified based on the relationship between mean shear strain rate (v/h) and driving stress (τ_d) along the North Croker Bay Glacier. Threshold values (red lines) separate each distinct ice flow regime based on changes in the relative slope of the clusters in each feature space. Coloured arrows in a, b, and c indicate the down-glacier direction of ice flow.
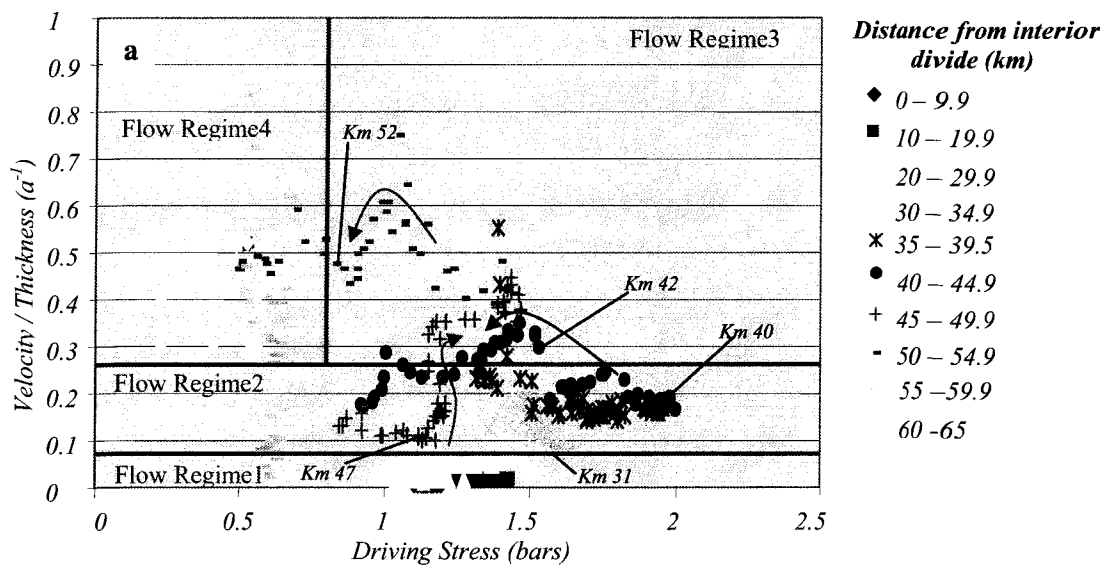
84

Figure 3.5b. The predominant modes of glacier flow across the Devon Island ice cap identified based on the relationship between mean shear strain rate (v/h) and driving stress (τ_d) along the Belcher Glacier. Threshold values (red lines) separate each distinct ice flow regime based on changes in the relative slope of the clusters in each feature space. Coloured arrows in a, b, and c indicate the down-glacier direction of ice flow.

85
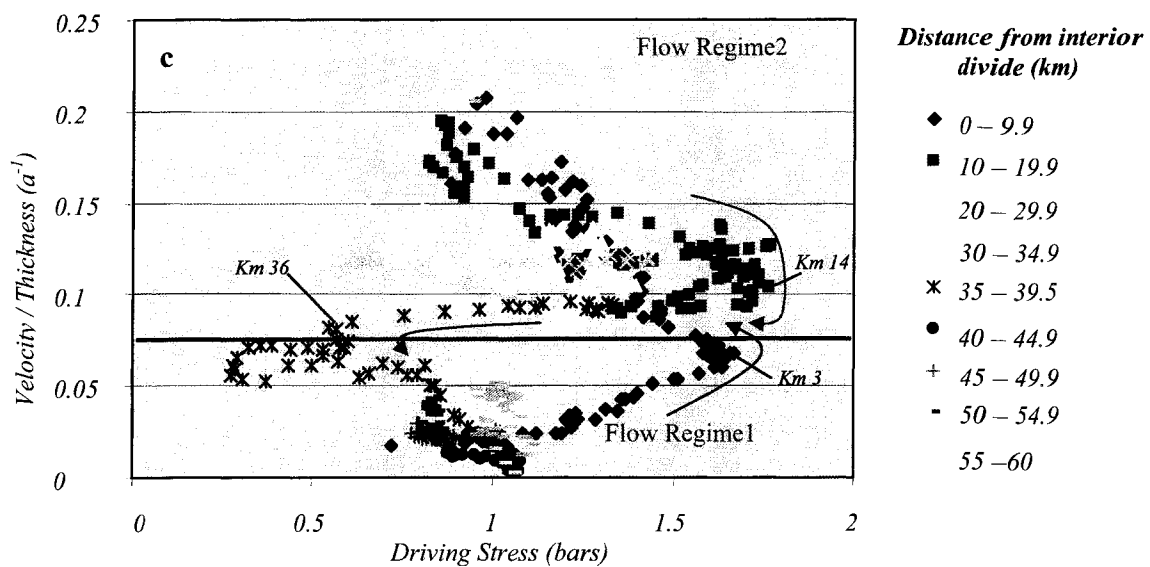
Figure 3.5c. The predominant modes of glacier flow across the Devon Island ice cap identified based on the relationship between mean shear strain rate (v/h) and driving stress (τ_d) along the Southeast 1 Glacier. Threshold values (red lines) separate each distinct ice flow regime based on changes in the relative slope of the clusters in each feature space. Coloured arrows in a, b, and c indicate the down-glacier direction of ice flow.
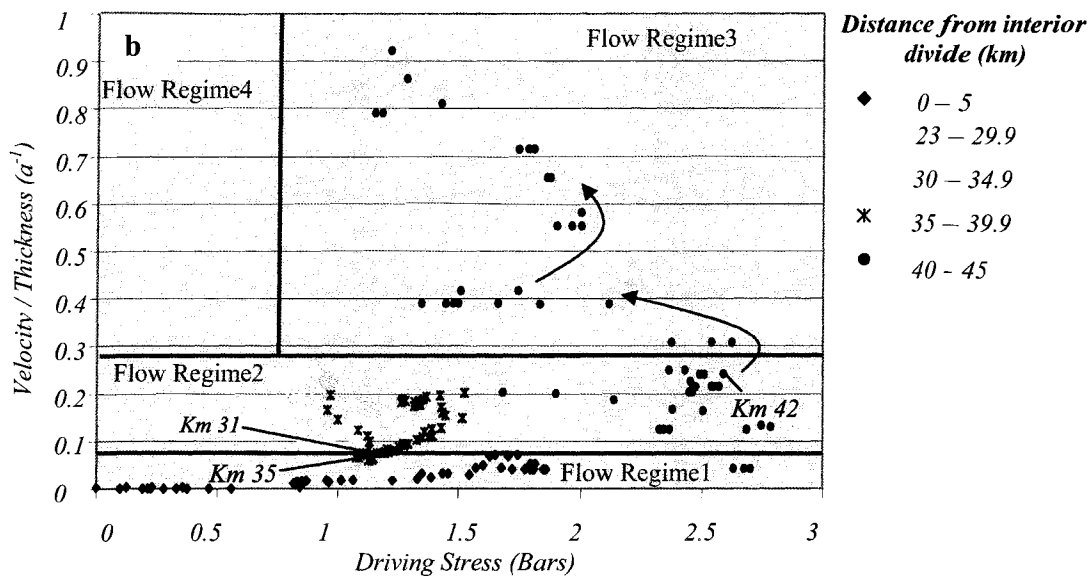
86
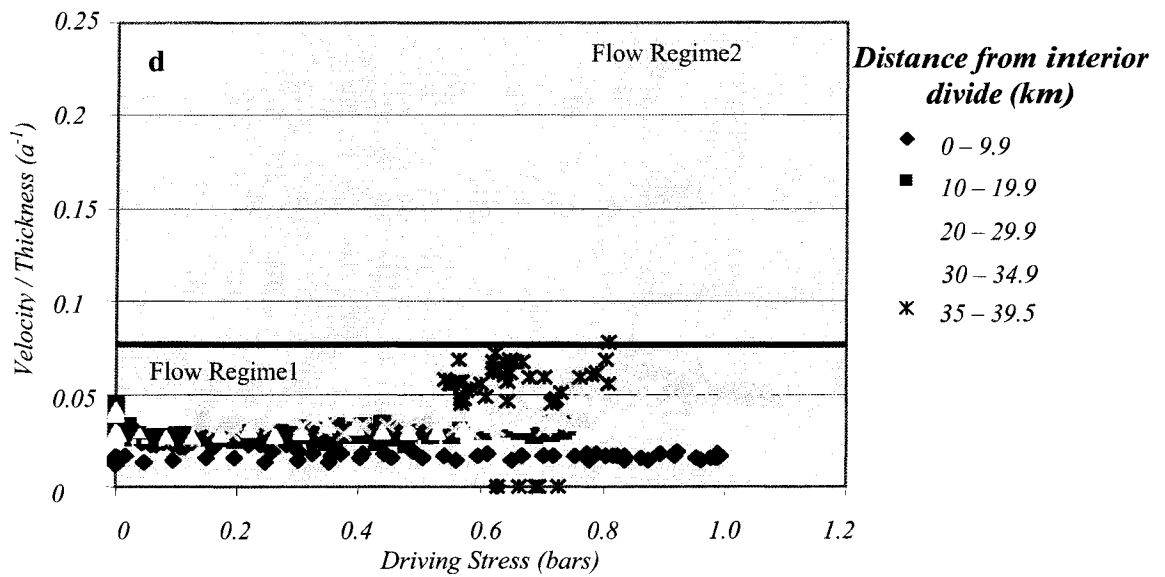
Figure 3.5d. The predominant modes of glacier flow across the Devon Island ice cap identified based on the relationship between mean shear strain rate (v/h) and driving stress (τ_d) along the Western Lobe. Threshold values (red lines) separate each distinct ice flow regime based on changes in the relative slope of the clusters in each feature space. Coloured arrows in a, b, and c indicate the down-glacier direction of ice flow.

87

a

Km 0

Km 31

Km 42

Km 48

Km 63

5 Km
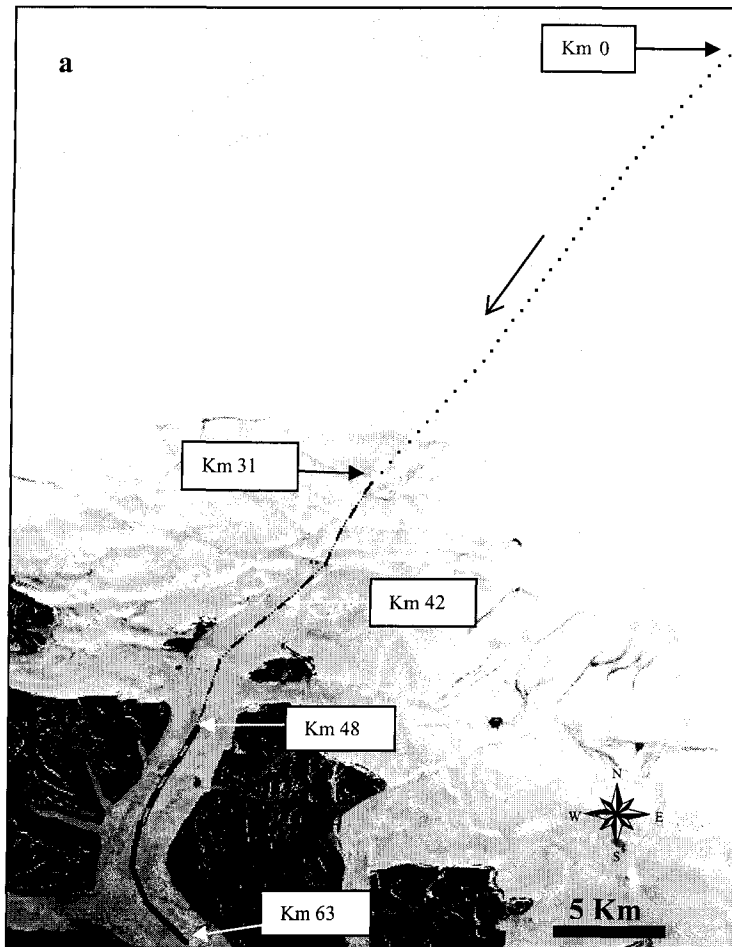
··········· Flow Regime1
————— Flow Regime2
Flow Regime3
Flow Regime4

⟵ Direction of
ice flow

Figure 3.6a. Planimetric view of the dominant flow regimes along the North Croker Bay Glacier. Centerline profiles are superimposed on a subset of the 1999 Landsat7 ETM+ satellite imagery. Location of image subset and profiles is identified in Figure 3.8.

88

Figure 3.6b. Planimetric view of the dominant flow regimes along the Belcher Glacier. Centerline profiles are superimposed on a subset of the 1999 Landsat ETM+ satellite imagery. Location of image subsets and profiles are identified in Figure 3.8.

89

Figure 3.6c. Planimetric view of the dominant flow regimes along the Southeast 1 Glacier. Centerline profiles are superimposed on a subset of the 1999 Landsat ETM+ satellite imagery. Location of image subsets and profiles are identified in Figure 3.8.

90

Figure 3.6d. Planimetric view of the dominant flow regimes along the Western Lobe. Centerline profiles are superimposed on a subset of the 1999 Landsat7 ETM+ satellite imagery. Location of image subsets and profiles are identified in Figure 3.8.
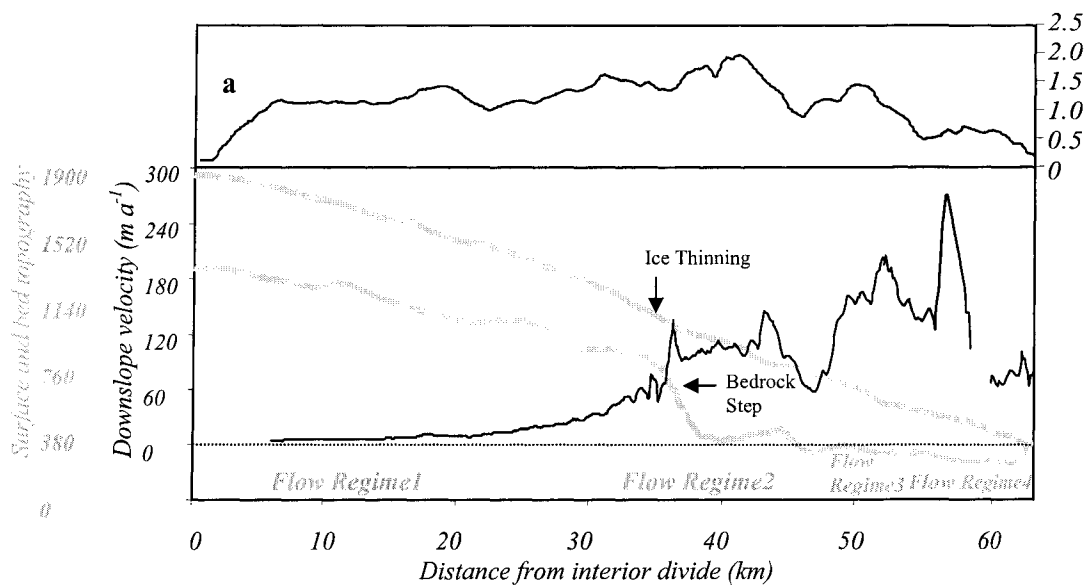
Figure 3.7a. Profiles of driving stress, surface and bed topography, and downslope velocity along the North Croker Bay Glacier. Gaps in the downslope velocity profile between km 0 – 5 and km 58 – 59 represent sections where InSAR data could not be derived.

92
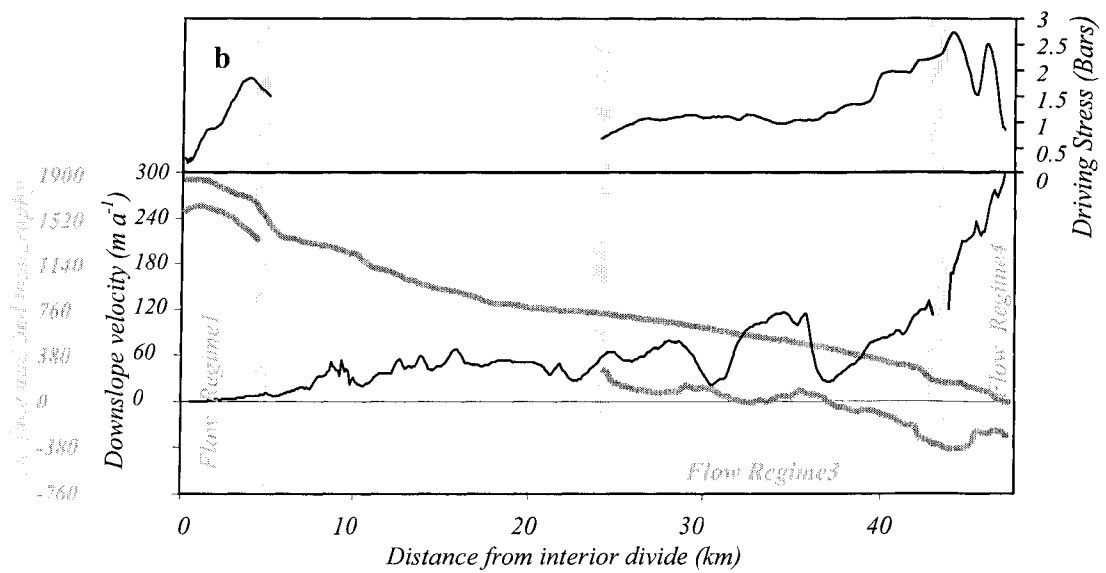
Figure 3.7b. Profiles of driving stress, surface and bed topography, and downslope velocity along the Belcher Glacier. The absence of bed topography data between km 4 − 24 precluded calculation of τ_d throughout this zone.

93
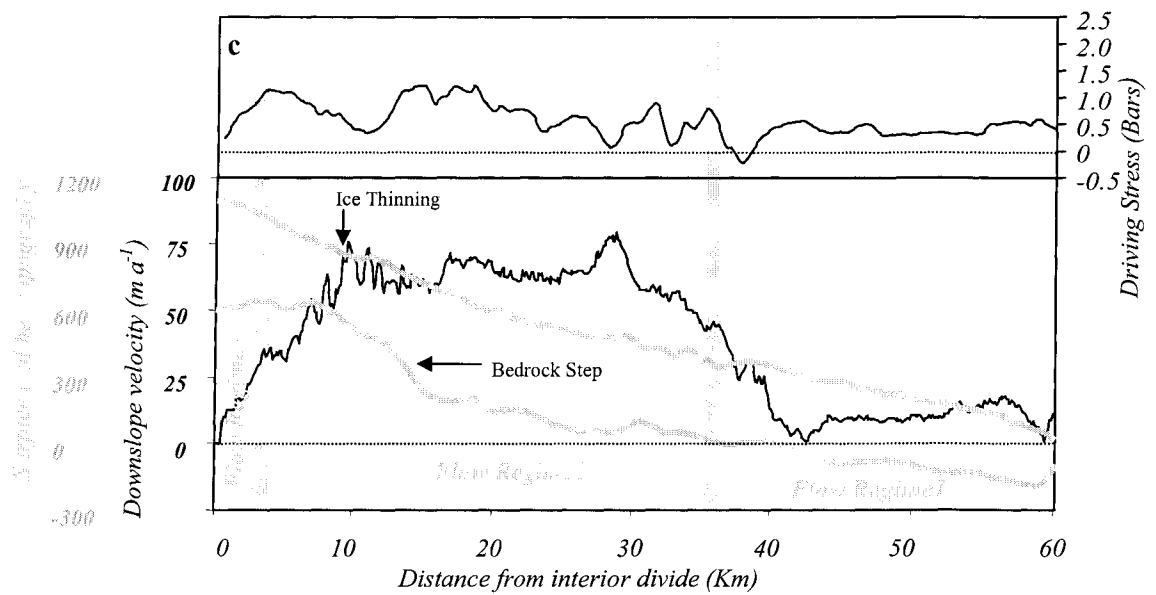
Figure 3.7c. Profiles of driving stress, surface and bed topography, and downslope velocity along the Southeast 1 Glacier.

94
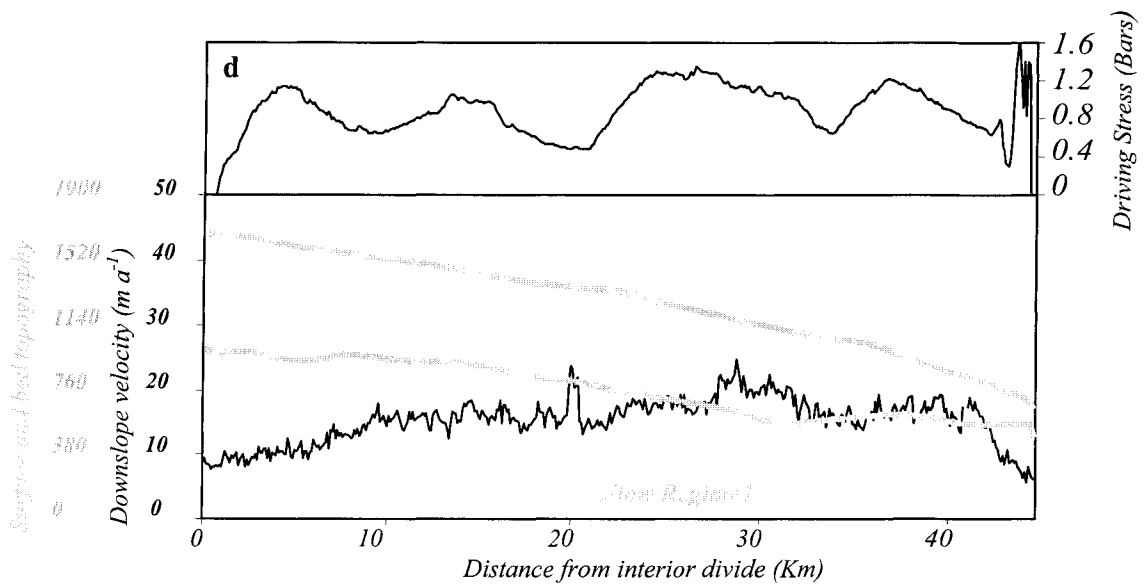
Figure3.7d. Profiles of driving stress, surface and bed topography, and downslope velocity along the Western Lobe.

95
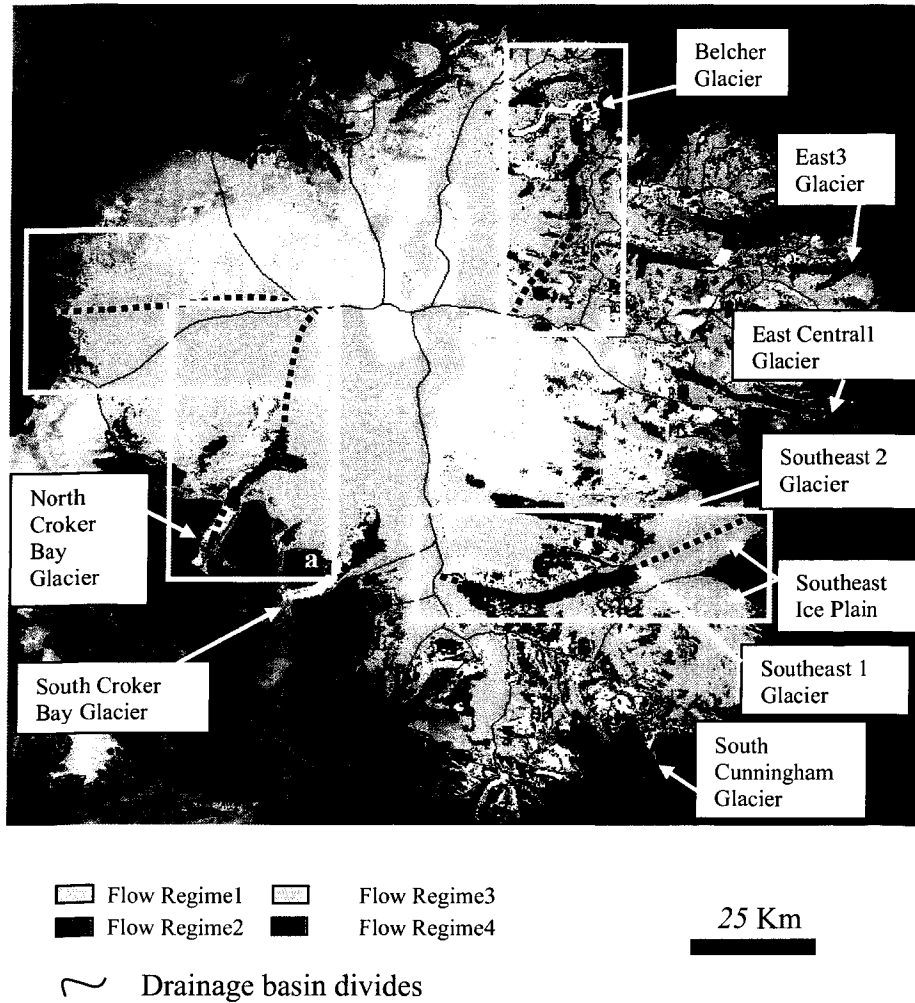
Figure 3.8. Mapped distribution of classified flow regimes across the Devon Island ice Cap. White boxes indicate the location of image subsets and centreline profiles in Figure 3.6.

96
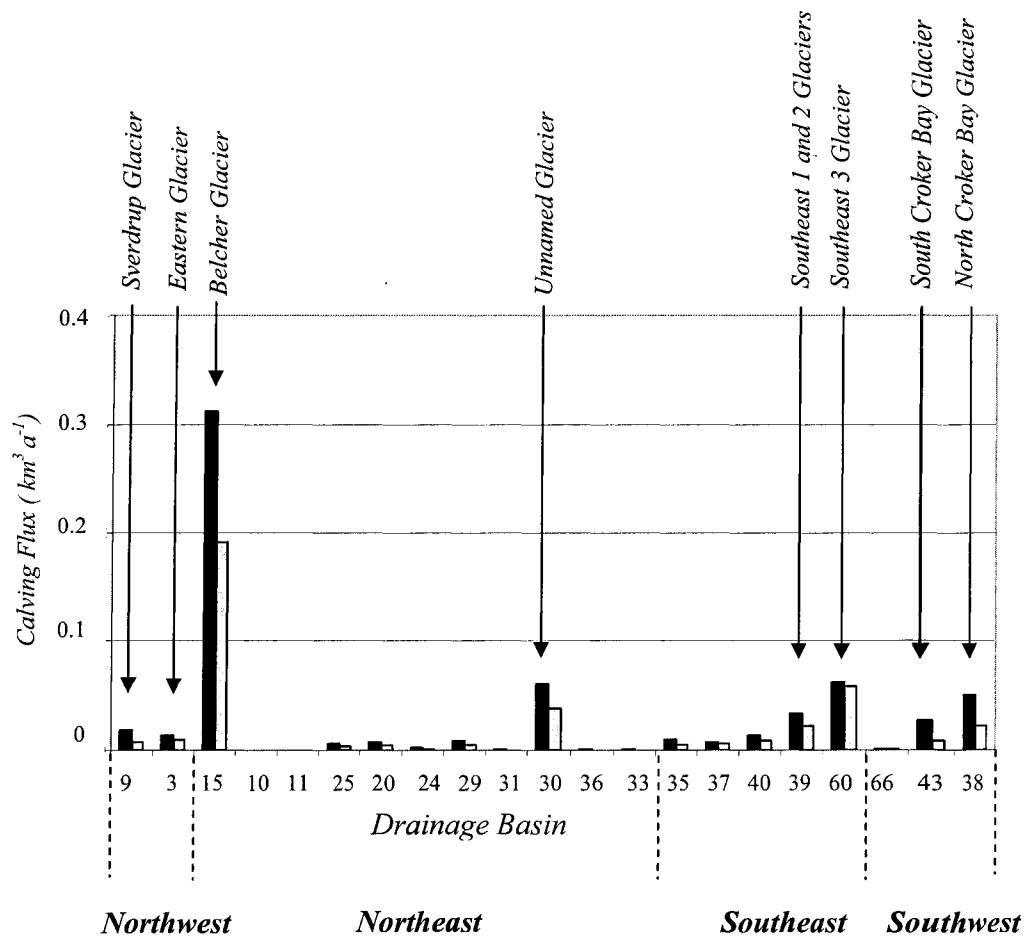
Figure 3.9. Distribution of iceberg calving rates on the Devon Island ice cap. Solid bars represent the upper calving flux estimate and the shaded bars represent the lower calving flux estimate.

97

CHAPTER 4

RECENT CHANGES IN THICKNESS OF THE DEVON ISLAND

ICE CAP

4.1 INTRODUCTION

Knowledge of the rates of thickness change of the Earth's large ice masses is crucial to understanding their state of balance and contribution to global sea level change. Combined, the Greenland and Antarctic ice sheets would raise sea-level by > 80 m if they were to disintegrate completely. Smaller ice caps and glaciers however pose a more immediate concern, and may have accounted for a significant fraction (> 50%) of total sea-level rise over the last century (Dyurgerov and Meier, 2005). In order to better quantify the current contribution of these ice masses to sea level rise and understand how they may respond to future climate warming that is predicted for the high northern latitudes (IPCC, 2001), it is essential to quantify their current rates of volume change and determine the main factors (i.e. changes in ice dynamics, net surface mass balance, iceberg calving) controlling the changes observed.

The Devon Island ice cap occupies ~14,000 km^2 of the eastern half of Devon Island (Figure 4.1), which makes it one of the largest ice masses in the Canadian high Arctic. This ice cap derives a significant proportion of its accumulation from the North Open Water Polynya in Baffin Bay, which is the primary precipitation source for ice in this region (Koerner, 1977). According to field measurements collected by Dr. R. Koerner of the Geological Survey of Canada, the average mass balance of the

98

northwest sector of the Devon Island ice cap (Figure 4.2) over the period 1961-2001

was –0.086 mWe a^{-1} (G. Cogley, personal communication, 2005). Inter-annual

variations in net mass balance on the ice cap, however, arise mainly from variations in

the summer balance (Koerner, 2002). Negative mass balance years tend to be

associated with anticyclonic conditions and the northward shift of the arctic front.

Conversely, melt is suppressed and snow accumulates in years when circulation over

the ice cap is dominated by the Baffin Bay Cyclone (Alt, 1978). Positive mass

balance can also occur in summers when snow is deposited by lows that track south

and southeast across the islands from the polar ocean (Alt, 1987). The duration of the

summer melt season on the ice cap is well correlated with the July 500 hPa height over

the ice cap (Wang and others, 2005).

An estimate of volume change of the Devon Island ice cap based primarily on

in situ mass balance data collected in the northwest sector of the ice cap by Dr. R.

Koerner between 1961 and 1991 indicates that the main part of the ice cap has

decreased in volume by ~42 km^3 water equivalent. This value however is a minimum

estimate as it does not account for losses due to iceberg calving. A similar estimate of

volume loss of ~32 km^3 water equivalent over the past 40 years was obtained through

extrapolation of surface elevation changes measured by repeat laser altimetry

measurements performed by NASA along 4 transects across the ice cap (Figure 4.2) in

1995 and 2000 (Abdalati and others, 2004). Both of these sets of observations are

invaluable for calibrating regional scale measurements but, due to their restricted areal

coverage, large uncertainties may be introduced when they are extrapolated to

compute volume change for the Devon Island ice cap as a whole.

99

Comparison of the ice margin identified on 1960 aerial photography and on 1999 Landsat ETM+ imagery highlights significant spatial variability in the rate and sign of fluctuations of the margins of the Devon Island ice cap (Burgess and Sharp, 2004). The dominant changes identified include retreat of most of the larger tidewater glaciers (by as much as ~ 3 km in the southeast region) and advance of the western margin by ~ 120 m. The net volume decrease of the main ice cap (excluding the stagnant southwest arm) was calculated to be 48 ± 5 km^3 using volume-area scaling techniques (Burgess and Sharp, 2004). Using a combination of ice-core derived estimates of net accumulation and melt modeling, Mair and others (2004) estimated the net volume reduction of the ice cap to be ~59.2 ± 26.6 km^3 due to net surface mass balance alone. They identified the southeast region as the area where the greatest volume changes appear to be occurring. Combined with mass loss due to iceberg calving (20.5 ± 4.7 km^3 between 1960 and 1999; Burgess and others, in press), it is estimated that total loss from the Devon Island ice cap over the past 40 years may be as high as ~ -79 km^3. It is evident that there is significant variability in the magnitude and sign of volume change across the Devon Island ice cap, and, accounting for this variability results in estimates of volume change that are consistently larger than those derived from 'localized' mass balance observations and altimetry.

In this study, estimates of the long term (40 years) rates of thickness change of the Devon Island ice cap, Nunavut, Canada, are derived using several approaches. First, average rates of thickness change were calculated for the accumulation zones of individual drainage basins as the area weighted difference between the measured ice flux and balance flux across the equilibrium line (ELA). For the ablation zones of

100

these basins, average rates of thickness change were calculated from the difference between the mass flux across the ELA, and the sum of the volume losses by surface mass balance and iceberg calving. Second, *in situ* measurements of rates of thickness change were obtained for 3 sites throughout the southwest region of the ice cap using (a) the 'coffee can' technique developed by Hamilton and Whillans (2000), and (b) measurements of the 40 year surface mass balance and vertical strain across a 1 km x 1 km grid. Third, thickness change rates were derived along 6 major outlet glaciers (the Belcher, Unnamed, North and South Croker Bay, and the Southeast 1 and 2 Glaciers) as a function of the difference in ice flux between successive gates spaced 5-8 km apart, and the average net surface mass balance between flux gate locations. Along the Belcher Glacier alone, direct measurements of surface lowering were quantified by comparing surface elevation values obtained from 1960's aerial photography with values obtained from radio-echo sounding surveys in 2000.

These measurements should allow us to answer important questions concerning the state of balance of the Devon Island ice cap. These include: (i) What is the magnitude of volume loss from the ice cap since 1960 and how much does this contribute to global sea-level change? (ii) How is volume change distributed between drainage basins? (iii) Is area change at the scale of individual drainage basins a good guide to volume change? (iv) How is volume change distributed between the accumulation and ablation zones? (v) Are there distinctive longitudinal patterns of elevation change along outlet glaciers, and how do these patterns compare with those at the basin wide scale? (vi) Do these patterns reflect enhanced terminal thinning in basins where iceberg calving is an important mass sink? and (vii) Is there evidence

101

from the patterns of thickness change, either within whole basins or along outlet glaciers, for recent changes in flow dynamics that have resulted in rates of thinning/thickening that are not easily accounted for by changes in surface mass balance alone?

4.2 DATASETS

Calculations of rates of thickness change were made possible by the recent development of ice thickness, topography, surface mass balance, and ice surface velocity datasets for the Devon Island ice cap. Ice thickness data were derived from airborne radio-echo sounding measurements obtained during the spring of 2000 (Dowdeswell and others, 2004). The ice thickness data are accurate to $\pm$ 10 m whereas the ice surface elevation values are accurate to $\pm$ 7 m. Surface mass balance data for the accumulation zone were derived from interpolation of long-term net accumulation rates measured at eight sites in the accumulation area of the ice cap. Net accumulation at each site was determined using down-borehole ^{137}Cs gamma-ray spectrometry to detect the depth to the 1963 "bomb" layer that was deposited as fallout from atmospheric thermonuclear weapons testing in the Russian high Arctic in 1962 (Mair and others, 2004). Mean net accumulation rates over the 37 year period (1963 – 2000) were calculated as a function of depth to the reference layer and the density of the overlying firn. Firn density profiles were determined by weighing and measuring individual core segments as they were extracted from each borehole. Based on field measurements of net accumulation performed at 3 sites in the southern region of the

102

ice cap in Spring 2005, the accumulation grid developed by Mair and others (2004) was modified to take into account accumulation rates that locally exceeded those shown by Mair and others (2004) by a factor of 1.5. The area affected encompassed the source regions of the South Croker Bay, Southeast 1, and Southeast2 Glaciers (see Figure 4.2). This modification had the effect of raising the mass balance of basin 38 by ~2.5% and basin 39 by ~6%, resulting in a net increase of 0.017 km^3 a^{-1} in the mass balance of the whole ice cap. For the ablation zone, the net balance was calculated using a positive degree-day model driven by air temperature data from Resolute Bay, Nunavut, corrected for conditions specific to the ice cap (Mair and others, 2004). Surface velocity fields for the ice cap were derived by satellite radar interferometry (InSAR) using ascending pass ERS 1 and 2 data obtained during the tandem mode mission in the spring of 1996 and the 3-day repeat pass mission acquired in February, 1992 (Burgess and others, in press). Errors associated with these data are $\pm$ 3 m a^{-1} throughout the interior regions of the ice cap, and from 10 – 30% of the measured velocity along the fast flowing outlet glaciers depending on the angle between the satellite look direction and the direction of ice flow. Since these data represent ice velocities over a 1 – 3 day time interval, uncertainties related to possible temporal variations in flow rates also exist when comparing InSAR derived ice fluxes with balance flux values derived from the 37 year accumulation values as described above. The lack of data on seasonal variability in rates of flow of the Devon Island ice cap precludes us from quantifying this uncertainty. Finally, the surface topography of the ice cap was obtained from the Canadian Digital Elevation Dataset (CDED), which was produced from 1:60,000 aerial photography acquired in 1959/1960 by the Government

103

of Canada. Errors associated with limited bedrock control, problems with photogrammetric data capture over low contrast regions, and conversion of data from analogue to digital format result in surface elevation errors of ±50 m along the main outlet glaciers and up to ±100 m throughout the ice cap interior. A second DEM of the Belcher Glacier was recently produced from this photography along the Belcher Glacier only. Ground control points obtained from differential GPS (DGPS) measurements in the Spring of 2005 indicate that these data are accurate to ± 2m.

4.3 METHODS

4.3.1 Basin-wide thickness changes

Average thickness changes were calculated for the accumulation and ablation zones of 10 major ($>\sim100$ km^2) drainage basins, excluding the western lobe of the ice cap, for which InSAR derived surface velocities are sparse. Basins for which the accumulation area comprises < 5% of the total basin area (basins 60, 37, and 25) were considered to consist of ablation zones only.

For the accumulation zone, the mean rate of thickness change was calculated from the difference between the balance and observed fluxes across the ELA:

$$\partial H / \partial t_{acc} = ((Q_{Balance} - Q_{InSAR}) / A_{acc}) \qquad (1)$$

where $\quad Q_{balance} = HV_{Balance}\, ELA_{length}$ $\qquad\qquad\qquad$ (2)

and $\quad Q_{InSAR} = HV_{InSAR}\, ELA_{length}$ $\qquad\qquad\qquad$ (3)

104

$V_{balance}$ is the balance velocity (the depth averaged flow rate required to maintain profile equilibrium in an ice mass [Paterson, 1994]; km a^{-1}), V_{InSAR} is the down-slope surface velocity derived from satellite radar interferometry (km a^{-1}) (Burgess and others, in press), and A_{acc} is the area of the accumulation zone within a particular basin (km^2). HV_{InSAR} ($HV_{balance}$) (km^2 a^{-1}) is the average of all grid cells along the ELA within a particular basin, where each grid cell is the product of V_{InSAR} ($V_{Balance}$) and ice thickness (H) (km) at that grid cell location. The long term ELA was estimated as 950 meters a.s.l. for the northwest, 800 meters a.s.l. for the southeast, and 875 meters a.s.l. for both the northeast and southwest regions (after Koerner, 1970). The boundaries of the ELA regions are indicated in Figure 4.3.

$V_{balance}$ was derived from the model of Budd and Warner (1994) using surface mass balance (Mair and others, 2004) modified as described above, ice thickness (Dowdeswell and others, 2004), and surface topography (CDED), as input data. The pattern of glacier flow produced by the balance velocity model (Figure 4.4) closely reflects the InSAR derived flow pattern (Figure 4.2), with the exception of 4 flow features that are not observed in the InSAR data (identified as A, B, C, and D in Figure 4.4). Since these features are embedded within much larger drainage basins, the misrouting of flow along them would not affect balance flux calculations at the basin scale. Flow unit A, however, appears to divert modeled flux from the South Croker Bay Glacier. Flow unit D is located in the southeast region and drains directly south from the summit region to join up with the Southeast2 Glacier approximately 30 km up glacier from its terminus. Discontinuous patches of enhanced velocity in the InSAR

105

data along the path of this feature support the existence of a major flow unit in this area (Unidentified Glacier – Figure 4.2). It is likely that this feature was not fully resolved by the InSAR data because ice flow in this region is nearly perpendicular to the look angle of the satellite ($52°$). Despite these differences, the overall similarity between the flow structures produced by the balance velocity model and the InSAR measurements provides confidence in the comparability of these data.

In order to make V_{InSAR}, which is a surface quantity, compatible with $V_{balance}$, which is a depth-averaged quantity, V_{InSAR} was multiplied by 0.8 over regions where the predominant mode of ice flow is inferred to be by internal deformation. This value is a conservative approximation based on the ratio of surface velocity to velocity measurements at depth measured near the summit of the Devon Island ice cap by Reeh and Paterson (1988). V_{InSAR} was assumed to be equal to the depth averaged velocity in areas where the predominant mode of ice flow is inferred to be by sliding. Although internal deformation may still occur where basal sliding dominates, this contribution is expected to be small (< 5%) relative to the uncertainties in the InSAR derived surface velocities (15 – 20%), which are accounted for in the calculations of ice flux. Inferences of whether ice movement is predominantly by internal deformation or sliding are based on an analysis of the relationship between the ratio of velocity to ice thickness (V/H) and the driving stress (Burgess and others, in press).

The total error associated with the application of equation 1 to each basin was estimated as:

$$\partial H / \partial t_{acc\_error} = (\sqrt{\Delta Q_{balance}{}^2 + \Delta Q_{InSAR}{}^2}) / A_{acc} \qquad (4)$$

where $\Delta Q_{balance}$ (ΔQ_{InSAR}) was calculated as the difference between an upper estimate of flux ($Q_{balance\_upper}$ (Q_{InSAR_upper})) and the best estimate of flux ($Q_{balance}$ (Q_{InSAR})) (see Table 1). $Q_{balance\_upper}$ was derived as the product of the upper estimate of ice thickness (H_{+10m}) and $V_{balance\_upper}$, where $V_{balance\_upper}$ was produced from the balance flux model using upper estimates of net surface mass balance ($b + b_{error}$; Mair and others, 2004) and H_{+10m}. Q_{InSAR_upper} was derived as the product of H_{+10m} and V_{InSAR_upper}, where V_{InSAR_upper} was derived by adding the estimated ice velocity error (specified in Burgess and others, in press), to V_{InSAR}. Error associated with A_{acc} had a negligible effect on the final value of $\partial H/\partial t_{acc}$.

For the ablation zones, the average thickness change was calculated from the difference between the measured flux across the ELA and the sum of the mass losses by surface ablation and calving:

$$\partial H/\partial t_{abl} = (Q_{InSAR} + Vol_{abl} + Q_{calving}) / Area_{abl} \tag{5}$$

where Vol_{abl} (see Table 1) is the volumetric net balance of the ablation zone as obtained from Mair and others (2004), $Q_{calving}$ (see Table 1) is the volume of ice lost by iceberg calving as computed by Burgess and others (in press), and $Area_{abl}$ is the total area of the ablation zone. As indicated in Table 1, mass loss due to net surface ablation and iceberg calving are negative values.

Since a positive net balance could have the effect of glacier advance as well as thickening, the apparent thickness change estimate for a basin experiencing growth was adjusted by the formula:

$$\partial H/\partial t_{abl\_advance} = \partial H/\partial t_{abl} - (Vol_{adv} / Area_{abl}) \tag{6}$$

where Vol_{abl} is the average annual volume increase due to advance of the basin since 1960 (Burgess and Sharp, 2004). This correction factor was applied to basin 38, which is the only ablation zone that has experienced growth over the past 40 years. Basin-wide thickness change rates of ablation zones with a negative balance are not affected by volume loss at the margin.

The total error associated with equation 5 was calculated as:

$$\partial H/\partial t_{abl\_error} = \left(\sqrt{\Delta Q_{InSAR}^2 + \Delta Vol_{abl}^2 + \Delta Q_{calving}^2} \right) / Area_{abl} \tag{7}$$

where ΔVol_{adv} was obtained from Mair and others (2004) and $\Delta Q_{calving}$ was obtained from Burgess and others (in press). Errors in $Area_{abl}$ had an insignificant effect on the estimate of $\partial H/\partial t_{abl.}$.

4.3.2 *In situ* measurements of thickness change

108

In situ measurements of ice thickness change were obtained at 3 locations (Site 1 – 1800 m, Site 2 – 1400 m, and Site 3 – 1000 m a.s.l.) in the southwest region of the ice cap in 2004 and 2005 (see Figure 4.2 for locations). These measurements, which were derived using two separate methods, provide independent checks on thickness change estimates produced using remote sensing techniques.

The first method was calculated from the thickness change equation:

$$\partial H / \partial t_{thickchg} = b_{40} - F \ (H \ (\dot{\varepsilon}_x + \dot{\varepsilon}_y) + u \ (\partial H / \partial x)) \tag{8}$$

(Paterson, 1994;pg 257)

where b_{40} is the accumulation rate averaged over a 40 year time period (1963 – 2003) measured using down borehole ^{137}Cs gamma spectrometry and firn core density profiling as described above. The majority of ice core segments extracted from all 3 sites were intact ranging from 30 – 50 cm in length with a diameter assumed to be 2 mm smaller than the inside diameter of the ice core barrel. Density measurements from all sites were estimated to be accurate to ~ ± 5% based on core length measurement and weight. $\dot{\varepsilon}_x$ and $\dot{\varepsilon}_y$ are surface strain rates in the along flow and transverse to flow directions respectively. Strain was calculated from the magnitude and direction of displacement between spring 2004 and 2005 of 4 stakes arranged in a 1 km x 1 km grid determined using repeat differential global positioning system (DGPS) techniques. F was assigned a value of 0.8 in order to relate strain rates measured at the ice cap surface to depth-averaged values. *u* is the downslope velocity

109

derived from repeat DGPS stake measurements, and ∂H was calculated over a 1 km

distance (∂x) from the ice thickness grid produced by Dowdeswell and others (2004).

The second method used was the 'coffee can' technique (Hamilton and

Whillans, 2000), which derives the long term rate of thickness change at a single point

according to:

$$\partial H/\partial t_{cc} = (b_{40}/\rho) + z + u\,v \qquad (9)$$

where b_{40} (positive for accumulation) is the net mass balance averaged over the

period from 1963 to 2003, ρ is firn density at the depth of a marker below the surface,

z is the vertical velocity of the ice surface derived from repeat differential GPS

measurements (negative downwards), and v is the slope angle at the ice surface

(negative downwards).

$\partial H/\partial t_{cc}$ is essentially the difference between b and z, where z is corrected for

firn compaction and the downslope component of motion. The validity of this method

relies on the assumption that ρ increases consistently with depth, which implies that b

and v have been relatively constant over the last 40 years or more. This was tested at

each site by assessing whether or not there is a linear relationship between z and $1/\rho$ at

depths of 20, 16, 12, 8, and 4 m, as would be expected from Sorge's Law (Hamilton

and Whillans, 2000). The data from sites 1 and 2 do show such a linear relationship,

indicating that compaction rates have not been significantly influenced by recent

changes in temperature or precipitation. The "coffee-can" method should therefore

result in valid calculations of the rate of thickness change at these locations (Hamilton

110

and Whillans, 2000). The upper 20 m of the ice cap at site 3 was composed entirely of ice with an assumed density of 917 kg m^3. Uncertainties of the resultant 'coffee can' measurements were based primarily on the accuracy of the GPS measurements which was ± 3, 5, and 6 cm a^{-1} in the vertical dimension for sites 1, 2, and 3 respectively.

4.3.3 Thickness changes along major outlet glaciers

Rates of dynamic thickness change were computed along 6 major outlet glaciers that drain the Devon Island ice cap (North and South Croker Bay, Southeast 1 and 2, Unnamed, and Belcher Glaciers) based on the divergence of ice flux between successive flux gates along the glaciers and net surface mass balance between these gates:

$$\partial H/\partial t_{Glacier} = (Q_{InSARg1} - Q_{InSARg2} + Vol_{bg1\_g2}) \; / \; (Area_{g1\_g2}) \tag{10}$$

where g1 and g2 are flux gates positioned on the up- and down-glacier ends of 5 − 8 km long glacier segments. Flux gates were chosen to enclose sections of the glacier that were relatively homogeneous in terms of lateral constraints along the margins. As with equation (3), Q_{InSAR} (m^3 a^{-1}) was derived as the product between HV_{InSAR} (m^2 a^{-1}) and the glacier width ($Width_{Glacier}$) (m), where HV_{InSAR} was obtained as an average value across $Width_{Glacier}$ at each flux gate location. $Area_{g1\_g2}$ (m^2) is the area between g1 and g2, and Vol_{bg1_g2} (m^3 a^{-1}) is the mass gain or loss derived as the product between the average net surface mass balance between flux gates (as obtained from Mair and others, 2004) and $Area_{g1\_g2}$.

111

The error associated with equation 10 was calculated as:

$$\Delta\partial H/\partial t_{\text{Glacier}} = (\sqrt{\Delta Q_{g1}^{\,2} + \Delta Q_{g2}^{\,2} + \Delta Vol_{bg1\_g2}^{\,2}}\,) / \text{Area}_{g1\_g2} \tag{11}$$

where

$$\Delta Q = Q(\sqrt{\frac{\Delta Width^2}{Width} + \frac{\Delta H^2}{H} + \frac{\Delta V_{InSAR}^{\,2}}{V_{InSAR}}}\,) \tag{12}$$

and

$$\Delta Vol_{smbg1\_g2} = \Delta b\text{Area}_{g1\_g2} \tag{13}$$

where Δb was obtained from Mair and others (2004).

Thickness change could only be computed for the lower 16 km of the Belcher Glacier due to missing or unreliable ice thickness measurements along much of the upper sections of the glacier (Burgess and others, 2005). Direct measures of surface elevation change were therefore computed along the entire length of this glacier as the difference between values derived from aerial photography obtained by the Government of Canada in 1960 (ELEV$_{1960}$; $\pm$ 2 m), and those derived from radio-echo

112

sounding data obtained by Dowdeswell and others (2004) in 2000 ($ELEV_{2000}$; ± 7 m). The accuracy of these measurements, estimated as the square root of the sum of the errors squared divided by the 40-year time interval between dataset acquisitions, is ± 0.18 m a^{-1}.

4.4 RESULTS

4.4.1 What is the post 1960 volume change for the whole ice cap and how much does this contribute to global sea level?

Volume loss derived from the basin-wide calculations was -53.2 ±6 km^3 water equivalent, (~ -4.3 mWe), averaged across the main portion of the Devon Island ice cap between 1960 and 1999. The basins on which this estimate is based constitute 78% of the main part of the ice cap. The volume loss from the remaining 22% of the ice cap was estimated as the sum of the volume losses from these basins by surface melt (-16.5 ±2 km^3 water equivalent; Mair and others, 2004) and iceberg calving (-0.014 ±0.007 km^3 water equivalent; Burgess and others, in press). This equates to a total loss of -67 ± 7 km^3 water equivalent (~ -5.6 mWe) between 1960 and 1999, or an average annual loss rate of -1.7 km^3 a^{-1} water equivalent (~ -0.14 mWe a^{-1}) over this period of time. Assuming that the total area of the Earth's oceans is 360 x 10^6 km^2, it is estimated that the Devon Island ice cap has contributed 0.19 ± 0.02 mm to global sea level between 1960 and 1999. This amounts to ~1% of the world-wide input from small ice caps and glaciers based on the current estimated contribution from these

113

sources to be ~0.59 mm a^{-1} averaged over the past 43 years (Dyurgerov and Meier, 2005).

4.4.2 How is volume change distributed between basins?

All basins examined in this study experienced net volume loss between 1960 and 1999, except for basin 38, where volume increased by 6.94 ±1.32 km^3 of ice over this period of time (see Table 2). The greatest losses were from basins 39 and 60 in the southeast region, where ice volume decreased by 17.18 ±1.23 km^3 and 20.75 ±0.26 km^3 respectively. Ice volume also decreased significantly in Basin 15 (by 12.29 ±1.44 km^3) in the northeast region. Basins 9, 25, 30, 37, 40, and 3 experienced an average net loss of 2.4 ± 0.25 km^3 of ice. Among these basins, the highest ice volume loss occurred from basin 30 (4.29 ±0.18 km^3).

4.4.3 How are thickness and volume changes distributed between accumulation and ablation areas and what are the factors controlling the changes observed?

Basin-wide estimates indicate that the accumulation zones of the northern basins (9, 3, and 15) are more-or-less in balance, while the accumulation zones of basins 30 and 40 along the eastern margin are slightly negative (Figure 4.3; Table 1). Basins 38 and 39 in the southern region appear to be thinning throughout their accumulation zones at rates of -0.12 ± 0.12 m a^{-1} and -0.23 ± 0.11 m a^{-1} respectively (Figure 4.3). *In situ* thickness change measurements indicating equilibrium conditions at Site 1 and slight thinning at Site 2 in the southwest accumulation zone (Table 3) agree closely with the basin wide values in this region. Significant thinning derived

114

across the 1 x 1 km grid at Site 3 (-0.23 ± 0.07 m a^{-1}) however is a result of ice drawdown due to accelerated flow towards the South Croker Bay Glacier. With the exception of this value, the *in situ* measurements are likely representative of thickness change over a broader area because they are located in regions of low dynamic activity (<15 m a^{-1}) where seasonal velocity fluctuations are minimal (<1 m a^{-1}). In addition, the horizontal mass balance gradient between the sites is shallow (0.11 kg m^{-2} a^{-1} m^{-1} [in elevation]).

The average rates of thickness change for the ablation zones of basin 39 in the southeast region, and basin 3 along the north coast are near zero (Figure 4.3). In these basins, mass loss due to surface melt is replaced almost entirely by influx across the ELA (see Table 1). In basin 38, flux across the ELA exceeds mass loss due to surface melt resulting in net thickening of the southwest ablation zone by 0.55 ± 0.22 m a^{-1}. The ablation zones of the remaining basins in the north and northeast regions (9, 15, and 30) are thinning by ~ -0.14, -0.62, and -0.28 m a^{-1} of ice respectively (Figure 4.3). Surface lowering by ~ -0.30 m a^{-1}, as detected along the NASA_EW2 (Figure 4.2) in basin 40, agrees with the basin-wide thinning rate of ~ -0.28 m a^{-1} at this location. Basins 9, 30, and 40 are losing mass primarily to surface melt alone (Table 1) whereas more than half of the annual mass loss within basin 15 is due to iceberg calving (~ -0.25 km^3 a^{-1} of ice) (Burgess and others, in press). Basins 25, 37, and 60 are situated almost entirely below the ELA and experience net losses of ~ -0.045, -0.053, and -0.53 km^3 a^{-1} of ice respectively due primarily to surface melt alone (see Table 1).

115

4.4.4 Is area change at the basin scale a good guide to volume change?

Volume change derived from areal change measurements for the Devon Island ice cap as a whole (Burgess and Sharp, 2004) is ~20 km^3 less than that estimated in this study. There is however a relatively close relationship ($r^2 = 0.8$) among the individual basins. Volume changes estimated using the 2 methods agree to within 1.2, 1.16, and 0.54 km^3 for basins 3, 30, and 37, and to within measurement uncertainty for basins 9, 25, and 40. The volume-area scaling technique therefore appears to provide a reasonable estimate of volume change for these basins. This is not, however, the case for basins 39, 60, 38, and 15 where estimates of volume change based on changes in area are lower than the values calculated in this study by 11.73, 6.39, 3.82, and 2.75 km^3 respectively (see Table 2). Three of these basins appear to be experiencing significant thickness change due to changes in ice dynamics within either their accumulation (basin 39) or ablation zones (basins 15 and 38) (see below), while basin 60 is thinning throughout due to primarily surface melt alone. In all of these cases, volume loss is not proportionally reflected at the ice cap margin.

4.4.5 Do outlet glaciers have distinctive longitudinal patterns of thickness change and how do these patterns compare with thickness changes at the basin wide scale?

Direct observations of surface elevation change along the Belcher Glacier indicate pronounced lowering by ~ -0.5 m a^{-1} within ~7 km of the head of this glacier and by ~ -0.6 m a^{-1} within 5 km of the terminus. Increases in the elevation of the ice surface by up to 1m a^{-1} at the ice front (as derived from the 1960-2000 elevation data) contradict thinning by ~ -2 m a^{-1} within ~10 km inland of the terminus as derived from

116

the flux difference method (Figure 4.5). This discrepancy may reflect time variant flow rates of this glacier that are not accounted for by the velocity measurements derived in this study. Close agreement between the annual rate of surface lowering obtained in this study, and the rate of surface lowering derived from the NASA airborne surveys between km 9 and 17 (NASA_BEL; Figure 4.2), indicate that the NASA measurements are representative of decadal scale rates of thickness change at this location. Basin-wide thinning by -0.62 ± 0.14 m a^{-1} of the ablation zone in basin 15 is in agreement with the rate of surface lowering derived from direct methods (-0.3 ± 0.2 m a^{-1}), averaged along the entire Belcher Glacier. Net thinning along the Belcher Glacier, which occupies ~37% of the ablation zone of basin 15, is therefore likely similar or slightly less than the changes that are occurring throughout the remainder of this ablation zone. The Unnamed Glacier appears to be thinning along most of its length with maximum rates of ~ -1.2 m a^{-1} which occur ~18 km from the ice front, decreasing to ~ -0.5 m a^{-1} ~10 km from the terminus. Rates of thickness change at ~15 and 7 km from the terminus however are indistingushable from zero (Figure 4.6). The lack of velocity data within 4 km of the terminus of this glacier precludes calculation of thickness change rates within this zone. In the southwest region, thickness changes along the upper ~12 km of the North and South Croker Bay Glaciers, which occupy only ~18% of the ablation zone of basin 38, are indistinguishable from zero. Thickening by up to ~2 m a^{-1} along the lower reaches of the North Croker Bay glacier (<400 m a.s.l.; Figure 4.7) is consistent with, but greater than, the pattern of thickening that prevails throughout the ablation zone of this basin (~0.55 ± 0.22 m a^{-1}). By contrast, thinning by ~ -2 m a^{-1} prevails throughout the lower reaches (<400 m a.s.l.)

117

of the South Croker Bay Glacier (Figure 4.8). Large uncertainties in the rate of thinning at the terminus of the South Croker Bay Glacier indicate that thinning at this location could range from ~ -0.5 to –3 m a^{-1}. In the southeast region (basin 39), thinning by up to ~ -1 m a^{-1} along the upper ~15 km of the Southeast 1 outlet glacier (Figure 4.9) is consistent with, but greater than, basin wide thinning of this accumulation zone by –0.23 ± 0.12 m a^{-1} (Figure 4.3). Thickening by up to ~1 m a^{-1} occurs ~20 km inland from the terminus along the Southeast 1 and 2 outlet glaciers where surface velocities decrease to < ~10 m a^{-1} (Figure 4.11). The Southeast 1 and 2 Glaciers occupy 50% of the ablation zone of this basin and represent the main pathways along which a sufficient supply of ice is delivered to the ablation zone to offset mass loss due to surface melt in this region.

4.4.6 Do thickness change patterns near the glacier termini reflect enhanced thinning where iceberg calving is an important sink?

The ice front associated with the Belcher Glacier is the most actively calving region on the Devon Island ice cap, discharging ~0.25 km^3 of ice annually (Burgess and others, in press). Flux imbalance calculations along the last 10 km of this glacier indicate apparent dynamic thinning by ~ 2 m a^{-1} at this terminus (Figure 4.5). Direct observations however indicate that net ice surface lowering (only ~ -0.6 m a^{-1} averaged over the past 40 years) is confined to between 6 and 7 km inland from the terminus while the region immediately behind the ice front is thickening. Despite this discrepancy, thinning, as indicated in both datasets, may be related to dynamic downdraw due to increasing ice flux towards the calving front. Unfortunately, velocity

118

data is not available within 4 km of the Unnamed Glacier, which is the second most important calving glacier on the Devon Island ice cap discharging ~0.04 km³ of ice annually. Intense transverse crevassing associated with this ice front however indicates that longitudinal extension, and possible dynamic thinning throughout this zone is occurring.

4.4.7 Is there evidence from the patterns of thickness change either within whole basins or along outlet glaciers for recent changes in flow dynamics that have resulted in rates of thinning/thickening that are not easily accounted for by surface mass balance?

It seems likely that thinning by -0.23 ± 0.11 m a^{-1} throughout the accumulation zone of basin 39 (where the average net surface balance is ~ 0.17 m a^{-1}) is the result of a recent increase in the rate of ice flow from this region. This increased flow is likely to have affected the upper region of the Southeast 1 Glacier (and possibly the Southeast 2 Glacier) where thinning currently occurs within ~ 5 km of the ice divide (Figure 4.9). In addition, it is evident from the balance velocity map that 'fast' glacier flow may extend to within ~10 km of the interior northern divide along flow unit D and a second flow unit to west of this feature (Figure 4.4). The relatively high number of "ice streams" that drain the accumulation zone of this basin may make it more sensitive to changes in ice dynamics than regions than are drained by sheet flow alone.

High ice fluxes across the ELA within basin 38 result in dynamic thickening of the ablation zone in this basin by ~0.55 ±0.22 m a^{-1}. Thinning by $\sim$ -2 m a^{-1} below ~400 m a.s.l. along the South Croker Bay Glacier is also attributable to changes in ice

119

dynamics as average surface ablation rates throughout this section are $\sim$ -0.5m a^{-1}. Conversely, dynamic thickening by $\sim$2 m a^{-1} occurs along the lower reaches of the North Croker Bay Glacier where net surface ablation rates are also $\sim$ -0.5m a^{-1}.

Dynamically induced thickening by up to $\sim$1 m a^{-1} occurs $\sim$20 km inland of the terminus of the Southeast 1 and 2 Glaciers where net surface ablation rates are $\sim$ -0.35 m a^{-1}. Ice flow decelerates dramatically along these glaciers from the topographically confined channel where basal sliding dominates to the non-confined channel where ice is flowing by internal deformation alone (see Figure 4.11). Downstream thickening along these glaciers may also be enhanced by the influx of ice along the margins, which occurs along most of the length of both glaciers. The presence of looped moraines and degraded flow stripes near the terminus (Burgess and others, 2005) (Figure 4.11) suggest that this section was flowing much faster in the past. An overdeepened subglacial trough ($\sim$250 m below sea-level) aligned with the Southeast 1 Glacier indicates a shift in the relative importance of fluxes from the Southeast 1 to Southeast 2 Glaciers, and is consistent with a shutdown of the Southeast 1 Glacier.

Recent increases in the flux rate at the terminus of the Belcher Glacier (Figure 4.5) are likely responsible for apparent dynamically induced thinning by $\sim$ -0.6 to -2 m a^{-1} within 10 km of this calving front. Similarly, pronounced surface lowering by $\sim$ -0.5 m a^{-1} between km 0 and km 7 along this glacier where the onset of 'fast' flow occurs (near the ELA), is also indicative of a dynamically driven changes in ice thickness.

4.5 DISCUSSION

120

Differences in magnitude and/or sign between the rates of thickness change along the major outlet glaciers, and those determined at the drainage basin scale in the southern basins are associated with differences in flow regime within a single drainage basin. This difference is particularly evident in basin 38, where dynamic thinning along the lower reaches of the South Croker Bay Glacier coincides with net thickening of the ablation zone in this basin. Dynamic thinning along the South Croker Bay Glacier is due to longitudinal extension where ice flux increases towards this terminus and ice movement is primarily by sliding at the glacier bed (Burgess and others, 2005). Thickening on the other hand, is most likely to occur throughout the remaining areas where flux rates decrease towards the terrestrially grounded margin. Thickening however also occurs along the lower sections of the North Croker Bay Glacier where reduced flux towards the terminus causes thickening despite basal sliding throughout this zone. Thickening along this section may be caused by increased sidewall drag caused by a sharp reorientation of the bedrock valley. Alternatively, a pro-glacial moraine, or shoal, beyond the terminus of this glacier may be the source of backpressure resulting in longitudinal compression and thickening up glacier from this terminus.

In the ablation zone of basin 39, the large-scale pattern of thickness change is likely one of thickening at higher elevations (600 – 800 m a.s.l.) where ice flux enters from the accumulation zone, and thinning near the margins where the maximum rates of surface ablation (up to -1.9 m a^{-1}; Mair and others, 2004) occur. Significant deviations from this pattern along the Southeast 1 and 2 Glaciers may be due to the fact that the upper reaches of these glaciers have accelerated resulting in thinning near

121

the ELA along the Southeast 1 Glacier (and possibly Southeast 2). Thickening due to longitudinal compression occurs ~20 km inland of the termini of these glaciers where velocities drop sharply, offsetting mass loss at the surface due to melt.

Total volume change of the main part of the Devon Island ice cap of ~32 km^3 water equivalent over the past 40 years, as estimated from extrapolation of the NASA airborne laser altimetry measurements (Abdalati and others, 2004), is significantly lower than our estimate of 67 ± 7 km^3 water equivalent. This may reflect a difference in thinning rates between the period covered by our assessment and that covered by the NASA measurements, but it may also derive from the fact that the NASA transects did not sample the regions where the most significant changes appear to be occurring. As shown in Figure 4.2, the NASA transects are confined primarily to the main east-west divide and the western lobe, which are relatively inactive regions. As indicated in this study, the most significant changes are occurring within the accumulation zone of the southeast region, the lower reaches of the South Croker Glacier, the ablation zone of basin 15 including the Belcher terminus region, and along the low-lying basins that are almost entirely below the ELA, such as basin 60 (see Table 2). Measurements of surface elevation change performed by NASA may be biased towards an underestimate of the total volume change that has actually occurred by excluding these areas in the 1995 and 2000 airborne laser surveys.

In many ways, the pattern of thickness changes observed over the Devon Island ice cap is similar to that measured by NASA's Program for Arctic Regional Climate Assessment (PARCA) over the Greenland ice sheet (Thomas and others, 2001). The broad scale pattern of thickness change over both Greenland and Devon is one of near

122

balance at high elevations and thinning near the ice cap margins (Krabill and others, 2000). Accumulation zone thinning rates of ~ -29 cm a^{-1} and ~ -23 cm a^{-1} do, however, occur in the southeast regions of Greenland (Thomas and others, 2000) and Devon respectively. In both cases, these basins appear to be influenced significantly by the behaviour of the major outlet glaciers that drain them (King Christian IV, Pikiutdleq, and Helheim for Greenland [Abdalati and others, 2001] and Southeast 1 and 2 for Devon). Thinning occurs well into the accumulation zones of the Devon Island ice cap and Greenland along these glaciers. Finally, several major tidewater glaciers that drain the Greenland Ice Sheet (Rink Isbrae, Kangerdlugsuup, Kjer, King Oscar, Humboldt North, Eqalorutsit East, Eqaloriutsit West, Storsstrommen North) have zones of dynamic thinning similar to those along the Belcher and South Croker Bay Glaciers on Devon. As on Greenland, the inferred changes in the dynamics of the Devon Island ice cap appear to contribute significantly to the overall volume change of the ice cap and must be included in measurements of surface elevation change if they are to provide a reliable basis for assessing volume change of the whole ice mass (Abdalati and others, 2001).

4.6 CONCLUSIONS

In this study, rates of long term (~40 years) thickness change computed from direct and indirect methods highlight significant spatial variability in the pattern of thickness change across the Devon Island ice cap. Thinning by -0.23 ± 0.11 m a^{-1} in the southeast accumulation zone may be enhanced by thinning of up to -0.8 m a^{-1}

123

along the upper reaches of the Southeast 1 glacier. Slight thinning by -0.12 ± 0.12 m a⁻¹ occurs in the southwest accumulation zone whereas the accumulation zones of the northern basins are generally in balance. In the ablation zone, near equilibrium conditions in the southeast region prevail where mass loss due to surface melt is offset by dynamic thickening of up to ~1 m a^{-1} 20 km of the terminus of the Southeast 1 and 2 outlet glaciers. Dynamic thickening (thinning) of the North (South) Croker Bay Glaciers in the southwest ablation zone coincides with ablation zone thickening by 0.55 ± 0.22 m a^{-1} in this region. Direct observations of surface elevation change averaged over the past 40 years indicate that localized thinning of ~ -0.7 m a^{-1} ~ 6 km of the terminus of the Belcher Glacier while the ice front is thickening. Thinning by ~ -2 m a^{-1} throughout the last 10 km of this glacier as derived from indirect methods however, suggest that recent changes in dynamics may have enhanced thinning within this zone. Basin-wide volume change calculations indicate that the main portion of the Devon Island ice cap (excluding the southwest arm) decreased by 67 ± 7 km³ water equivalent between 1963 and 2000, resulting in a total contribution of ~0.19 mm to global sea level rise over this period of time.

4.7 REFERENCES

Abdalati, W., W. Krabill, E. Frederick, S. Manizade, C. Martin, J. Sonntag, R. Swift, R. Thomas, W. Wright, and J. Yungel. 2001. Outlet glacier and margin elevation changes: Near-coastal thinning of the Greenland Ice Sheet. *J. Geoph. Res.*, **106**(D24), 33,729-33,741.

Abdalati, W., W. Krabill, E. Frederick, S. Manizade, C. Martin, J. Sonntag, R. Swift, R. Thomas, J. Yungel, and R. Koerner. 2004. Elevation changes of ice caps in the Canadian Arctic Archipelago. *J. Geophys. Res.* **109**, F04007, doi: 1029/2003JF000045.

Alt, B.T. 1978. Synoptic climate controls of mass-balance variations on Devon Island ice cap. *Arc. and Alp. Res.* **10**(1). 61-80.

Alt, B. T., 1987. Developing synoptic analogs for extreme mass balance conditions on Queen Elizabeth Island ice caps. *J. Clim. Appl. Meteorol.,* **26** (12), 1605-1623.

Benham, Toby. 2004. Personal communication. Scott Polar Research Institute, University of Cambridge and Centre for Polar Observation and Modelling, Cambridge, U.K.

Budd, W.F. and R.C. Warner. 1996. A computer scheme for rapid calculations of balance-flux distributions. *Ann. Glaciol.* **23**, 21-27

Burgess, D.O., and M.J. Sharp. 2004. Recent changes in areal extent of the Devon Ice Cap, Nunavut, Canada. *Arctic, Antarctic, and Alpine Research.* **36**(2), 261-271.

Burgess, D.O., M.J. Sharp, D.W.F. Mair, J.A. Dowdeswell, and T.J. Benham. Flow dynamics and iceberg calving rates of the Devon ice cap, Nunavut, Canada. *J Glaciol* . **51**(173), 219-238.

Cogley, J.G., Adams, W.P., Ecclestone, M.A., Jung-Rothenhausler, F., and Ommanney, C.S.L. 1996. Mass balance of White Glacier, Axel Heiberg Island, N.W.T., Canada, 1960-91. *J. Glaciol.* **42**, 548-563.

Cogley, J.G. 2005. Personal communication. Department of Geography, Trent University, ON, Canada.

Dowdeswell and 10 others. 1997. The mass balance of Circum-Arctic glaciers and recent climate change. *Quat. Sci. Res.* **48**, 1 – 14.

Dowdeswell, J. A., T. J. Benham, M.R. Gorman, D. Burgess, and M. Sharp. 2004. Form and flow of the Devon Island ice cap, Canadian Arctic. *J. Geophys. Res.* **109**, F02002, doi:10.1029/2003JF000095.

Dyurgerov, M.B. and M.F. Meier. 2005. Glaciers and the Changing Earth system: A 2004 snapshot. *University of Colorado Institute of Arctic and Alpine Research Occasional Paper 58.*

Hamilton, G.S. and I.M. Whillans. 2000. Point measurements of mass balance of the Greenland Ice Sheet using precision vertical Global Positioning System (GPS) surveys. *J. Geophys. Res.,* **105**(B7), 16,295-16,301.

Intergovernmental Panel on Climate Change. 2001. *Climate Change 2001: Impacts, Adaptation, and Vulnerability,* edited by J.J. McCarthy et al., Cambridge Univ. Press, New York.

Koerner, R. 1970. Mass balance of the Devon Island ice cap, Northwest Territories, Canada, 1961 – 66. *J. Glaciol.,* **6**(45), 383-392.

Koerner, R. 1977. Ice thickness measurements and their implications with respect to past and present ice volumes in the Canadian High Arctic ice caps. *Can. J. Earth Sci.,* **14**, 2697-2705.

Koerner, R. 2002. Glaciers of the High Arctic Islands, in *Satellite Image Atlas of Glaciers of the World. Glaciers of North America – Glaciers of Canada.* Edited by R.S. Williams, Jr. and J.G. Ferrigno, U.S. Geological Survey Professional Paper 1386-Jj111-j146.

126

Krabill, W., W. Abdalati, E. Frederick, S. Manizade, C. Martin, J. Sonntag, R. Swift, R. Thomas, W. Wright, and J. Yungel. 2000. Greenland Ice Sheet: High-elevation balance and peripheral thinning. *Science, 289,* 428-429.

Mair, D.W.F., D.O. Burgess, and M.J. Sharp. 2004. Thirty-seven year mass balance of the Devon Ice Cap, Nunavut, Canada determined by shallow ice coring and melt modelling. *J. Geophys. Res.* **110**, F01011, doi:10.1029/2003JF000099.

Paterson, W. S. B. 1994. *The Physics of Glaciers.3rd.* Oxford, etc., Elsevier.

Reeh, N. and Paterson, W.S.B., 1988, Application of a flow model to the ice-divide region of Devon Island Ice Cap, Canada: Journal of Glaciology, v. 34, no. 116, p. 55Ð63.

Thomas, R.H., T. Akins, B. Csatho, M. Fahnestock, P. Gogineni, C. Kim, and J. Sonntag. 2000. Mass balance of the Greenland Ice Sheet at high elevations. *Science*, **289**, 426-429.

Thomas, R. H., and PARCA Investigators. 2001.Program for Arctic regional climate assessment (PARCA): Goals, key findings, and future directions. *J. Geophys. Res.*, **106**(D24), 33,691 -33,705.

Wang, L., M. J. Sharp, B. Rivard, S. Marshall, and D. Burgess. 2005. Melt Season Duration on Canadian Arctic Ice Caps, 2000-2004. *Geophys. Res. Let.,* **32**, L19502, doi:10.1029/2005GL023962

	Accumulation Zone	Ablation Zone			
Basin ID	Net volume change (km^3 a^{-1})	Net volume change (km^3 a^{-1})	Q_{InSar} (km^3 a^{-1})	b_{abl} (km^3 a^{-1})	$Q_{calving}$ (km^3 a^{-1})
3	-0.036(.020)	-0.015(.024)	0.097	-0.075	-0.037
9	-0.003(.025)	-0.043(.016)	0.063	-0.092	-0.014
15	-0.013(.031)	-0.302(.070)	0.081	-0.162	-0.221
25	n/a	-0.045(.006)	n/a	-0.041	-0.004
30	-0.029(.013)	-0.100(.026)	0.064	-0.104	-0.041
37	n/a	-0.053(.008)	n/a	-0.051	-0.002
38	-0.213(.180)	-0.392 (.111)	0.522	-0.072	-0.059
39	-0.385(.137)	-0.071(.142)	0.558	-0.606	-0.023
40	-0.018(.010)	-0.044(.141)	0.029	-0.066	-0.008
60	n/a	-0.532(.042)	n/a	-0.528	-0.004

Table 4.1. Values of ice volume change throughout the accumulation and ablation zone of the major tidewater terminating basins across the Devon Island ice cap. Net volume change of the accumulation zone represents the difference between balance and observed flux at the ELA. Individual components contributing to net volume change of the ablation zone are shown separately.

128

Basin ID	Volume change derived from flux imbalance x 39 years (km^3 a^{-1})	Volume change derived from areal changes 1960 – 1999(km^3 a^{-1})
9	-1.83 ± 0.19	-2.07 ± 0.25
25	-1.76 ± 0.04	-1.87 ± 0.23
40	-2.46 ± 0.88	-3.00 ± 0.36
37	-2.07 ± 0.05	-1.72 ± 0.21
30	-4.29 ± 0.18	-5.45 ± 0.67
3	-1.98 ± 0.20	-0.78 ± 0.10
15	-12.29 ± 1.44	-9.51 ± 0.73
38	6.94 ± 1.32	3.12 ± 0.38
39	-17.78 ± 1.23	-6.05 ± 0.73
60	-20.75 ± 0.26	-14.36 ± 1.74
Total	**-58.27 ± 5.8**	**-41.69 ± 5.4**

Table 4.2. Estimates of the change in ice volume of all major drainage basins according to (a) flux imbalance as derived in this study and (b) the maximum thickness area change technique as derived in Chapter 2. Shaded cells represent volume changes that agree to within the specified margin of error.

129

Site Number	$\partial H / \partial t_{cc}$ (mWe a^{-1})	$\partial H / \partial t_{thickchg}$ (mWe a^{-1})
1	-0.02 ± 0.03	+0.03 ± 0.04
2	-0.11 ± 0.05	-0.05 ± 0.05
3	+0.04 ± 0.06	-0.23 ± 0.07

Table 4.3. Ice thickness change rates derived from *in situ* measurements at 3 study sites in the southwest region in 2004/2005.

130
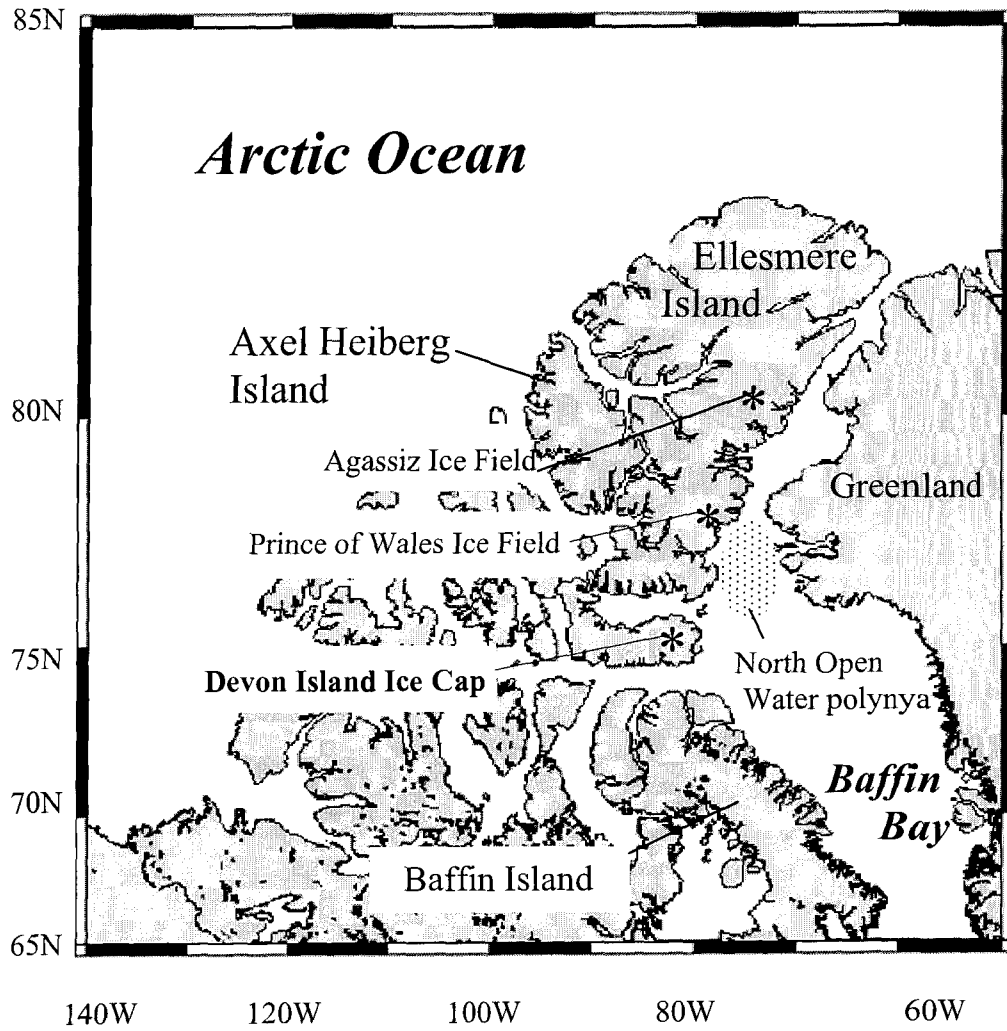
Figure 4.1. Location of the Devon Island ice cap within the Canadian Arctic Archipelago.

131
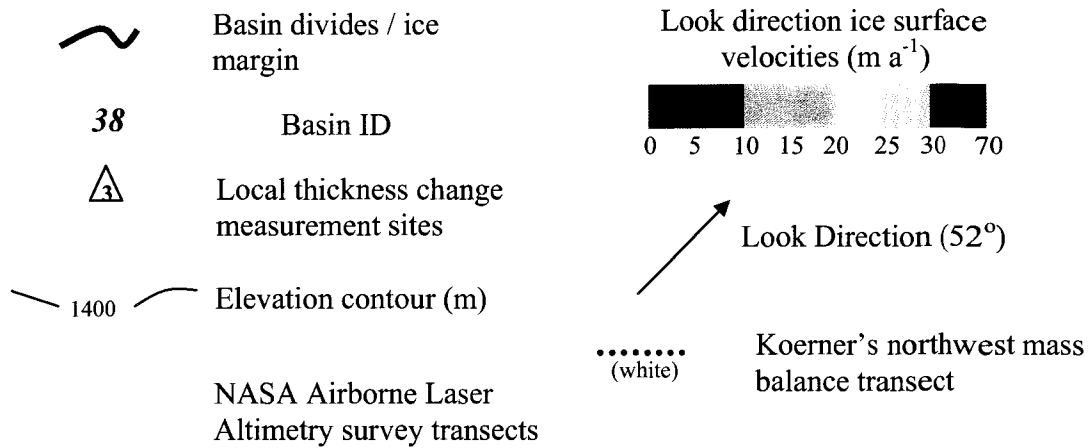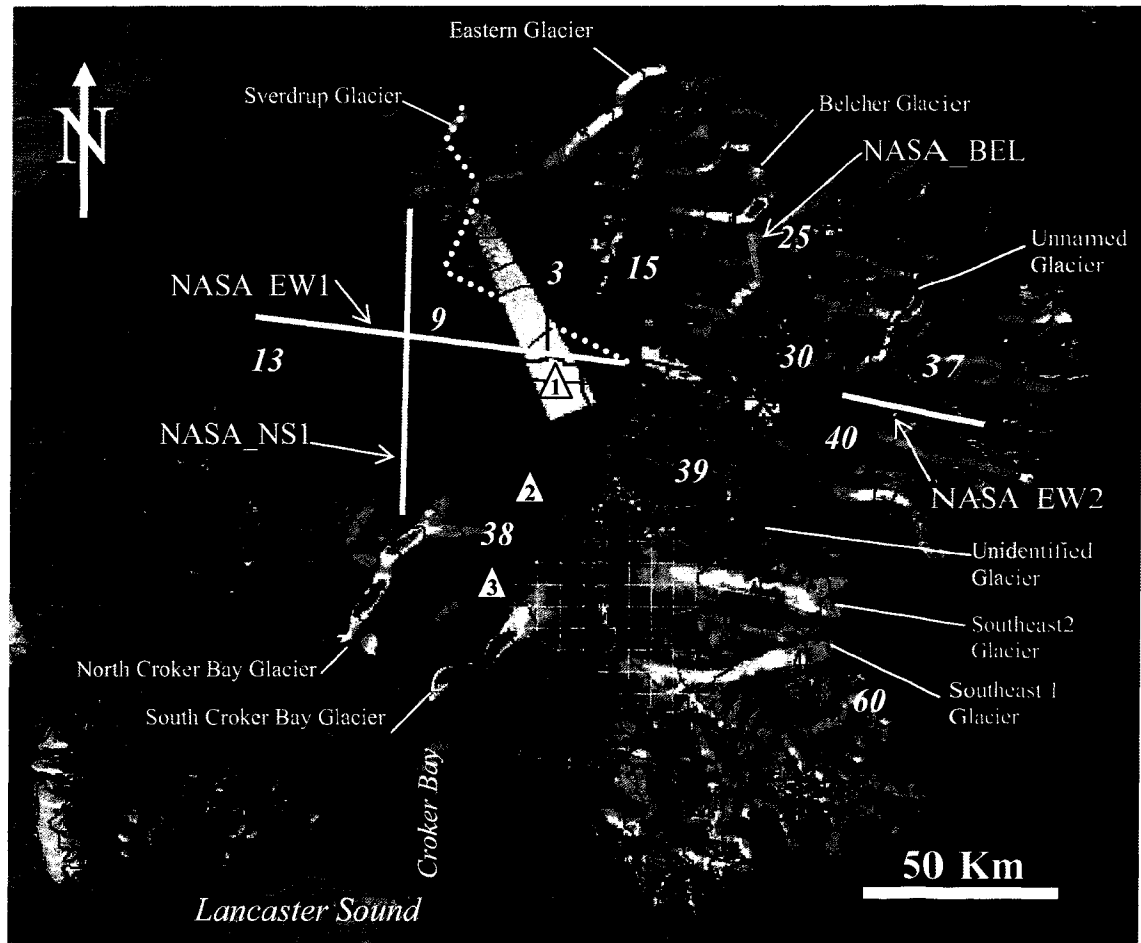
Figure 4.2. InSAR look direction surface velocities across the Devon Island ice cap derived from the ERS 1/2 satellite data. The grey gridded area in the southern region of the ice cap indicate the location where surface accumulation rates were increased by 1.5 times the amount derived by Mair and others (2004).

132
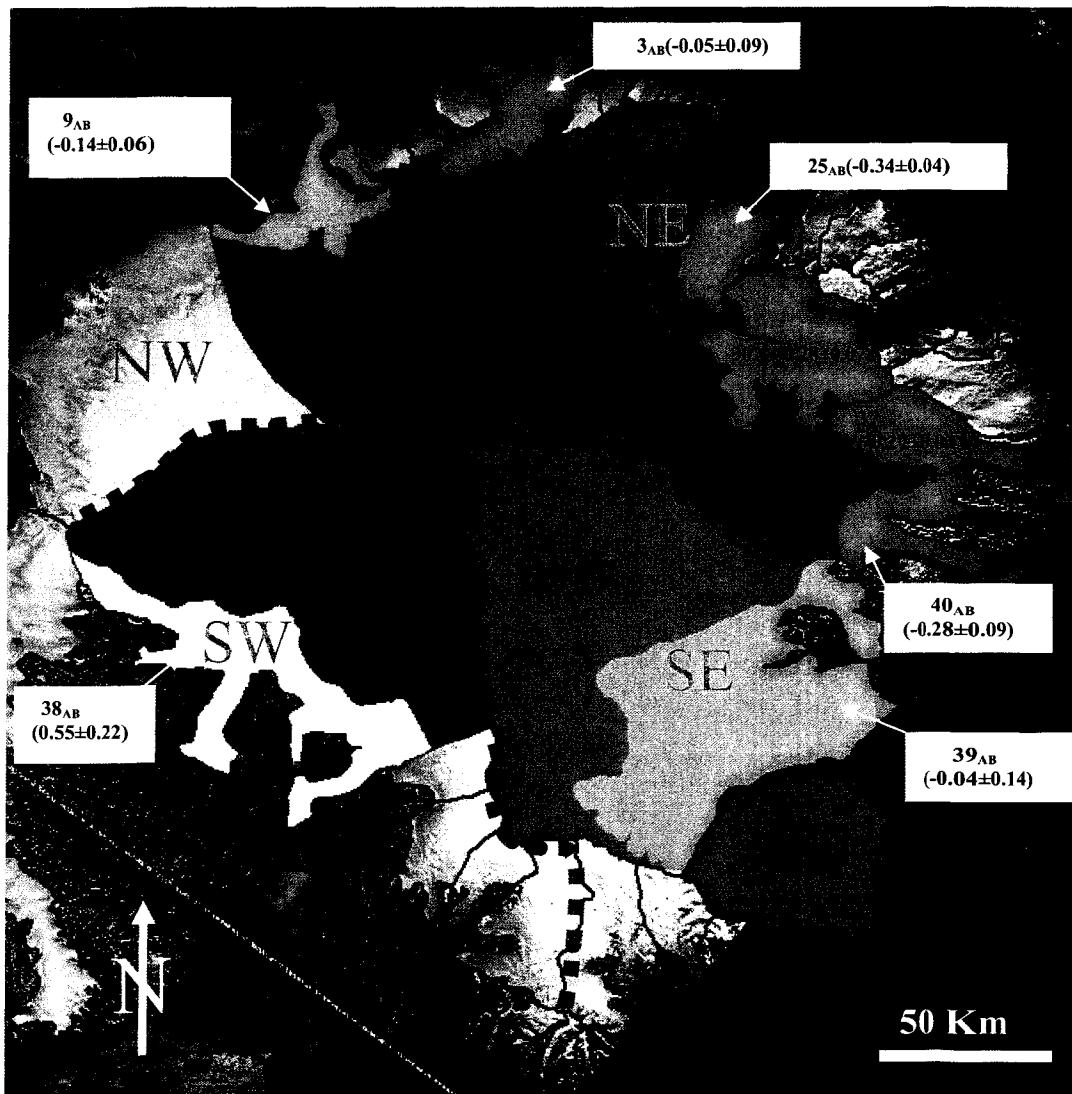
Figure 4.3. Basin-wide thickness changes of the accumulation (AC) and ablation (AB) zones across the Devon ice cap (m a^{-1}). The ELA is specified at 950 m in northwest (NW), 800 m in the southeast (SE), and 875 m in the southwest (SW) and northeast (NE) quadrants (Koerner, 1970).

133
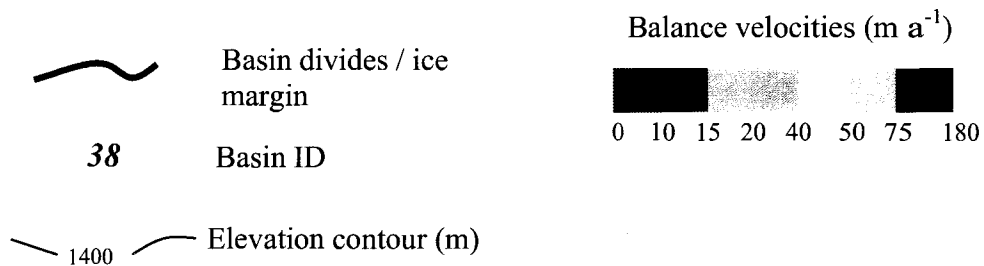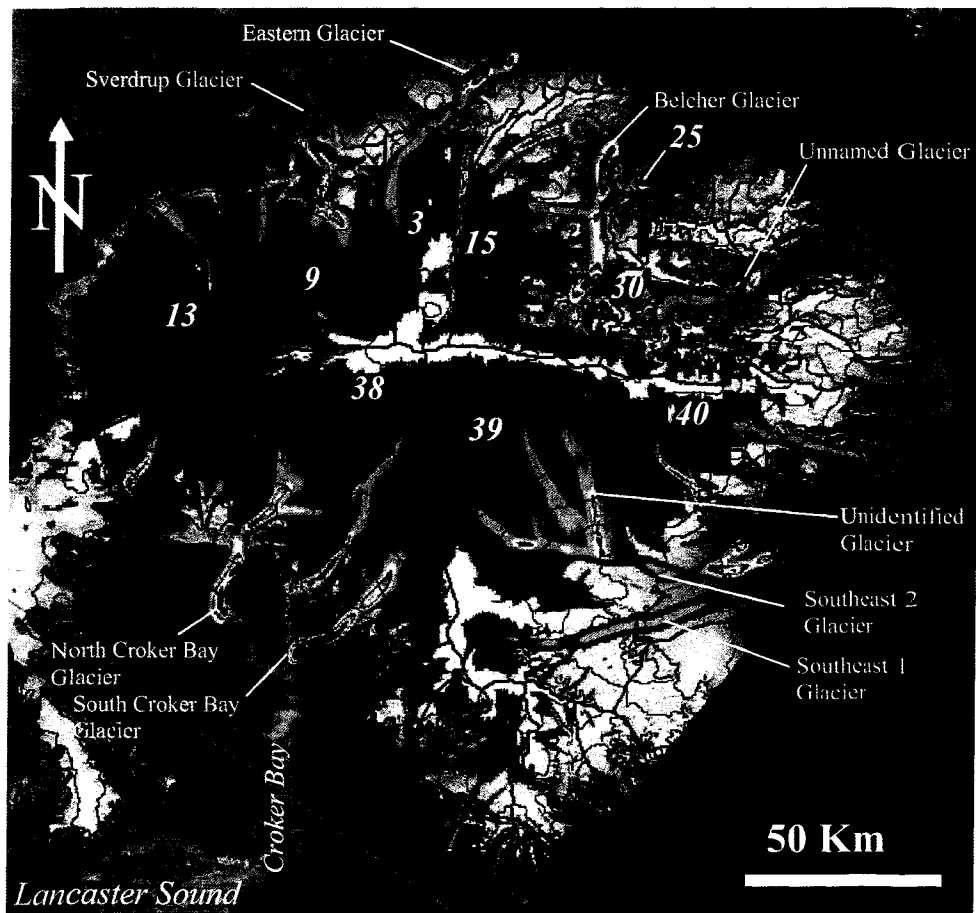
Figure 4.4. Modelled balance velocities across the Devon Island ice cap. Areas of missing data represent sections of the ice cap where the modeled balance velocity is less than 1 m a^{-1}. Flow units not evident in the InSAR derived velocity fields are indicated as A, B, C, and D.

134
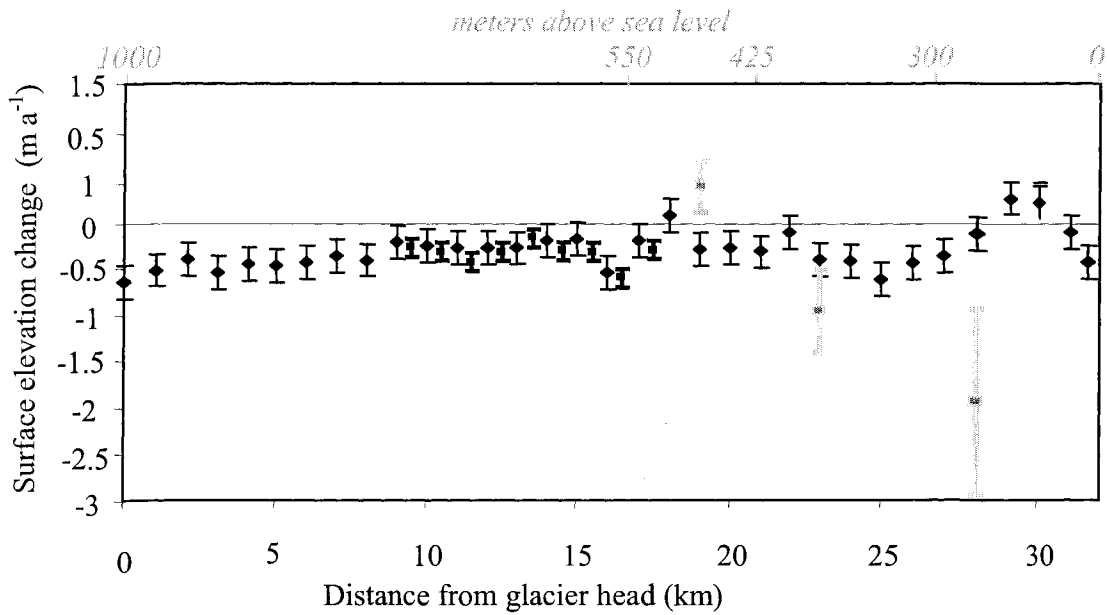
Figure 4.5. Average annual surface elevation change along the Belcher Glacier derived from 1960's aerial photography and 2000 radio-echo sounding data (Dowdeswell and others, 2004). Thickness change rates due to ice dynamics are indicated by the large grey data points at km 23 and 29. Annual surface lowering rates derived from the NASA airborne laser altimetry surveys are plotted in bold between km 9 and 17. Values along the top axis indicate the elevation at each flux gate location.

135
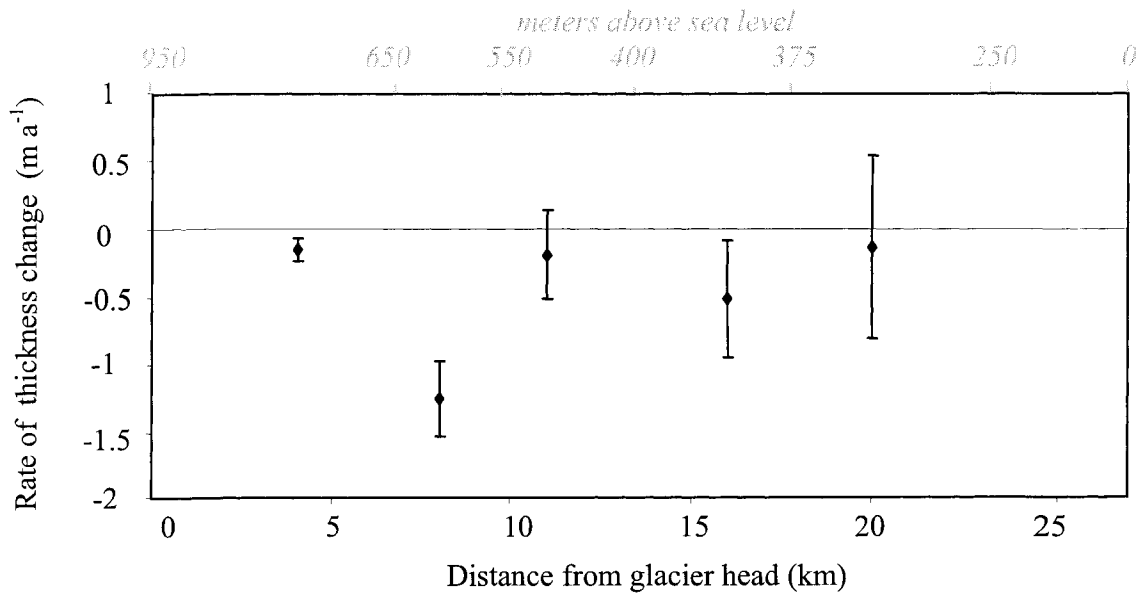
Figure 4.6. Rates of thickness change due to ice dynamics along the Unnamed Glacier. Values along the top axis indicate the elevation at each flux gate location.

136
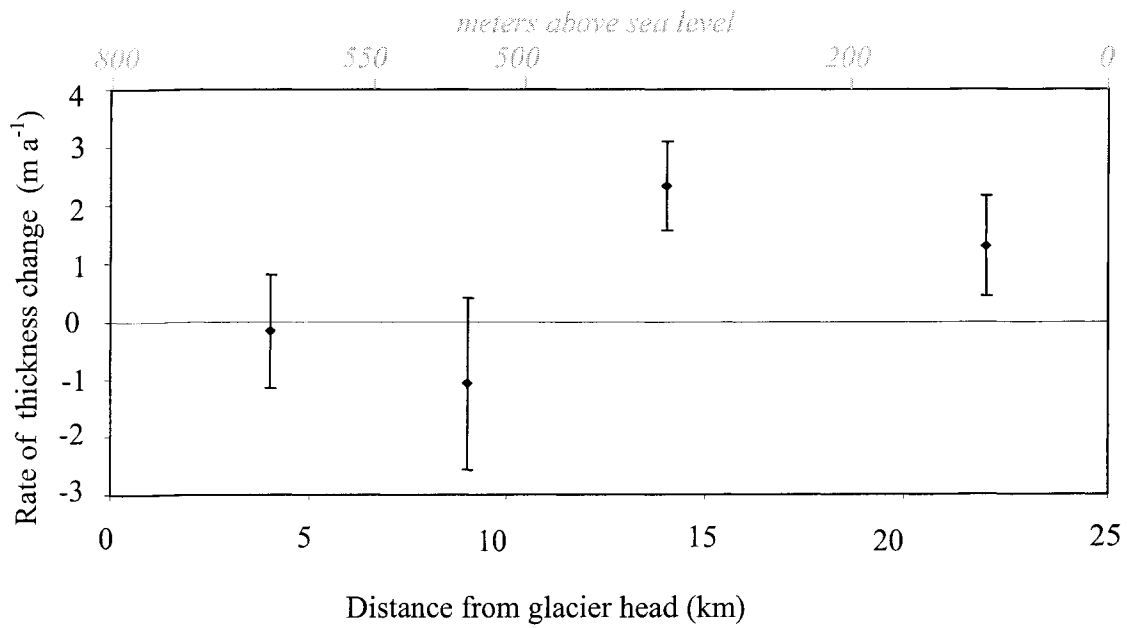
Figure 4.7. Rates of thickness change due to ice dynamics along the North Croker Bay Glacier. Values along the top axis indicate the elevation at each flux gate location.

137
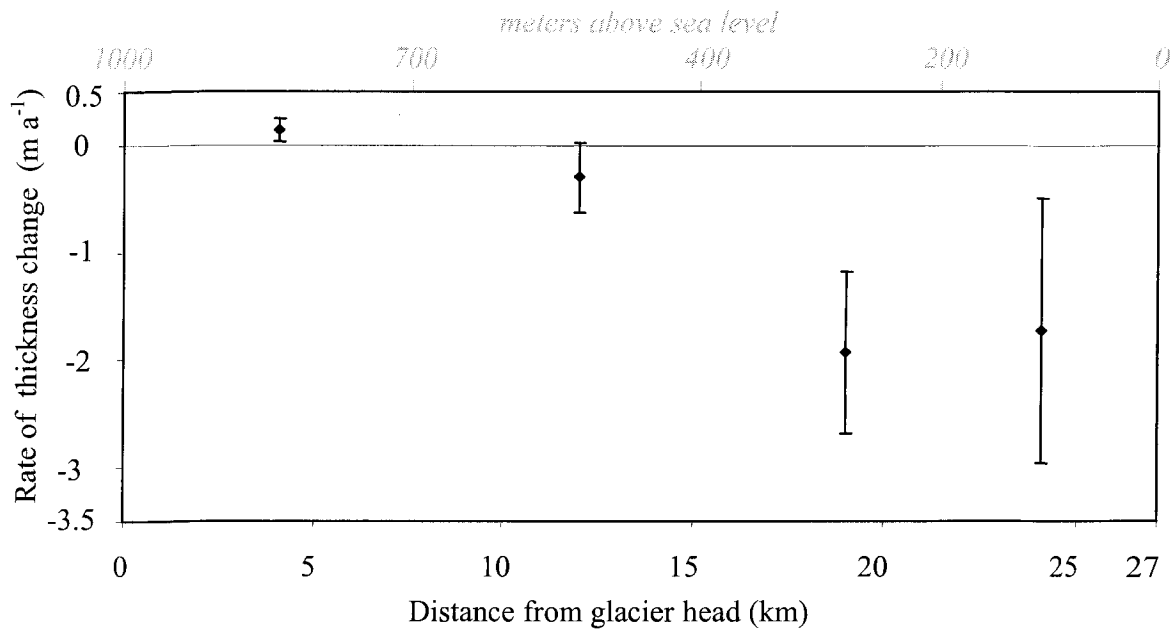
Figure 4.8. Rates of thickness change due to ice dynamics along the South Croker Bay Glacier. Values along the top axis indicate the elevation at each flux gate location.

138
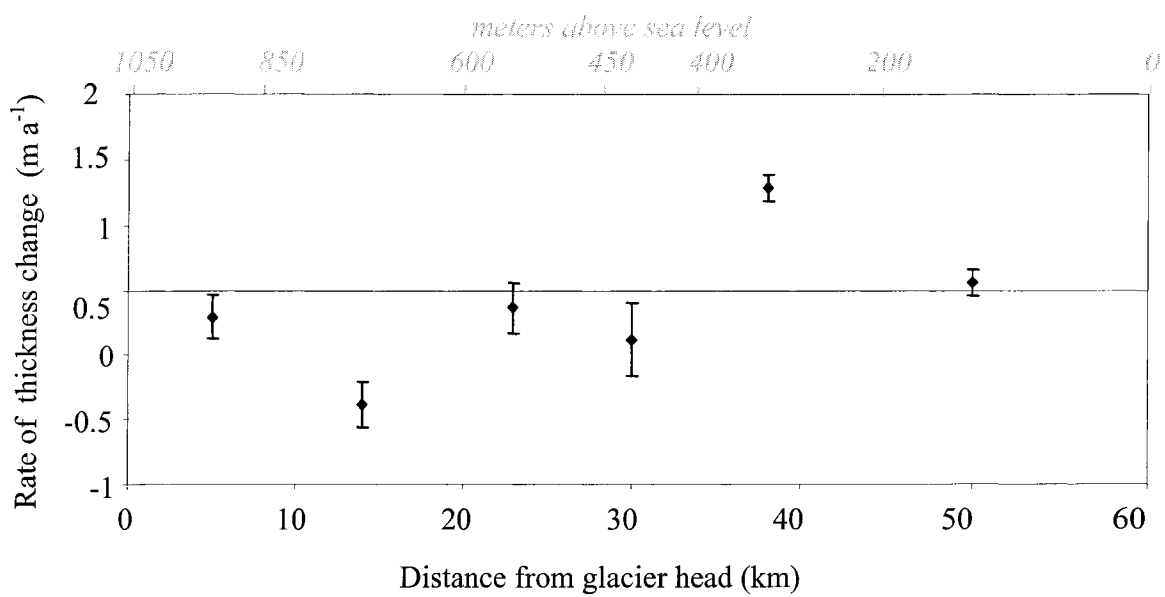
Figure 4.9. Rates of thickness change due to ice dynamics along the Southeast 1 Glacier. Values along the top axis indicate the elevation at each flux gate location.

139
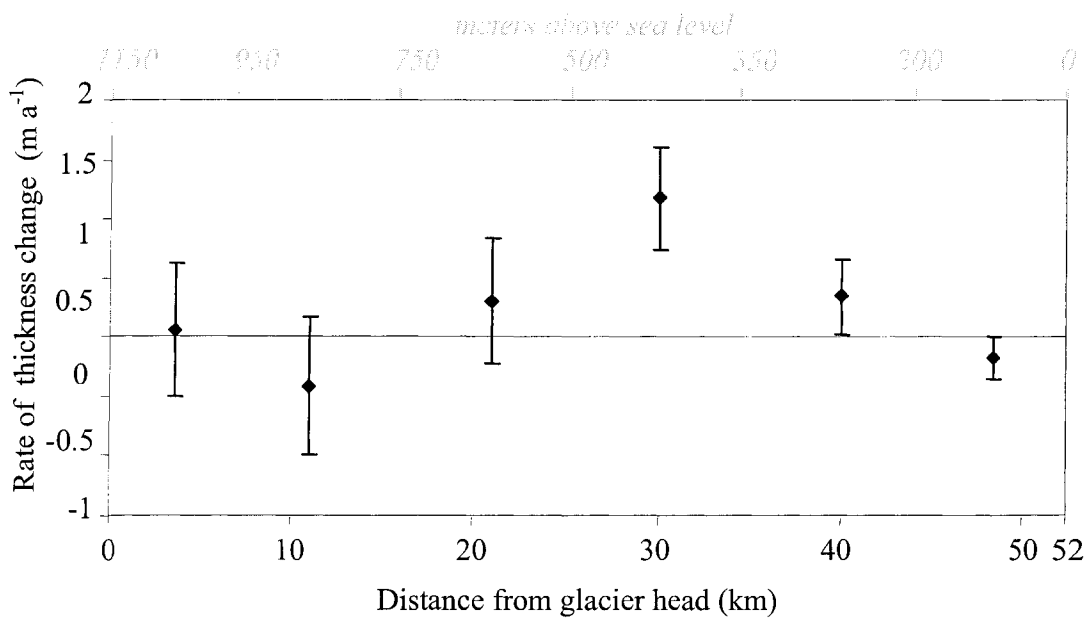
Figure 4.10. Rates of thickness change due to ice dynamics along the Southeast 2 Glacier. Values along the top axis indicate the elevation of each flux gate location.

140
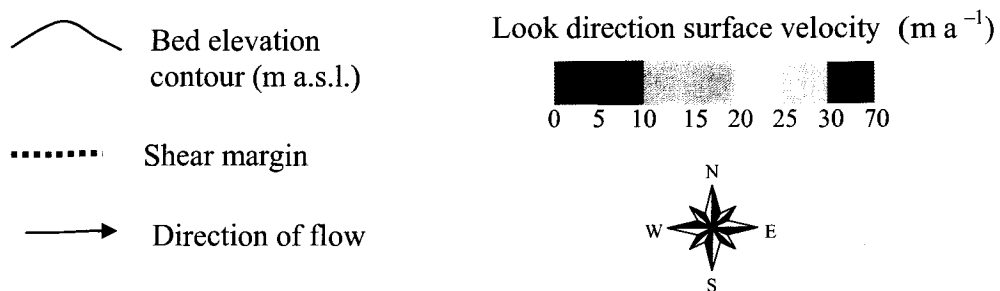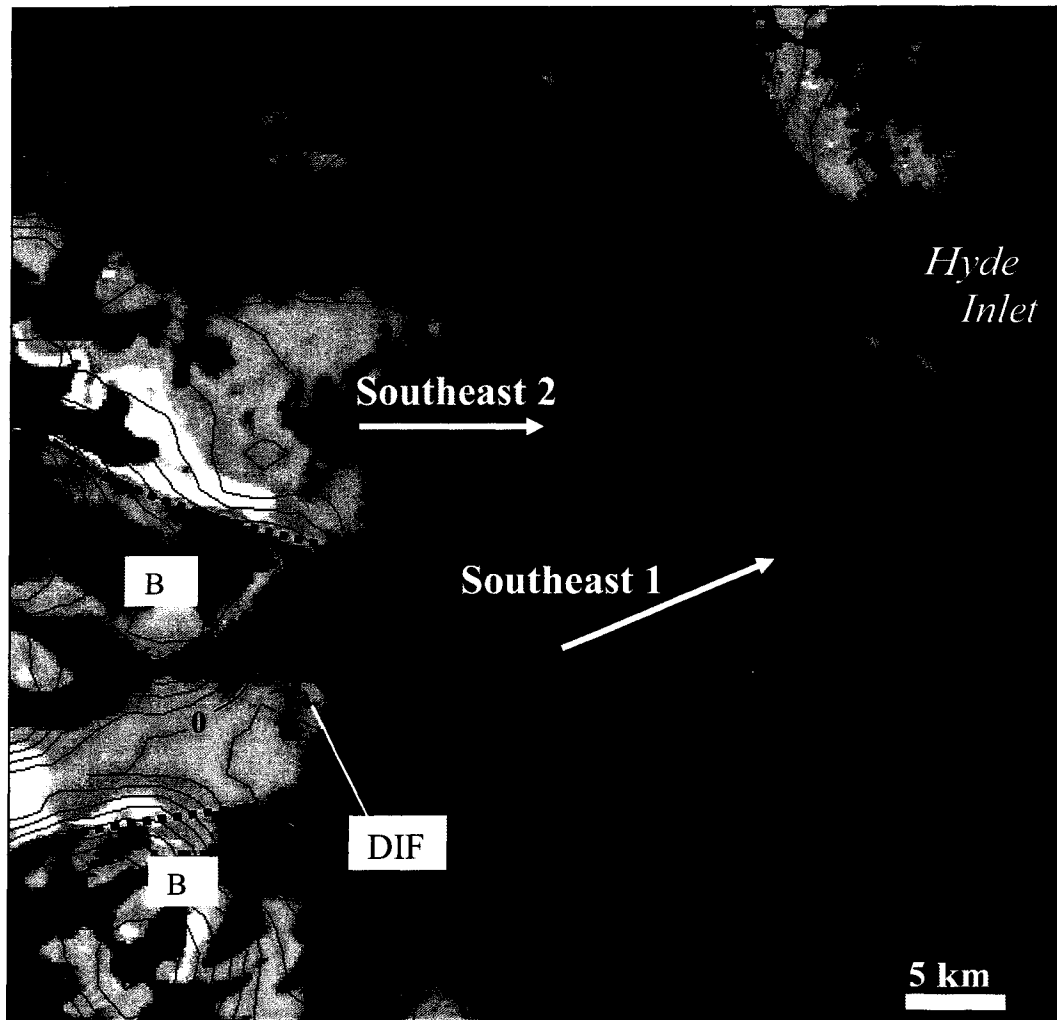
Figure 4.11. InSAR derived velocity pattern and bed topography throughout the terminus region of the Southeast 1 and 2 Glaciers. The elevation contours of the glacier bed highlight an erosional trough aligned with ice flow along the Southeast 1 Glacier. DIF indicates the zone of decelerating flow, which occurs beyond the channel constricted by bedrock topography (BT) on either side. Ice flow at this location transforms from movement primarily by basal sliding to movement by internal deformation alone as derived Burgess and others, 2004.

CHAPTER 5

SUMMARY AND CONCLUSIONS

5.1 SUMMARY

Through the use of satellite remote sensing and field-based measurements, this thesis provides unique insight into the dynamics and recent changes in geometry and volume of the Devon Island ice cap. In addition to the 3 papers that comprise the main body of this work, contributions were also made to 2 additional non-thesis papers – *Flow and form of the Devon Island ice cap* (Dowdeswell and others, 2004) and *Thirty-seven year mass balance of Devon Ice Cap, Nunavut, Canada, determined by shallow ice coring and melt modeling* (Mair and others, 2004). Ice thickness data from Dowdeswell and others (2004) and net surface mass balance data from Mair and others (2004) were integrated into Chapters 3 and 4 in order to derive ice flow regimes, iceberg calving rates, and rates of thickness change across the ice cap.

Results from this thesis represent the most complete assessment of the mass balance and recent geometric changes of a large polar ice cap to date. The major findings include:

1)   The Devon Island ice cap has decreased by 332 ± 40 km^2 over the past 40 years. This areal decrease equates to a loss of 65 ± 12 km^3 of ice (or ~0.17 mm sea-level rise) for the entire ice cap as derived from volume-area scaling methods.

142

2) The dominant changes in area that occurred include (a) retreat of all major tidewater glaciers by up to 3 km along the east coast, (b) advance of up to 120 m along the western margin, (c) shrinkage of the southwest arm by 200 $\pm$ 17 km^2, and (d) increase in exposed bedrock in the interior regions of the ice cap by 28 $\pm$ 5 km^2.

3) Surface velocity fields mapped from satellite radar interferometry (InSAR) revealed uniform sheet flow across most of the western half of the ice cap while the eastern region is drained by several large outlet glaciers, some of which extend up to 60 km inland from the ice margin.

4) Flow across the ice cap is governed by 4 main ice flow regimes. Flow Regime 1 represents ice motion by internal deformation only; Flow Regime 2 represents ice motion by basal sliding and internal deformation; Flow Regime 3 represents ice motion by enhanced basal sliding and internal deformation; and Flow Regime 4 represents ice motion by basal sliding only. Continuous mapping of the main ice flow regimes indicate that ~22% of eastern half of the ice cap is warm-based as opposed to only ~8% of the western region.

5) Iceberg calving, calculated as the sum of ice flux at the tidewater terminating glaciers and volume loss at these termini due to glacier retreat, accounts for ~20.5 km^3 of ice, or ~30% of the total mass ablated from the ice cap, since 1960. The ice front associated with the Belcher Glacier was identified as the most important calving outlet, accounting for ~50% of the net annual iceberg flux from the ice cap.

143

6)	Thickness change results indicate that the north accumulation zone is in balance while net thinning occurs within the south and east accumulation zones with maximum rates of -0.23 ± 0.11 m a^{-1} in the southeast basin. The ablation zones of the northern basins are in equilibrium or thinning by -0.14 to -0.34 m a^{-1}. Thinning by –0.62 ± 0.14 m a^{-1} of the ablation zone in basin 15 is enhanced by ice calved from the terminus of the Belcher Glacier. The ablation zone in the southwest sector is thickening by 0.55 ± 0.22 m a^{-1} while net equilibrium prevails in the southeast ablation zone. Along glacier thickness changes reveal thinning by ~ -0.8 m a^{-1} above the ELA along the Southeast 1 Glacier and thickening by up to ~1 m a^{-1} below the ELA along the Southeast 1 and 2 outlet glaciers. Thickening (thinning) by ~2 m a^{-1} (~ -2 m a^{-1}) occurs below ~400 m a.s.l. along the North (South) Croker Bay Glacier. Surface lowering of up to ~ –0.7 m a^{-1} averaged over the past 40 years is evident near the terminus of the Belcher Glacier. Flux difference calculations however indicate that this region may currently be experiencing thinning of up to ~ -2 m a^{-1}.

7)	Volume changes based on mass loss due to net surface mass balance and iceberg calving rates indicate that the Devon Island ice cap as a whole has decreased by -74 ± 9 km^3 (or -67 ± 7 km^3 water equivalent) between 1960 and 1999, contributing ~0.19 mm to global sea-level rise over this time period.

144

It is apparent from this study that significant variability in the spatial pattern of geometric change occurs across the Devon Island ice cap. The western region of the ice cap has experienced net increase in mass of ~3.5 km^3 of ice since 1960. Most of this region terminates terrestrially between 400-600 m a.s.l. where surface ablation rates are relatively low (~ -0.35 m a^{-1}; Mair and others, 2004). Also, low driving stresses throughout this region (< 50 kPa; Dowdeswell and others, 2004) inhibit rapid ice drainage from the interior region towards the margins. These characteristics have buffered this region from the effects of post Little Ice Age warming that have had an otherwise negative impact on the mass balance of most land ice in the northern hemisphere (Dowdeswell and others, 1997). By contrast, changes in ice dynamics and surface melt have significantly influenced the mass balance, and hence geometry, of the eastern half of the ice cap. In the southeast sector, maximum driving stresses (>100 kPa) above ~900 m a.s.l. (Dowdeswell and others, 2004) likely contribute to enhanced ice flow across the ELA resulting in dynamic thinning of the accumulation zone in this region. With the exception of the southwest arm, the eastern half of the ice cap also loses ~90% more volume as a result of surface ablation than the west half of the ice cap. In addition, >95% of the total amount of ice lost due to calving originates from glaciers along the eastern margin. Iceberg calving and surface melt are therefore both important contributors to mass loss from the eastern sector of the Devon Island ice cap resulting in a net decrease of ~ -79 km^3 of ice from this region over the past 40 years.

145

5.2 CONCLUSIONS

Net shrinkage of the Devon Island ice cap as quantified in this study, is consistent with the other indicators of global climate warming that commenced in the mid 19th century (Overpeck and others, 1997; IPCC, 2001). In the Arctic region, dramatic responses to this warming are evident in (1) a net reduction of Arctic sea ice since the late 1970's (Serreze and others, 2003), (2) a positive trend in the areal extent over which surface melt on the Greenland ice sheet occurs (Abdalati and Steffen, 2001), and (3) overall retreat of most glaciers in the circumpolar region from which mass balance data are available (Dowdeswell and others, 1997). In addition, important linkages observed between these and other biological, hydrological, and societal changes indicate that system-wide changes in the Arctic are also occurring in response to post Little Ice Age warming in the northern high latitudes (Heinzman and others, 2005). Of these changes, decreases in volume of land-based ice are having, and will continue to have, the greatest impact on global sea-level change. Large uncertainties in the overall importance of eustatic (from glaciers) versus steric (thermal expansion) components of net sea-level rise however still currently exist (Dyurgerov and Meier, 2005).

The most recent estimate provided by Dyurgerov and Meier (2005) indicates that the eustatic sea-level rise is ~0.59 mm a^{-1} when averaged over the past 40 years, but as high as ~0.93 mm a^{-1} over the past decade. By including recent mass balance estimates from the Alaskan glaciers (Arendt, 2002) and the Patagonia ice fields (Rignot and others, 2003), accounting for accelerated warming since the late 1980's,

146

and using a new estimate of the total areal coverage of land ice, this new estimate has increased over previous estimates which ranged from ~0.25 mm a^{-1} (Dyurgerov and Meier, 1997) to ~0.5 mm a^{-1} (Meier and Wahr, 2002). Contributions from land ice in the Canadian Arctic however are still based on the ice volume changes derived by extrapolating point measurements of surface mass balance data collected by Dr. R. Koerner of the Geological Survey of Canada since 1960. This estimate contains significant uncertainty due to extrapolations over large regions and does not include mass loss due to iceberg calving. These shortcomings are likely to be responsible for the much lower, previous estimate of volume change for the Devon Island ice cap since 1960 (~42 km^3 water equivalent) than the value derived in this study (-67 ± 7 km^3 water equivalent) which was obtained for individual drainage basins and includes mass loss due to iceberg calving. This discrepancy implies that recent contribution towards global sea-level rise due to net volume decrease from the Devon Island ice cap, and likely all land-ice in the Canadian Arctic, is still underestimated by up to ~40%.

A second independent estimate of volume change, as derived from repeat NASA laser altimetry surveys (Abdalati and others, 2004), is also significantly lower (~ -32 km^3) than estimated in this study. This discrepancy likely reflects the sparse coverage of the NASA measurements that failed to sample regions that are changing most rapidly. These regions include the southeast accumulation zone, the ablation zone of basin 15 and the low-lying basins situated around the ice cap margin. In addition, the current NASA transects do not provide insight into net changes of individual drainage basins, which vary significantly across the ice cap. In order to

derive accurate measures of volume change for the ice cap as a whole, future surveys should therefore be designed to measure changes across complete glacier systems and include areas that are most likely to be affected by dynamically driven changes in ice thickness.

From a global perspective, the impact of recent climatic conditions on the relative volume decrease of the Devon Island ice cap has been low. This assessment is based on a quantitative measure of relative volume change (annual rate of volume loss divided by ice mass area; VC:A) for which current rates of volume change, and area of major ice masses are known. Of the small ice caps and glaciers ($<$ 14, 000 km^2), the Patagonia ice fields (Rignot and others, 2003) currently experience the greatest rate of volume loss per unit area (VC:A = 0.001 m a^{-1}). The Alaskan Glaciers (Arendt and others, 2002) experience the second highest rates (VC:A = 0.0006 m a^{-1}), while the Devon Island ice cap and the ice caps in Svalbard (Dowdeswell and Hagen, 2003) have been affected least (VC:A = 0.0001 m a^{-1} for both). This trend highlights the significantly greater impact of recent climate forcing on land ice at lower latitudes that are influenced mainly by maritime climatic regimes, as opposed to land ice in the more arid polar region. Within the Arctic, the Greenland ice sheet exhibits a VC:A value that is an order of magnitude lower (VC:A = 0.00003 m a^{-1}; based on the most recent estimate of volume change by Krabill and others, 2000) than that of the ice caps on Devon Island and Svalbard. This difference is mainly a function of the size of the Greenland ice sheet (~1.7 x 10^6 km^2 in area and up to ~3000 m in elevation), which

148

has buffered this ice mass from the effects of post Little Ice Age warming relative to the smaller ice caps.

Despite the low impact of recent climate warming on the health of the Greenland Ice Sheet, similarities in the patterns of recent geometric change between this ice mass and the Devon Island ice cap do however exist. Both ice masses are currently experiencing net loss due to surface melt below ~1000 m a.s.l. with a significant proportion of the total loss accounted for by mass discharge directly into the ocean (~30% from Devon Island ice cap and ~50% from the Greenland ice sheet). Over Greenland, mass loss due to ice dynamics is evident mainly from enhanced surface lowering of near the terminus of most outlet glaciers as identified from repeat airborne laser surveys performed by NASA between 1993 and 2000 (Abdalati, 2001). On the Devon Island ice cap, thinning by ~0.62 m a^{-1} of the ablation zone in basin 15 (situated in the northeast sector) is enhanced by mass loss due to iceberg calving associated with the terminus of the Belcher Glacier. Both ice masses are also experiencing dynamic drawdown of the accumulation zones of the inland region of their southeast sectors. Other than the fact that the Greenland ice sheet is <200 times greater in volume than the Devon Island ice cap, the primary difference between the two ice masses is that ~50% of the Greenland ice sheet rarely, if ever, experiences summer melt. On the Devon Island ice cap, despite significant interannual variability in the duration of melt, surface melt routinely occurs at the summit (~1900 m a.s.l.) (Wang and others, 2005). These important differences imply that the Greenland ice sheet is at an earlier stage in terms of fully responding to the impact of post Little Ice Age warming relative to the Devon Island ice cap. Knowledge of the predominant

149

mechanisms controlling geometric changes of the Devon Island ice cap may therefore provide a better understanding of the response of the Greenland ice sheet to future climate warming.

5.3 FUTURE RESEARCH

It is apparent from this study that further investigation into three main aspects of the Devon Island ice cap is required in order to improve our understanding of the current changes experienced by the ice cap, and how the ice cap is likely to respond to future climate warming. The priorities for further investigation include (1) validation of the measurements of thickness change derived from indirect methods in this study, (2) quantification of seasonal and long term variability in rates of ice flow of the tidewater glaciers and the inland extent of this variability, and (3) reducing the uncertainties in long term net surface mass balance of the southeast region where significant mass losses from the ice cap occur.

(1) Validation of the 'long term' thickness change rates derived from indirect methods in this study require accurate historical surface elevation data to be compared with current sources, such as from the NASA airborne laser altimetry ($\pm$ ~0.1 m) or surface elevations derived from radio-echo sounding data obtained by Dowdeswell and others (2004) ($\pm$ 7m). Unfortunately, the topographic data that represents the 1960 surface over the Devon Island ice cap (Canadian Digital Elevation Dataset) are only accurate to ~ $\pm$ 100 m throughout the interior regions and ~ $\pm$ 50 m along the main outlet glaciers rendering them unusable for detecting subtle changes over the decadal time scale. Along the main outlet glaciers however, surface elevations can be produced

150

from the 1960's photography using conventional photogrammetric techniques where sufficient image contrast exists. These methods were successfully employed to produce a DEM along the Belcher Glacier accurate to ± 2 m and should be applied to all outlet glaciers in order to provide baseline surface elevation data from which current and/or future measurements can be compared. Throughout the ice cap interior, accurate surface data may be obtained from the high resolution photographic data that was acquired during the CORONA mission between 1960 and 1972. Since these images were collected as continuous strips that span the width of the ice cap, it may be possible to employ photogrammetric techniques that utilize high precision optics to extract surface elevation measurements over low contrast areas (Ayman Habib, personal communication, 2005).

Besides validation of long term thickness change, it is also important to monitor ongoing thickness change along the main outlet glaciers where flow is most likely to be influenced by external climate forcing (Copland and others, 2003; Cress and Wyness, 1961). In order to monitor short-term changes over these areas, it is essential to obtain surface elevation measurements along the main outlet glaciers on a regular basis (every 1-2 years) using repeat airborne laser altimetry or ground-based kinematic GPS surveys. Correlations with temporal variations in flow rate and possible linkages to melt intensity (as discussed below) will provide important insight into the sensitivity of these areas to climatically induced changes in ice thickness.

(2) The second area of research that must be pursued in order to improve our understanding of the current behaviour and vulnerability of the Devon Island ice cap

151

to future climate change is to fill gaps in the spatial coverage of the current velocity measurements across the ice cap and to quantify the temporal variability (seasonal and long term) in rates of ice flow along the main outlet glaciers. In this study, gaps in the velocity structure of the Devon Island ice cap occurred along the termini of several tidewater glaciers (including the Belcher, Eastern, Unnamed Glaciers) where intense crevassing and high velocities caused decorrelation of the radar image pairs. Gaps also remain over ~25% of the interior region of the ice cap where direction of ice flow is nearly perpendicular to the look direction of the ascending mode ERS1 / 2 satellites. Over the tidewater glaciers, improved velocity mapping may possibly be obtained from intensity mapping (Luckman and others, 2003) or speckle tracking techniques (Short and Gray, 2005) using SAR data acquired since 2000 when the original velocity mapping on Devon was performed. Since the intensity and speckle tracking techniques are only sensitive to ice motion > ~30 m a^{-1}, gaps in the coverage of the continuous velocity field within the interior regions must be obtained from descending mode InSAR data. Although these data are unavailable from the existing (or past) configuration of satellites, it may be possible to fill these gaps with data from Radarsat2 provided that (a) perpendicular baselines during this mission are maintained below ~ 100 m and (b) the rate of flow in 1992 is not significantly different from the rate of flow when future InSAR data are acquired (possibly by 2007).

In order to better understand the potential influence of external climate forcing on the dynamics of the Devon Island ice cap, it is imperative that variability in the rates of ice flow (seasonal or long-term) is quantified. Field studies are planned for 2006 to install GPS receivers along the length of the Belcher Glacier in order to track temporal

152

flow rates over a 2-year period (Martin Sharp, personal communication, 2005). Ice flow rates derived from GPS data will be linked to temperature and hydrological conditions along the glacier in order to provide insight into the impact of external climate forcing on the dynamics of the glacier. A relationship between these parameters would be useful for quantifying the annual variability in calving flux rates and their sensitivity to climate warming. If successful, this technique should be applied to the other major tidewater outlet glaciers (North and South Croker Bay, Unnamed, and Eastern Glaciers) in order to constrain estimates of seasonal variability in rates of iceberg calving from the ice cap.

Longer term changes in ice velocity (>1 year) may be detected by comparing velocity patterns obtained from speckle tracking techniques applied over regions of 'fast' flow in successive years (Short and Gray, 2005). In order to detect subtle changes of inland flow rates and potential instabilities throughout the interior regions, it would be necessary to acquire repeat InSAR observations over these regions on an operational basis. Unfortunately however this option is not available from the current constellation of radar satellites.

(3) The third aspect of the Devon Island ice cap that requires further investigation is to gain a better understanding of the spatial pattern of net surface mass balance in the southeast region. Previous work has determined that this region receives the highest rates of accumulation (Mair and others, 2004; Koerner, 1970), which is due primarily to the proximity of the Baffin Bay moisture source (Koerner, 1977). Long term (40-year) mass balance measurements performed in this region during the spring of 2005

153

however indicated that (a) the net surface mass balance near the head of Southeast 1 and 2 outlet glaciers is currently underestimated and (b) spatial variability in mass balance within this region may be higher than the existing data suggest. In addition, ablation rates in the extreme southeast sector of this drainage basin have not yet been quantified directly, resulting in large uncertainties in the melt rates. This basin comprises the single largest catchment area on the ice cap ($\sim$2100 km^2) in which the greatest mass 'turnover' occurs. An accurate assessment of the long-term net surface mass balance throughout this sector would therefore significantly improve our understanding of the mass balance of the ice cap as a whole.

To achieve this goal, efforts should be focused on obtaining a relatively dense network of point and continuous measurements of long-term mass balance throughout the southeast region. Long-term mass balance at point locations should be quantified by detecting the depth to, and density above the 1963 radio active reference layer deposited as fallout from thermonuclear weapons testing in the Russian high Arctic in 1962 (Mair and others, 2004). Continuous mapping of ice layers at depth between core locations from $\sim$250 – 500 Mhz ground penetrating radar (GPR) would provide insight into the spatial gradients in net accumulation throughout this region (Dowdeswell and Evans, 2004). This technique has been used successfully to map the continuity of ice layers at depth along transects extending hundreds of kilometres in length over the Antarctic Ice Sheet (Morse and others, 2002; Welch and Jocobel, 2003). Conventional mass balance surveys should be performed in the southeast ablation zone where melt rates are currently poorly understood. Collection of meteorological data from *in situ* instrumentation, and melt duration and intensity from QuickSCAT remote sensing

154

data (Wang and others, 2005) should also be monitored in order to gain a better understanding of the factors that control melt throughout this sector of the ice cap.

5.4 REFERENCES

Abdalati, W. and K. Steffen. 2001. Greenland ice sheet melt extent: 1979-1999. *J. Geophys. Res.* **109**, D24, 33,983-33,988

Abdalati, W., W. Krabill, E. Frederick, S. Manizade, C. Martin, J. Sonntag, R. Swift, R. Thomas, W. Wright, and J. Yungel. 2001. Outlet glacier and margin elevation changes: Near-coastal thinning of the Greenland Ice Sheet. *J. Geophys. Res.,* **106**(D24), 33,729-33,741.

Abdalati, W., W. Krabill, E. Frederick, S. Manizade, C. Martin, J. Sonntag, R. Swift, R. Thomas, J. Yungel, and R. Koerner. 2004. Elevation changes of ice caps in the Canadian Arctic Archipelago. *J. Geophys. Res.* **109**, F04007, doi: 1029/2003JF000045.

Arendt, A., Eckelmeyer, K., Harrison, W.D., Lingle, C.S., and Valentine, V.B., 2002: Rapid wastage of Alaska glaciers and their contribution to rising sea level. *Science,* **297**(5580): 382-386.

Cogley, J.G., Adams, W.P., Ecclestone, M.A., Jung-Rothenhausler, F., and Ommanney, C.S.L. 1996. Mass balance of White Glacier, Axel Heiberg Island, N.W.T., Canada, 1960-91. *J. Glaciol.* **42**, 548-563.

Copland, L., M. Sharp, P. Nienow, and R. Bingham. 2003. The distribution of basal motion beneath a high Arctic polythermal glacier. *J. Glaciol.,* **49**(106).

Cress, P., and Wyness, R. 1961, The Devon Island expedition, observations of glacial

155

movements. *Arctic*, **14**(4), 257-259.

Dowdeswell and 10 others. 1997. The mass balance of Circum-Arctic glaciers and recent climate change. *Quat. Res.* **48,** 1 – 14.

Dowdeswell, J.A. and Hagen, J.O. 2003. Arctic ice caps and glaciers in Mass balance of the cryosphere: Observations and modeling of contemporary and future changes. *Cambridge University Press.* Eds. Jonathan L. Bamber and Antony J. Payne. 527-557

Dowdeswell, J. A., T. J. Benham, M.R. Gorman, D. Burgess, and M. Sharp. 2004. Form and flow of the Devon Island ice cap, Canadian Arctic. *J. Geophys. Res.* **109**, F02002, doi:10.1029/2003JF000095.

Dowdeswell, J.A., and S. Evans. 2004. Investigations of the form and flow of ice sheets and glaciers using rado-echo sounding. *Rep. Prog. Phys.* **67**, 1821-1861.

Dyurgerov, M.B. and M.F. Meier. 1997. Mass balance of mountain and subpolar glaciers: a new global assessment for 1961-1990, *Arct. Alp. Res., 29*, 379-391.

Dyurgerov, M.B. and M.F. Meier. 2005. Glaciers and the Changing Earth system: A 2004 snapshot. *University of Colorado Institute of Arctic and Alpine Research Occasional Paper 58.*

Grove. J.M. 1988. The Little Ice Age. *Methuen, London.*

Habib, Ayman. 2005. Personal communication. Associate Professor, Department of Geomatics Engineering University of Calgary, Calgary, Alberta, Canada.

Hinzman, L.D., and 34 others. 2005. Evidence and implications of recent climate change in northern Alaska and other Arctic regions. *Climatic Change*, **72**, doi: 10.1007/s10584-005-5352-2. 251-298.

156

Intergovernmental Panel on Climate Change. 2001. *Climate Change 2001: Impacts, Adaptation, and Vulnerability,* edited by J.J. McCarthy et al., Cambridge Univ. Press, New York.

Krabill, W., W. Abdalati, E. Frederick, S. Manizade, C. Martin, J. Sonntag, R. Swift, R. Thomas, W. Wright, and J. Yungel. Greenland Ice Sheet: High-elevation balance and peripheral thinning. *Science.* **289**.428-430.

Koerner, R.M., 1970. The mass balance of Devon Island ice cap Northwest Territories, Canada, 1961-1966. *J. Glaciol.*, **9**(57): 325-336.

Koerner, R.M., 1977. Ice thickness measurements and their implications with respect to past and present ice volumes in the Canadian High Arctic ice caps. *Can. J. of Earth Sci.,* **14**, 2697-2705.

Luckman, A., T. Murray, H. Jiskoot, H. Pritchard, and T. Strozzi. 2003. ERS SAR feature-tracking measurement of outlet glacier velocities on a regional scale in east Greenland. *Ann. of Glaciol.,* **36**, 129-134.

Mair, D.W.F., D.O. Burgess, and M.J. Sharp. 2004. Thirty-seven year mass balance of the Devon Ice Cap, Nunavut, Canada determined by shallow ice coring and melt modelling. *J. Geophys. Res.* **110**, F01011, doi:10.1029/2003JF000099.

Meier, M.F. and J.M. Wahr. 2002. Sea level is rising: Do we know why? *Proc. Natl. Acad. Sci. USA, 99*,6524-6526.

Morse, D.L., D.D. Blankenship, E.D. Waddington, and T.A. Neumann. 2002. A site for deep ice coring in West Antarctica: results from aerogeophysical surveys and thermo-kinetic modeling. *Ann. Glaciol.* **35**, 389-98.

157

Overpeck, J., K. Hughen, D. Hardy, R. Bradley, R. Case, M. Douglas, B. Finney, K. Gajewski, G. Jacoby, A. Jennings, S. Lamoureux, A. Lasca, G. MacDonald, J. Moore, M. Retelle, S. Smith, A. Wolfe, and G. Zielinski. 1997. Arctic environmental change of the last four centuries. *Science,* 278: 1251-1256.

Rignot, E.S., A. Rivera and G. Casassa. 2003. Contribution of the Patagonia icefields of South America to sea level rise. *Science,* **302**, 434-437.

Serreze, M.C., Maslanik, J.A., Scambos, T.A., Fetterer, F., Stroeve, J., Knowles, K., Fowler, C., Drobot, S., Barry, R.G., and Haran, T.M. 2003. A record minimum arctic sea ice extent and area in 2002. *Geophys. Res. Let.* **30**(3), 1110, doi:10.1029/2002GL016406

Sharp, M.J. 2005. Personal communication. Professor, Department of Earth and Atmospheric Sciences, University of Alberta, Edmonton, Alberta, Canada.

Short N.H., and A.L. Gray. 2005. Glacier dynamics in the Canadian high Arctic from RADARSAT-1 speckle tracking. *Can. J. Rem. Sens.,* **31**(3), 225-239.

Welch, B.C. and R. W. Jocbel. 2003. Analysis of 2001 US-ITASE traverse deep-penetrating radar studies in West Antarctica. *Geophys. Res. Lett.* **30**,(1444). Doi:10.1029/2003GL017210.

Wang, L., M. J. Sharp, B. Rivard, S. Marshall, and D. Burgess. 2005. Melt Season Duration on Canadian Arctic Ice Caps, 2000-2004. *Geophys. Res. Let.,* **32**, L19502, doi:10.1029/2005GL023962

158